SOME OBSERVATIONS OF MIDDLE LATITUDE FORCED PLANETARY WAVES

Jacques Derome
Department of Meteorology
McGill University
Montreal

SOME OBSERVATIONS OF MIDDLE LATITUDE FORCED PLANETARY WAVES

1. Introduction

The type of atmospheric disturbances that we want to consider are the zonal asymmetries which are observed when the state of the atmosphere is averaged over a period of roughly one month or more. These asymmetries are associated with (or manifestations of) the well-known fact that two points having the same latitude and the same elevation above mean sea level, but different longitudes, can have quite different climates.

The fact that the zonal asymmetries on the mean monthly maps occur at approximately the same location year after year suggests that they owe their existence to zonal asymmetries of the lower boundary, such as the presence of mountain barriers and land-sea thermal contrasts (Saltzman, 1968). For that reason we commonly say that the disturbances are "forced" by the lower boundary. As we shall see in more detail later, this does not necessarily imply that the energy associated with these disturbances is maintained against dissipative forces by a flux of energy through the lower boundary. In the case of disturbances "forced" by topography, for example, there is no flux of energy through the earth's surface; there is simply a redistribution of energy from the axisymmetric to the nonaxisymmetric part of the flow through the action of mountains which deflect the zonal flow.

2. The Observed Structure

2.1 Mean annual conditions

To fix ideas, we have in Fig. 1 the 500 mb geopotential height averaged over each day in the period 1965-1967. Naturally the field contains only ultra-large scale features, the more notable being the troughs on the east coasts of Asia and North America.

2.2 Average Winter Conditions in the Wave Domain

To obtain more detailed information about the scales of motion present in time-averaged fields we can perform a Fourier analysis along latitude circles, i.e., we can write, for any atmospheric variable Z at a given time t_o,

$$Z(\lambda,\varphi,p) = A_o(\varphi,p) + \sum_{n=1}^{\infty}\left[A_n(\varphi,p)\cos n\lambda + B_n(\varphi,p)\sin n\lambda\right]$$

$$= A_o(\varphi,p) + \sum_{n=1}^{\infty} C_n(\varphi,p)\cos n\left[\lambda-\gamma_n(\varphi,p)\right]$$

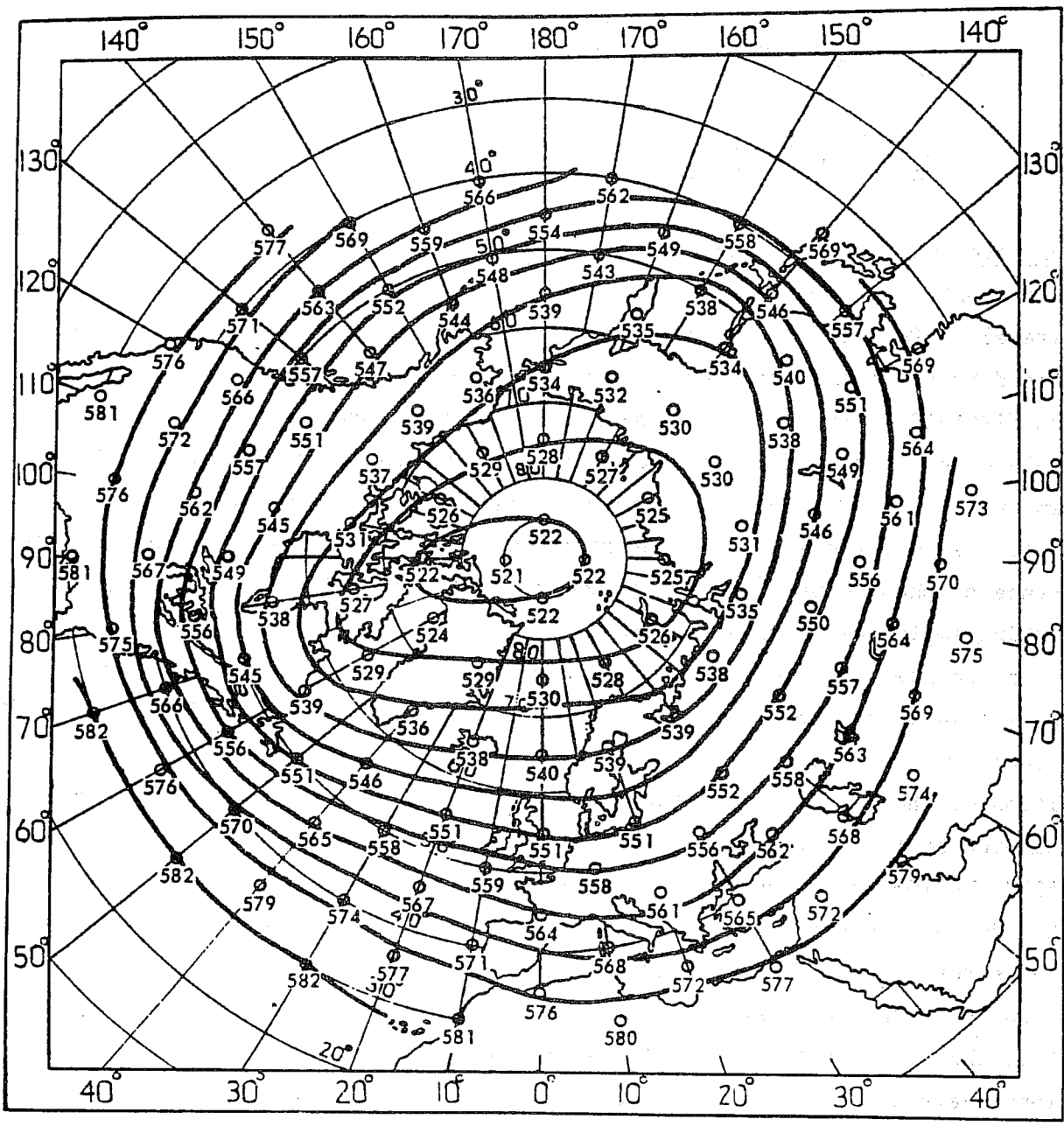

Fig. 1. The average 500 mb geopotential height field for the period 1965-1967, in gdm (After Craddock and Flood, 1969).

where λ, φ, p are the longitude, latitude and pressure respectively, and

$$A_o = \frac{1}{2\pi} \int_0^{2\pi} Z d\lambda$$

$$\{A_n, B_n\} = \frac{1}{\pi} \int_0^{2\pi} Z\{\cos n\lambda, \sin n\lambda\} d\lambda \quad , \qquad n \geq 1$$

$$C_n = (A_n^2 + B_n^2)^{\frac{1}{2}} = \text{amplitude of wavenumber n}$$

$$\gamma_n = \frac{1}{n} \tan^{-1}(B_n/A_n) = \text{phase of wavenumber n.}$$

Zonal wavenumber 1. This type of analysis has been done by van Loon et al. (1973) on mean monthly height data for January and July, the two months being treated separately. For each of these two months an average height distribution was obtained by averaging over seven years (1964-1970) in the troposphere and over five years (1966-1970) in the stratosphere. The Fourier analysis of the resulting mean monthly maps yielded, for zonal wavenumber 1, the amplitude and phase distribution shown in Fig. 2. We see that in the troposphere zonal wavenumber 1 has a maximum amplitude slightly over 150m at about 50°N, in the upper troposphere. We note the presence of phase clusters in the troposphere at about 15°N and 72°N, indicating a vanishing amplitude at those points.

In the lower stratosphere the wave maximum amplitude shifts northward and reaches a value of about 600m at p = 10 mb (Z ≃ 30 km) and φ ≃ 70°N, a fourfold increase over the value in the upper troposphere. As for the phase, which gives the position of the ridge, we see that it is such that in the middle latitude the wave is sloping to the west with height. The tilt is rather pronounced, considering that at 50°N the 1000 mb ridge is located at 60°E whereas at 10 mb it is at 180°, a shift of 240 degrees to the west. This means that at some intermediate level (50 mb) the ridge is vertically above the 1000 mb trough. In the horizontal we find in general that south of the wave amplitude maximum the phase lines are tilted from the south-west to the north-east. North of the wave amplitude maximum, at least in those regions where the amplitude is relatively large, there is a tendency for the wave to tilt from the south-east to the north-west. We will return later to a discussion of these phase tilts, both in the horizontal and the vertical, and show how they are related to the direction of wave energy propagation.

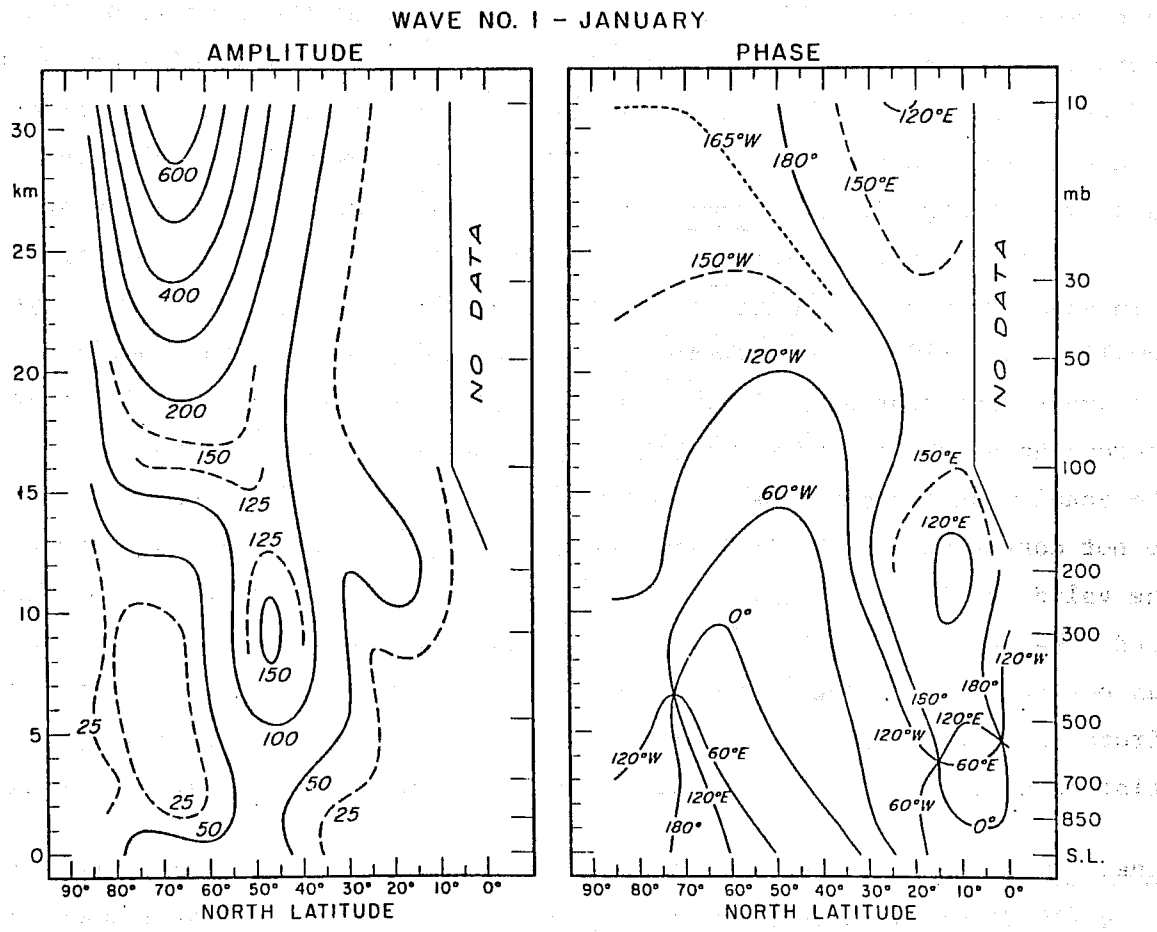

Fig. 2. Latitude-height section of stationary zonal wavenumber 1 amplitude (metres) and phase (longitude of ridge) in January, averaged over the years 1964-1970 in the troposphere and over 1965-1969 in the stratosphere. (After van Loon et al., 1973).

To get some idea of the representativeness of the average wave structure of Fig. 2 we can compare it with that shown in Fig. 3, for January 1958, a month not included in the data set of Fig. 2. We find again: (a) a relative maximum in the amplitude in the upper troposphere at 50°N, (b) a shift northward and an increase in the amplitude up to at least 10 mb (30 km), with roughly a factor 4 difference between the amplitudes at 200 mb and 10 mb, (c) a westward tilt with height in middle latitudes, (d) a tendency for the wave, at constant pressure, to tilt from the south-west to the north-east south of the amplitude maximum and the opposite tilt further north. The notable difference occurs in the intensity of the wave, which is roughly 50% higher in 1958 than during the average of the several years used to construct Fig. 2. We note also that the phase cluster in the northern mid troposphere of Fig. 2, which indicates a zero value for the amplitude, probably resulted from the averaging process; it was not observed in 1958. This is not a particularly significant feature since the amplitudes in this region are quite small.

It is interesting to compare the stationary wave structure of Fig. 2 with the mean zonal wind averaged over the period December-February for several years, from Newell et al. (1972), as seen in Fig. 4. We find that the wave amplitude maximum in the upper troposphere is about 15 degrees north of the subtropical jet and that with increasing height in the stratosphere the amplitude maximum tends to coincide with the zonal wind maximum. As the data set which was used to construct Figs. 2 and 4 do not correspond to the same time period, there can naturally be some question as to the validity of the above relationship between wave structure and the mean zonal wind. We can see from Fig. 5, however, that generally the same close relationship was observed in the lower stratosphere of January 1966. Fig. 5 is from a paper by Hirota and Sato (1969) who, in fact, seem to have been the first to point out this relationship. In the case of Fig. 5 all data apply to the same time period.

Zonal wavenumber 2. The structure of the second zonal harmonic from van Loon et al.'s (1973) analysis is shown in Fig. 6. As in the case of wavenumber 1 (Fig. 2), the height variance of this wave is concentrated in the middle and high latitudes. North of 40°N the amplitude increases monotonically from the middle troposphere to 30 km and the wave slopes westward with height, although much less than the gravest harmonic. The tropospheric amplitudes are as large as those of wavenumber 1 (in some areas larger) but at 30 km wavenumber 1 is larger by a factor of at least two. South of 40°N the amplitude of wavenumber 2 is insignificant, except near 12 km, which coincides with the southward bulge of the mean zonal wind (Fig. 4) maximum. We note that zonal wavenumber 1 also had a weak amplitude maximum in that region.

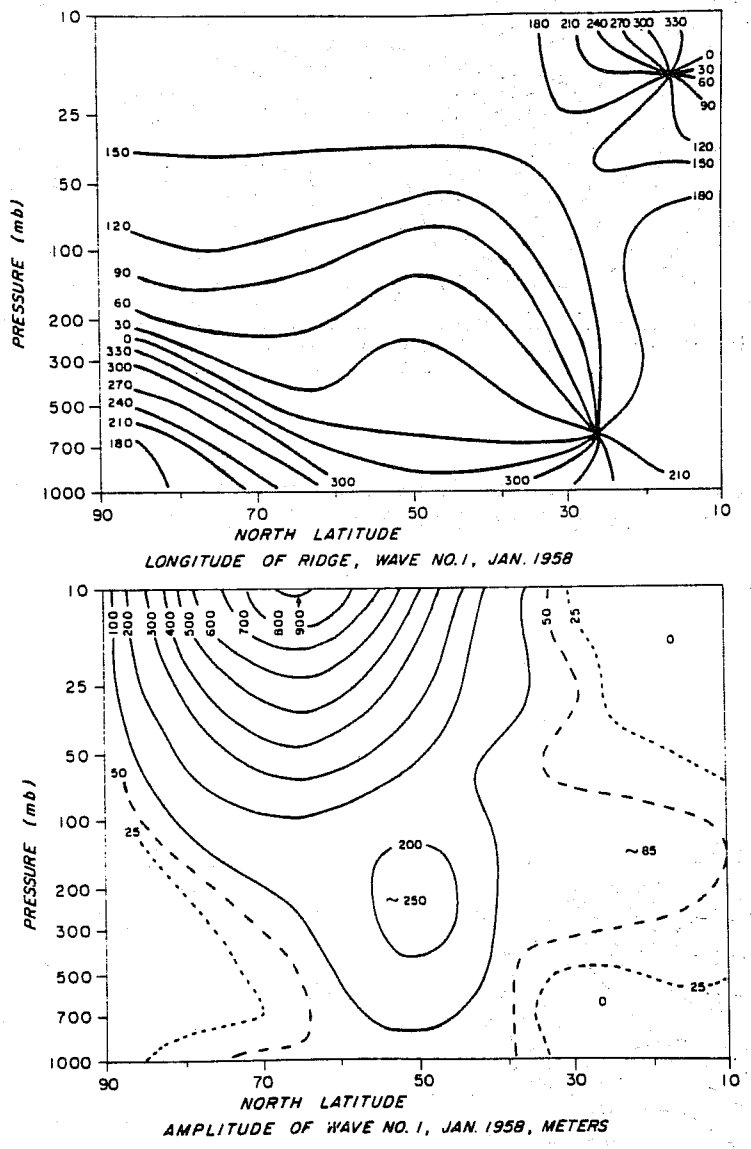

Fig. 3. Amplitude and phase angle of stationary wavenumber 1 versus latitude and height, for January 1958 (After Muench, 1967).

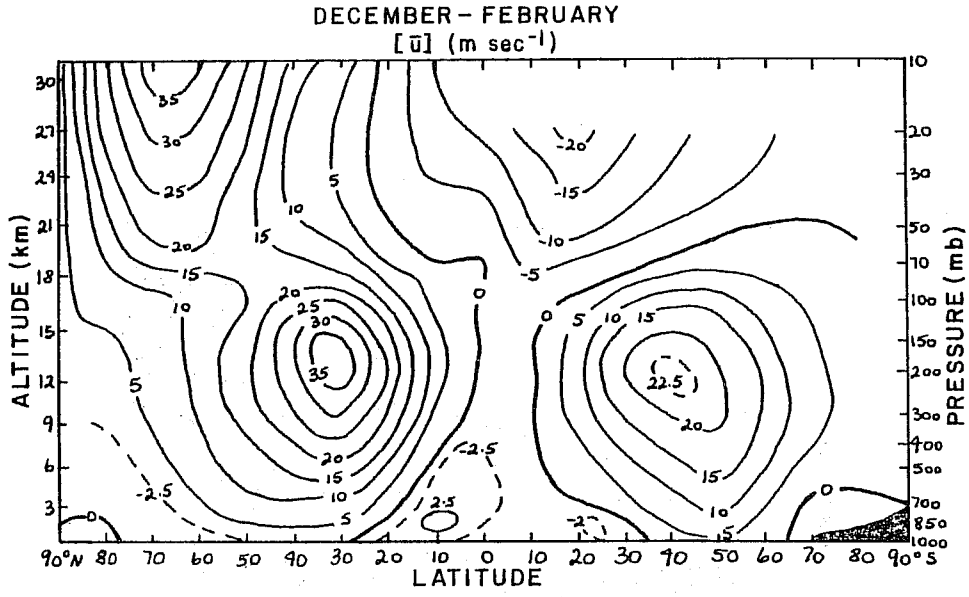

Fig. 4. Latitude-height section of the mean zonal wind (m/s) for the period December-February (After Newell et al., 1972).

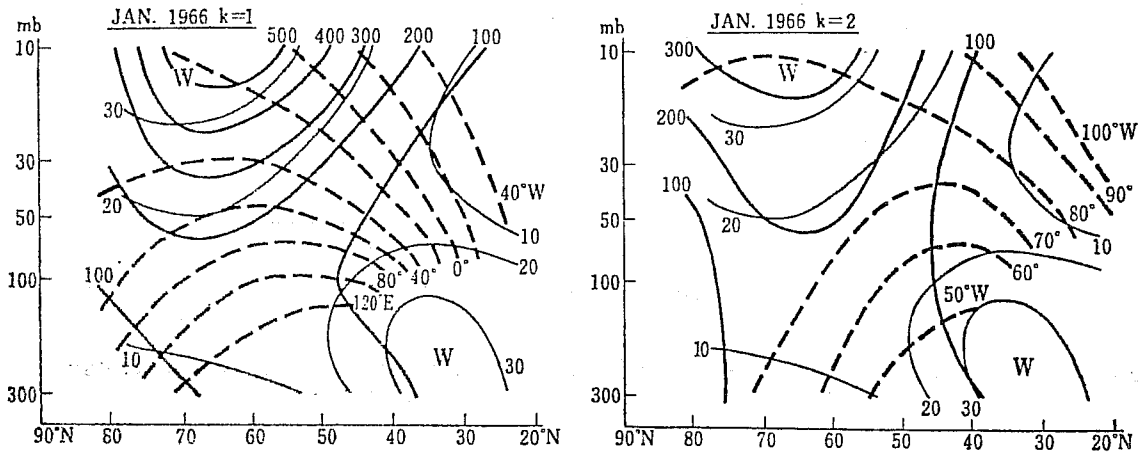

Fig. 5. Mean monthly zonal wind (thin full lines; in metres per second), amplitude of the mean monthly height waves (heavy full lines; in metres) and phase angle of the trough (broken lines) for January 1966. Wavenumber 1, left; wavenumber 2, right (After Hirota and Sato, 1969).

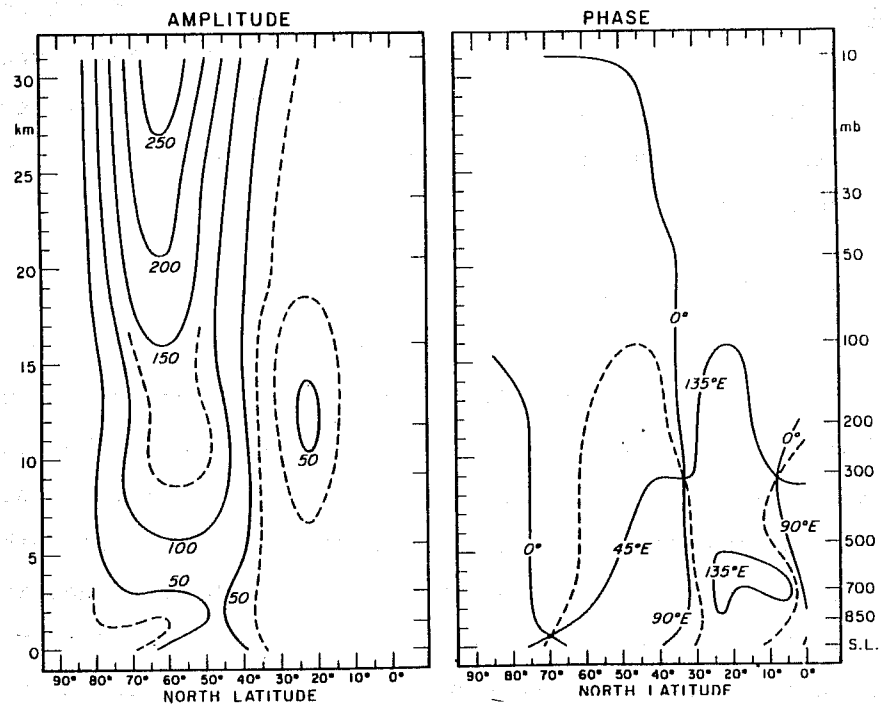

Fig. 6. Latitude-height section of the amplitude (metres) and phase (longitude of ridge) for stationary wavenumber 2 in January. In the stratosphere south of 10°N no analysis was made (After van Loon et al., 1973).

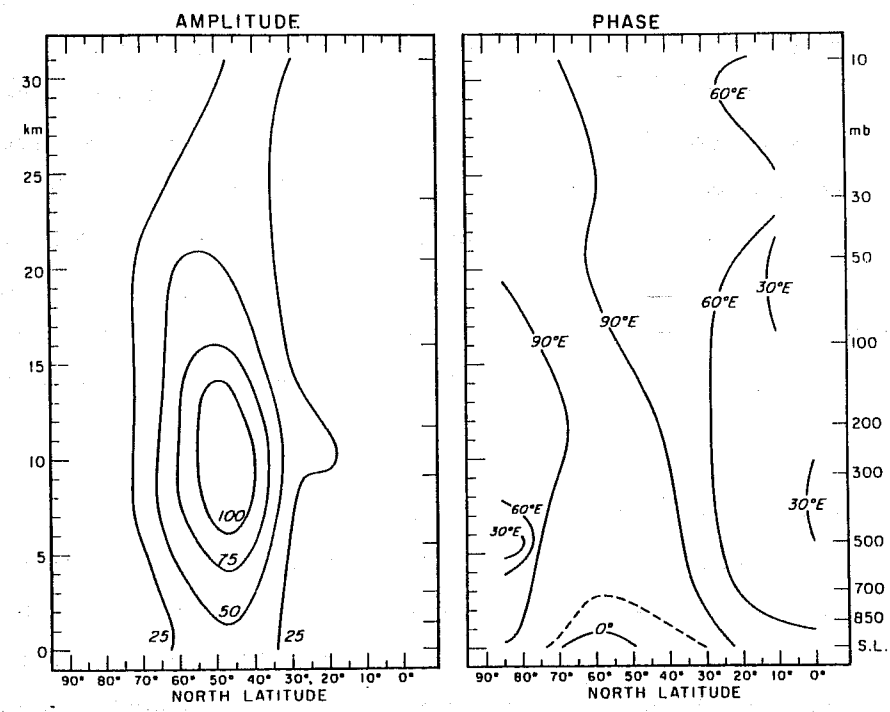

Fig. 7. Latitude-height section of the amplitude (metres) and phase (longitude of ridge) for stationary wavenumber 3 in January. In the stratosphere south of 10°N no analysis was made (After van Loon et al., 1973).

Zonal wavenumber 3. The results of van Loon et al. (1973) for this wavenumber appear in Fig. 7. Clearly the height wave is confined to the troposphere and the first few kilometres of the stratosphere, where its intensity is comparable to that of the first two harmonics. The tilt of the wave is seen to be rather small both in the vertical and in the horizontal.

2.3 Sum of Zonal Harmonics

Constant pressure maps - January. The contributions from zonal wavenumbers 1, 2 and 3 published by van Loon et al. (1973) were added together by Avery (1978) to produce the 500 and 10 mb maps shown in Fig. 8. It is seen that the mean height field is becoming smoother with altitude, as expected from our discussion of the harmonics. We also observe the northern progression of the disturbances from 500 to 10 mb. We should bear in mind that while the height variance is concentrated in the polar region the wind field tends to have relatively more variance in the mid and southern latitudes than the mass field because of the geostrophic nature of the flow and the decrease of the Coriolis parameter with decreasing latitude. This was pointed out, in particular, by Simmons (1978).

Zonal Cross-sections - v, January. To give some idea of the wind velocities associated with the mean January height field we present in Fig. 9 zonal cross-sections of the meridional velocity component from Saltzman and Sankar-Rao (1963). The data are presented at 30°N, 45°N and 60°N up to 100 mb only. The largest values are found near 300 mb and reach about 16 m s^{-1}. If we compare these speeds with that of the mean zonal wind in Fig. 4 we see that they represent a rather substantial disturbance of the mean zonal flow. This implies that linear models of the forced planetary waves, which assume that disturbance velocities are much smaller than the mean zonal wind, cannot be expected to simulate in detail the structure of the waves, at least in the troposphere. The importance of the nonlinear terms in the potential vorticity equation applicable to the stationary waves has been demonstrated by Saltzman and Sankar-Rao (1963).

2.4 Average Summer Conditions in the Wave Domain

The mean July zonal asymmetries differ radically from those found in January. As can be seen in Fig. 10 taken from van Loon et al. (1973), which applies to the same years as the January data from the same authors presented earlier, the maximum geopotential height amplitude in zonal wavenumber 1 is found at about 30°N in the upper troposphere. Near the surface a secondary maximum of about 75 m is also

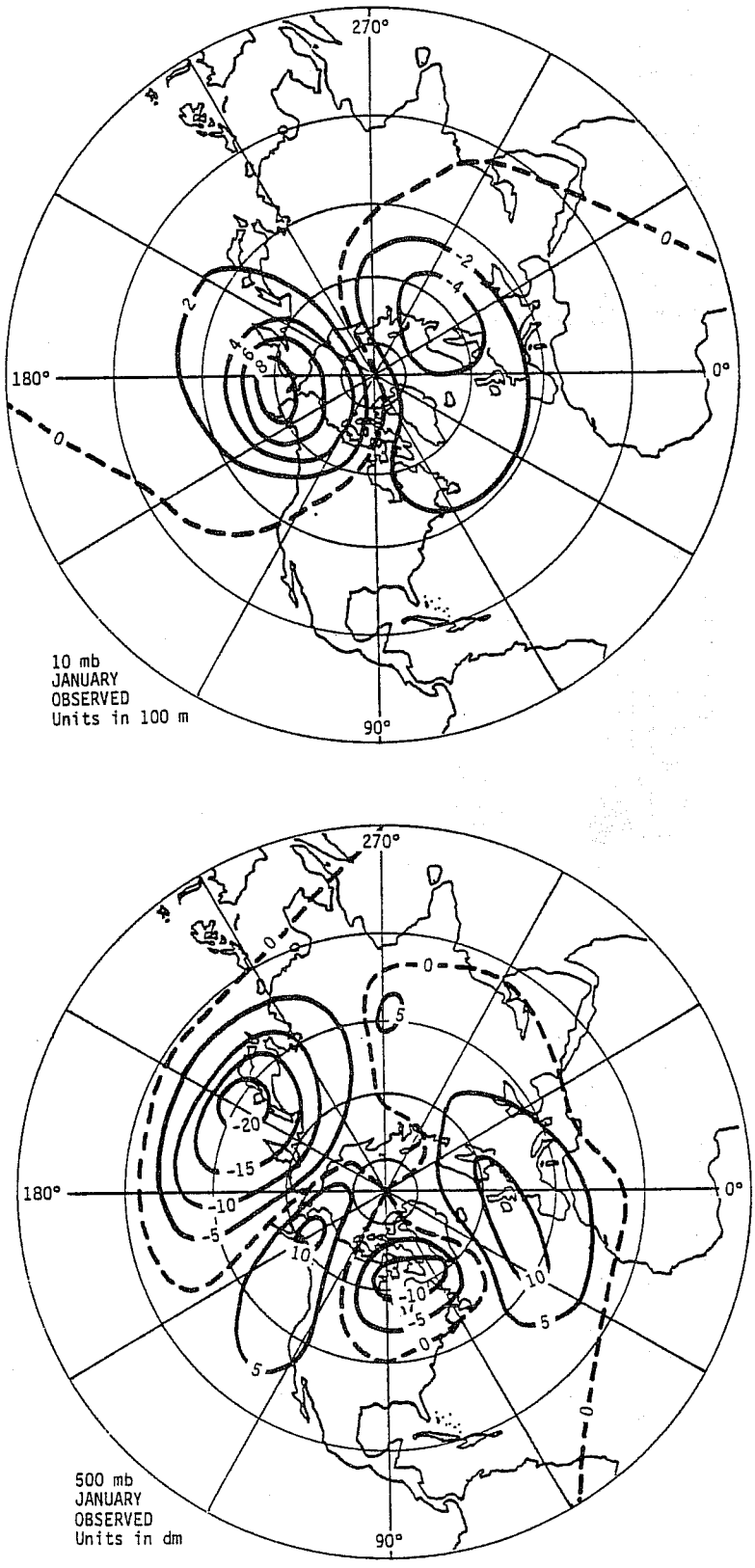

Fig. 8. Observed January planetary wave height pattern due to zonal wavenumbers 1, 2 and 3 at (a) 10 mb, and (b) 500 mb (After Avery, 1978; data from van Loon et al., 1973).

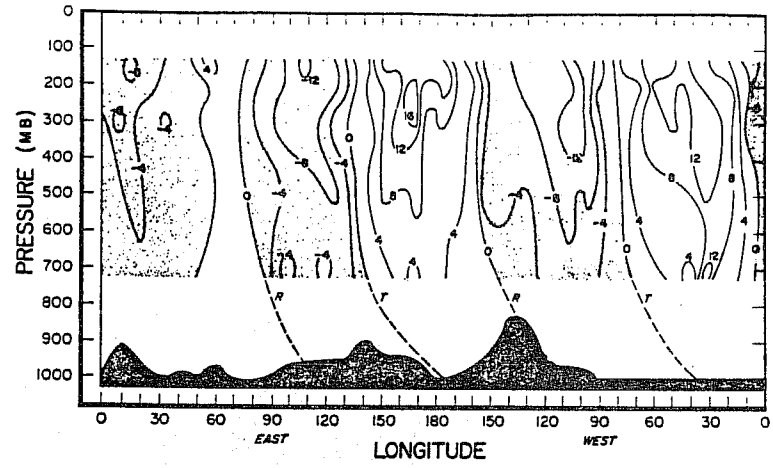

v_1, January, 60N.

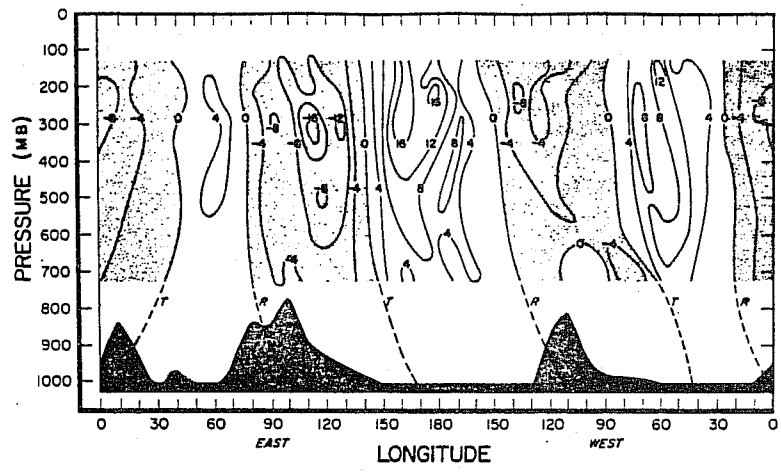

v_1, January, 45N.

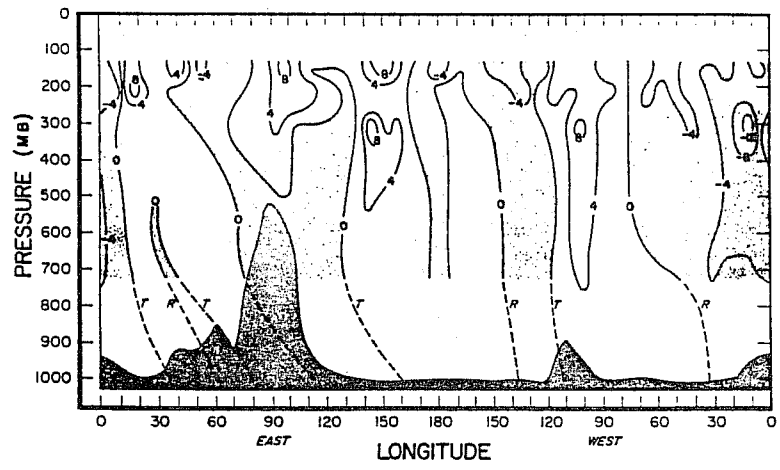

v_1, January 30N.

Fig. 9. Longitude-pressure section of the meridional wind component associated with the January stationary flow at 60°N (top), 45°N (middle) and 30°N (bottom) (After Saltzman and Sankar-Rao, 1963).

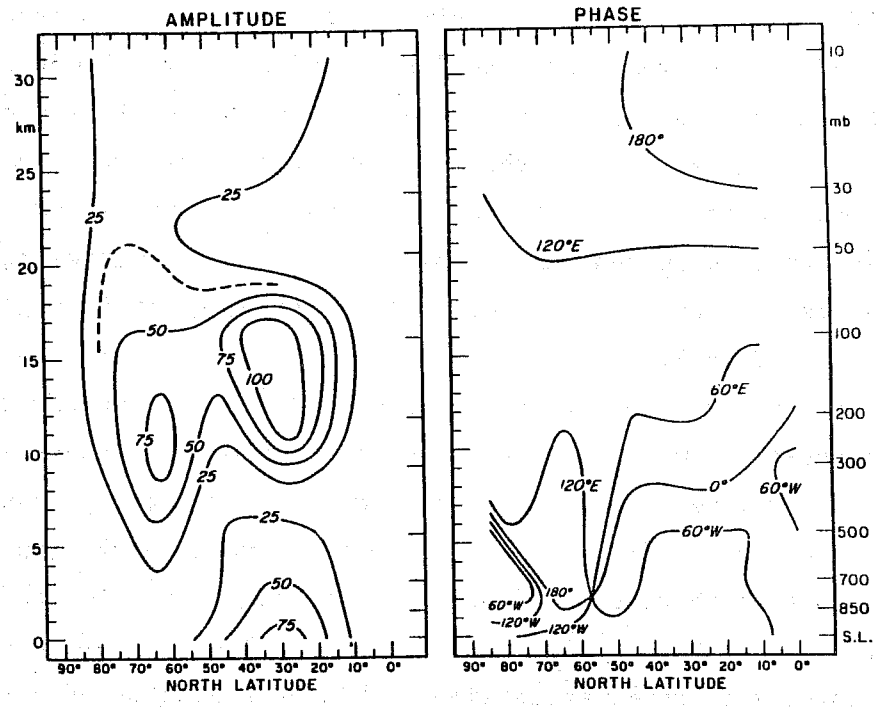

Fig. 10. Latitude-height section of the amplitude (metres) and phase (longitude of ridge) for stationary wavenumber 1 in July. In the stratosphere south of 10°N no analysis was made (After van Loon et al., 1973).

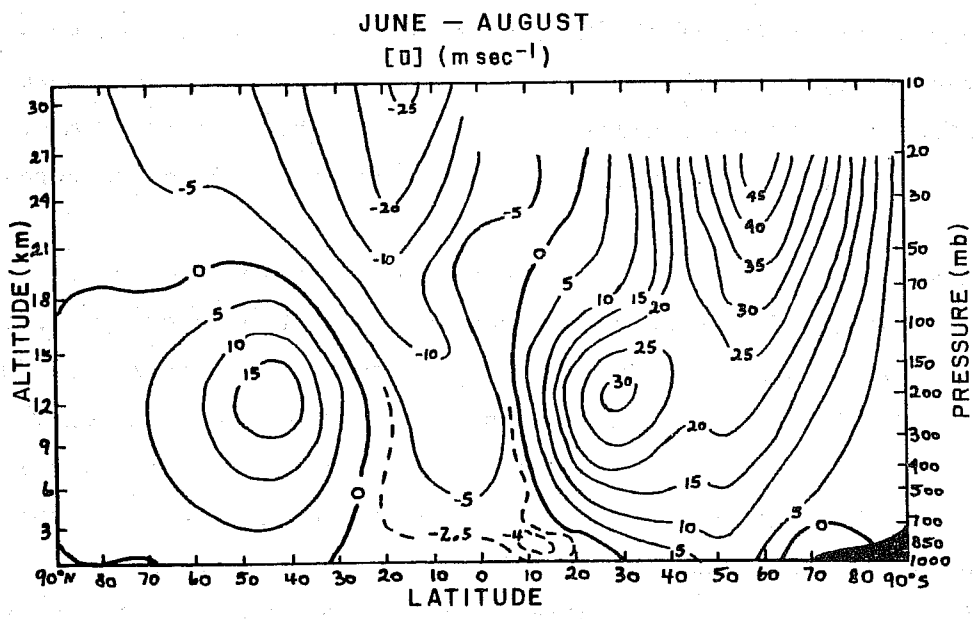

Fig. 11. Latitude-height section of the mean zonal wind (m/s) for the period June-August (After Newell et al., 1972).

found near 30°N; in winter (Fig. 2) a similar amplitude is observed near the surface but at 50°N. The most striking feature of the wave, however, is the fact that in opposition to January, the wave now tilts to the east with height from about 10°N to 60°N. This requires that the temperature maximum lies to the east of the height maximum and similarly the temperature minimum is east of the height minimum. It is easily seen that this implies that on the average along a latitude circle warm air is flowing south and cold air is flowing north (neglecting transports by transient eddies).

We note also that the amplitude of the wave decreases rapidly with height in the lower stratosphere. We have seen in our discussion of January conditions that the structure of zonal wavenumber 1 for that month is related to that of the mean zonal wind. If we look at Fig. 11, which gives the mean summer (in Northern Hemisphere) zonal wind distribution, we find that the height at which the wave decays rapidly corresponds to the transition zone from the lower level mean zonal westerlies to upper level mean zonal easterlies. This near-absence of a zonal wavenumber 1 in the stratospheric easterlies and the eastward tilt of the tropospheric wave in the troposphere are two important features of the July observations which atmospheric models should be able to reproduce.

Zonal wavenumbers 2 and 3 are described by van Loon et al. (1973) as being similar to the gravest harmonic and they will not be discussed in detail here.

2.5 Seasonal Variations in the Temperature Field

The annual variation of the mean monthly 500 to 1000 mb thickness along 45°N is presented in Fig. 12. The data were extracted from maps published by the German Weather Office (Die Grosswetterlagen Europas) for the period November 1977 through September 1978 at bimonthly intervals. A thickness of 10m corresponds to 0.49 degrees K.

Broadly speaking the curves can be collected in two groups, the November to March period and the May to September period. Within each group the curves are clearly positively correlated, while there is obviously a marked difference between the groups. To highlight the summer-winter difference the July curve has been superimposed (dashed) on the January one. The negative correlation is quite obvious.

In winter the coldest areas are found on the eastern part of the two land masses and the warmest areas over the Atlantic and the eastern Pacific. It thus appears likely that the warming influence of the oceans in winter plays an important role in determining the position and amplitude of the mean monthly temperature wave up to 500 mb.

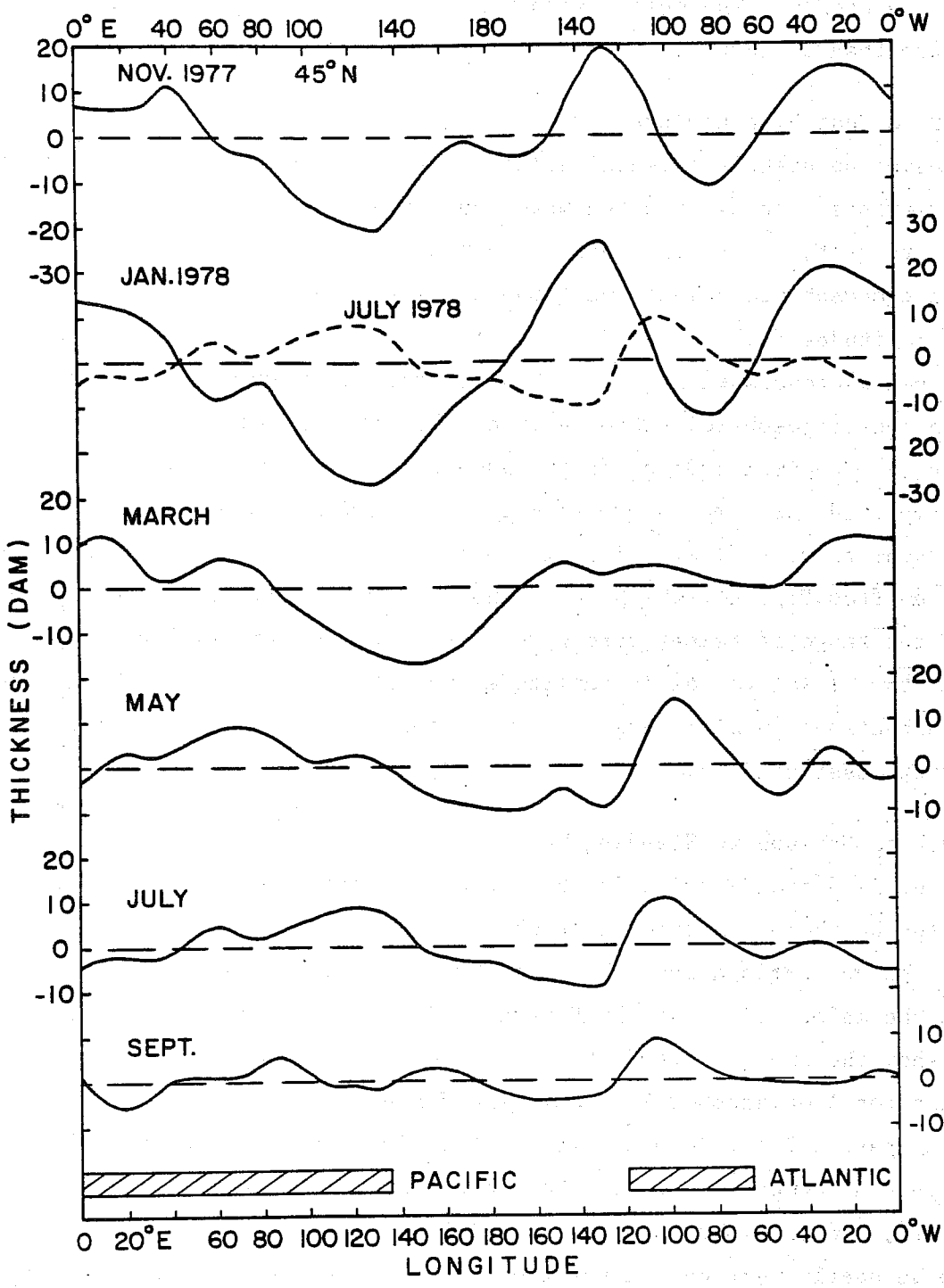

Fig. 12. Deviation from the zonal average of the mean monthly 500 to 1000 mb thickness along 45°N for 6 months of the year. A thickness of 10m corresponds to 0.49 degrees K.

In July the sign of the temperature disturbance is almost everywhere opposite to that of January. The warm air is generally over the continents and the cooler air over the oceans. The summer standing wave is seen to be weaker than the winter one by more than a factor 2.

2.6 Year to Year Fluctuations

Whenever we present climatological averages the question of representativeness naturally arises. To see how the mean monthly height and temperature fields change from year to year, we present data again from van Loon et al. (1973). Fig. 13 shows the tropospheric height and temperature for zonal wavenumbers 1, 2 and 3 at selected latitudes for 1964-1970. We note first that while the amplitude of the height waves increases with height, that of the temperature waves decreases with height in the troposphere. Observe in particular the large year to year fluctuations in (a) the amplitude of height wave 3; (b) the phase of height wave 1; (c) the amplitude of temperature wave 2 in the lower levels.

The year to year fluctuations are much larger in the lower stratosphere, as can be seen from Fig. 14, which shows the five years 1965-1969. At 10 mb, for example, the range of temperature wave 1 is about 19 degrees K while the height wave 1 at that level ranges in amplitude from 150 to 1100m. We should keep these large fluctuations in mind later when we compare the results of General Circulation Models with observed data.

2.7 Southern Hemisphere Standing Waves

As the land distribution in the Southern Hemisphere differs radically from that in the Northern Hemisphere, it should be interesting to compare the forced waves of the two hemispheres. Fig. 15 shows the radiosonde station network which provided the information used by Knittel (1976) to produce Figs. 16 and 17. These figures show the amplitude and phase distribution, in meridional cross-sections, for height zonal wavenumber 1 in July and January.

By comparing Figs. 16 and 2 we see that in winter the Southern Hemisphere wave has a magnitude comparable to its Northern Hemisphere counterpart, at least in the troposphere; in the lower stratosphere it is weaker. The Southern Hemisphere wave seems to be nearly vertical in the troposphere where its amplitude is largest, in contrast to the Northern Hemisphere wave which tilts westward with height. By refering to Fig. 11 we see that in the stratosphere the wave amplitude maximum nearly coincides with the zonal wind maximum, just as previously observed in the Northern Hemisphere.

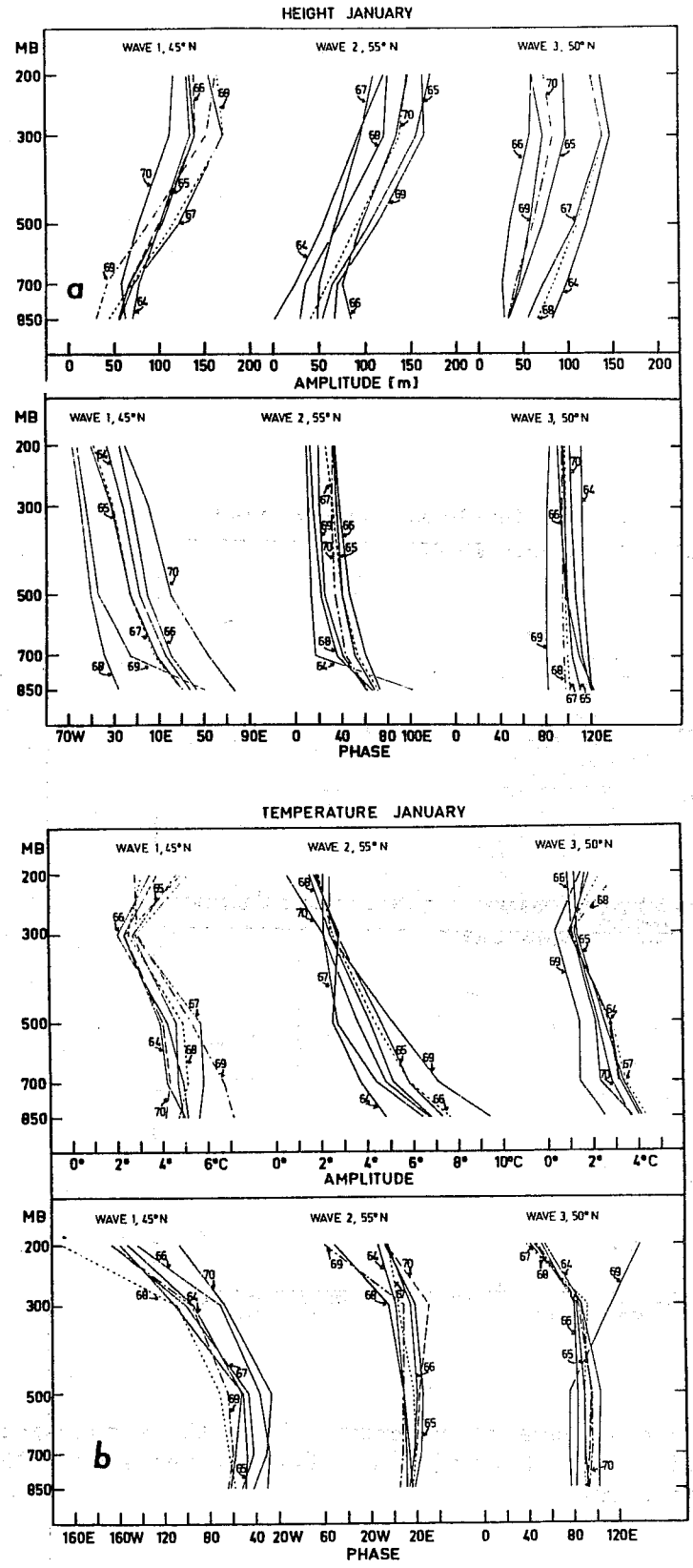

Fig. 13(a). Amplitude in metres and phase of wavenumbers 1 - 3 for the geopotential height of different years (After van Loon et al., 1973).

Fig. 13(b). Amplitude in degrees Celsius and phase of wavenumbers 1 - 3 for the temperature of different years (After van Loon et al., 1973).

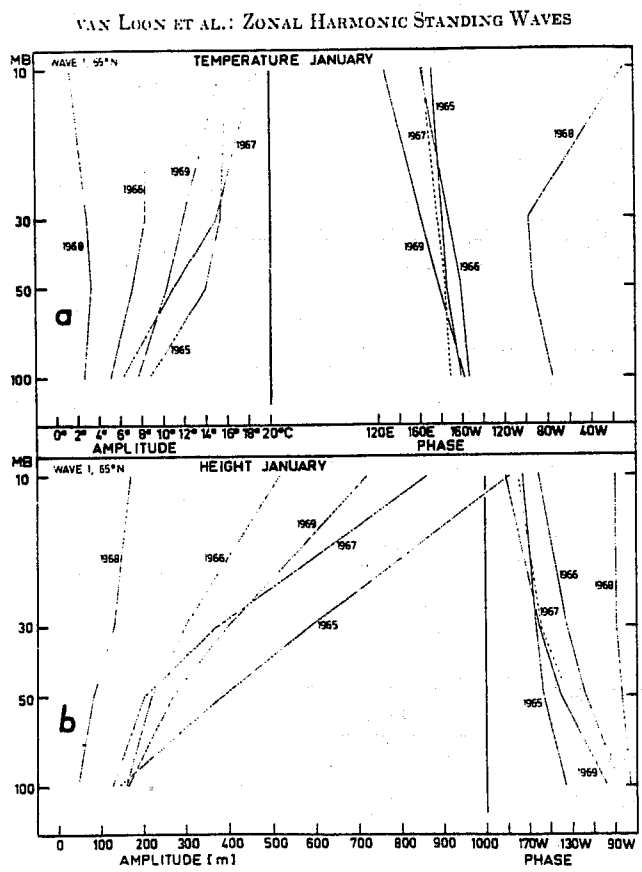

Fig. 14. Amplitude and phase of wavenumber 1 in the stratosphere temperature (top) and height (bottom) for different years at 65°N (After van Loon et al., 1973).

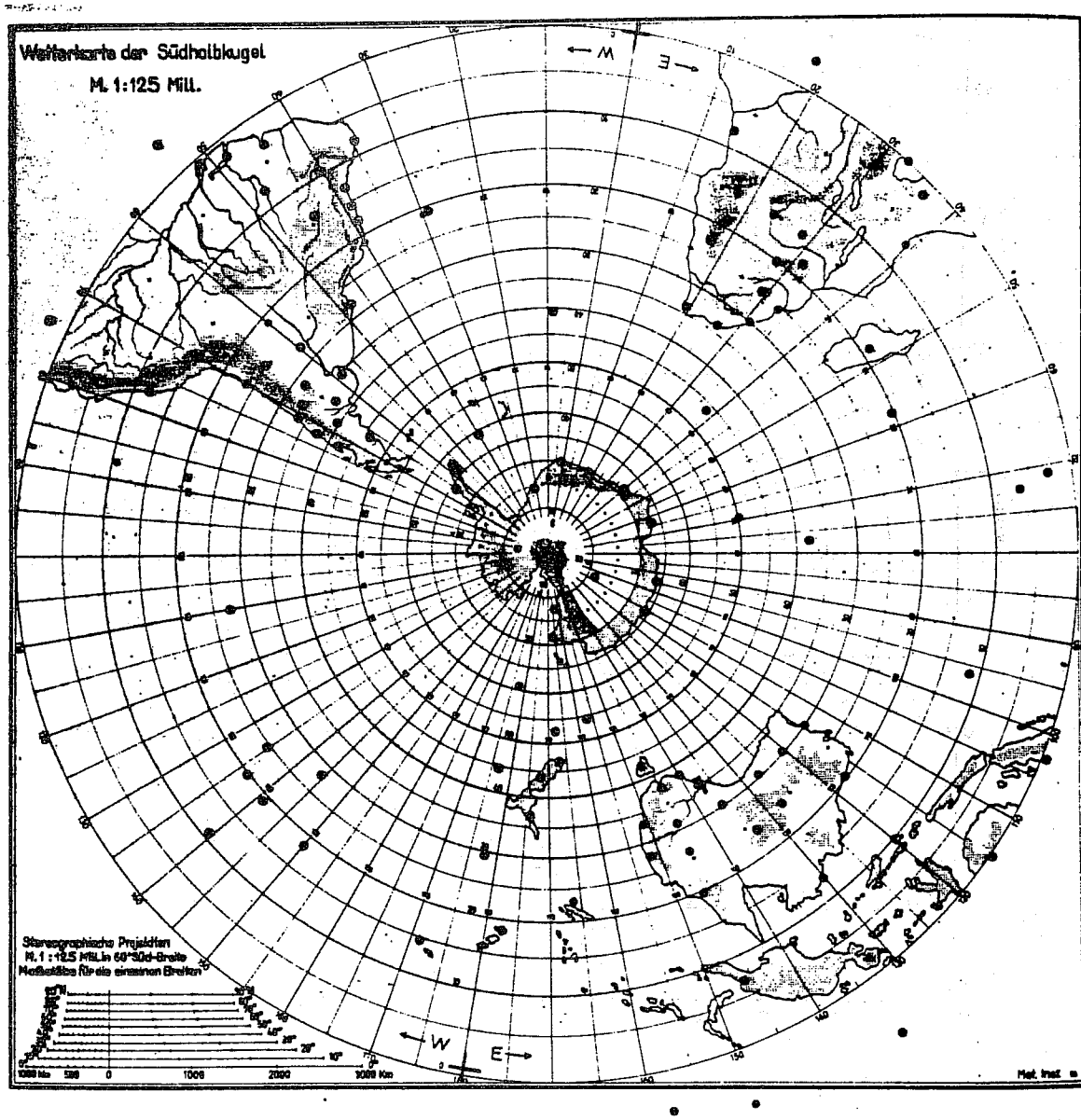

Fig. 15. Radiosonde stations with observations at the 30 mb-level in the Southern Hemisphere (After Knittel, 1976).

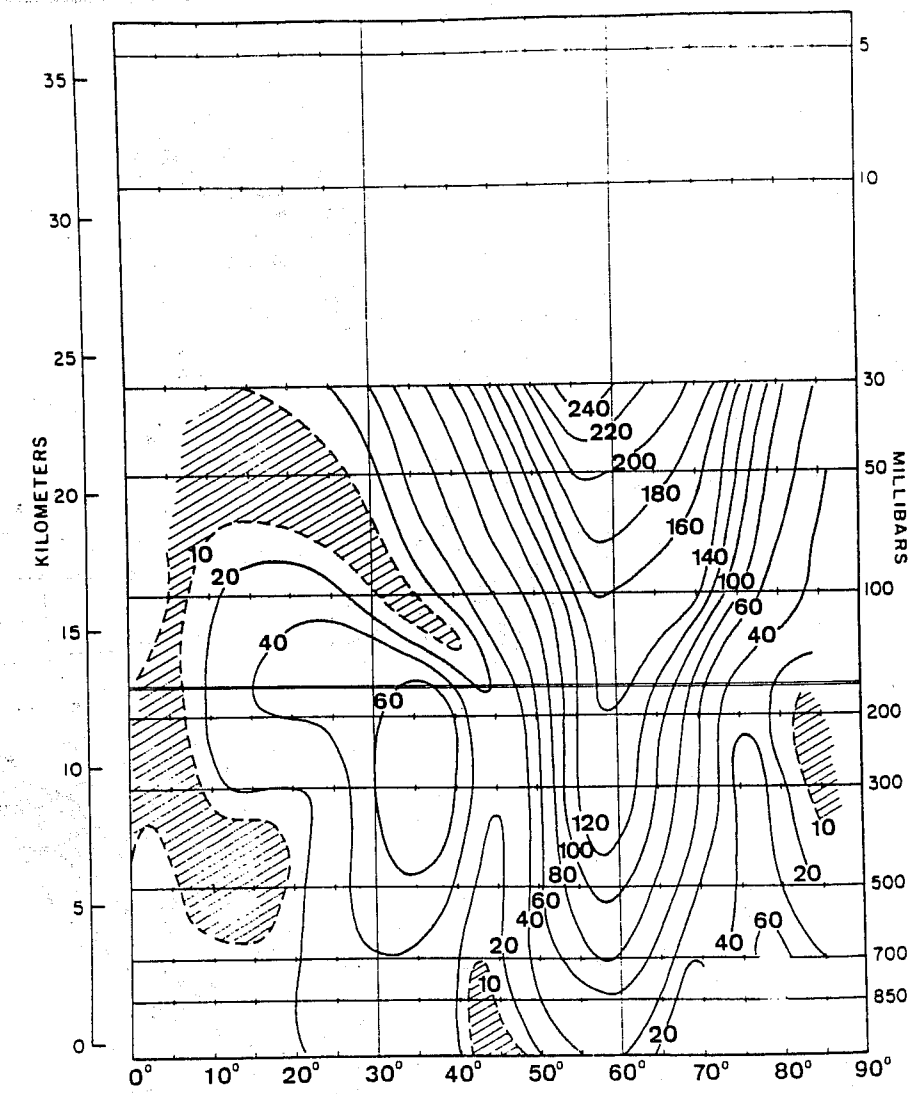

Fig. 16a. Latitude-height section of wavenumber 1 height amplitude in metres in July in the Southern Hemisphere; average of 1968-1972 (After Knittel, 1976).

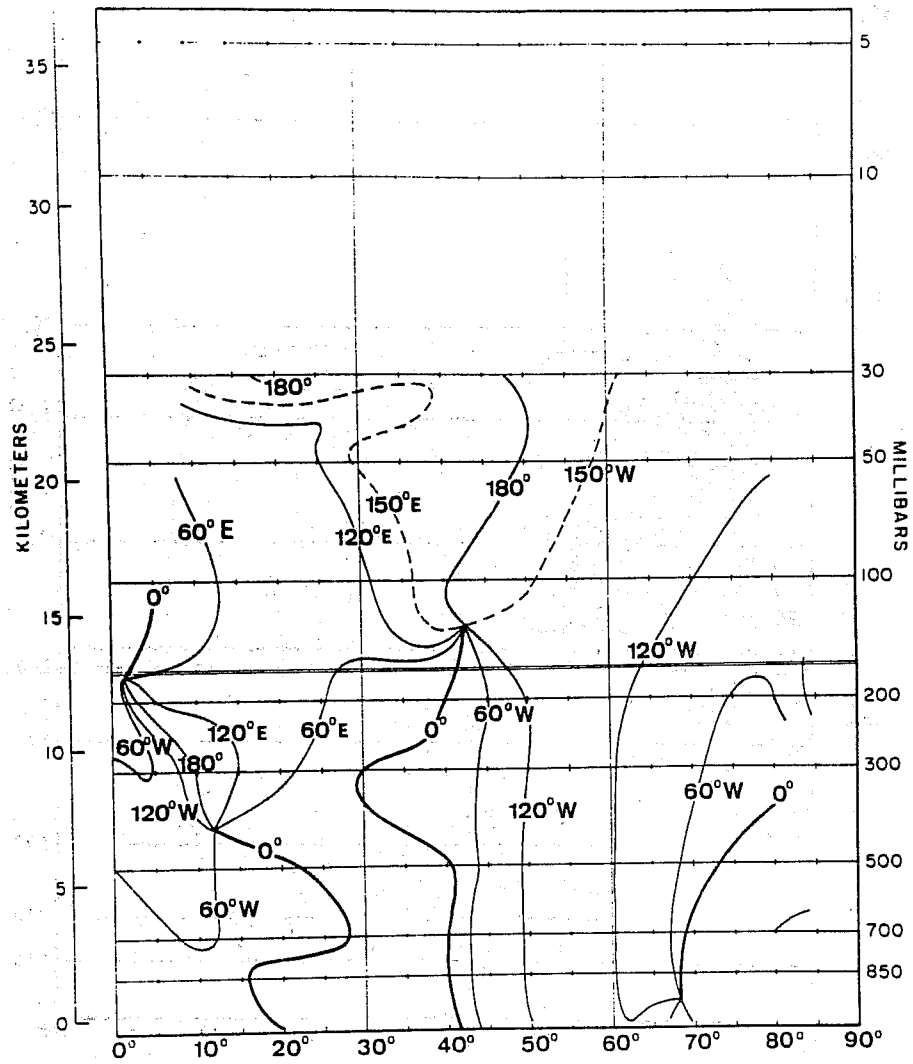

Fig. 16b. As in Fig. 16a but for the phase (longitude of ridge).

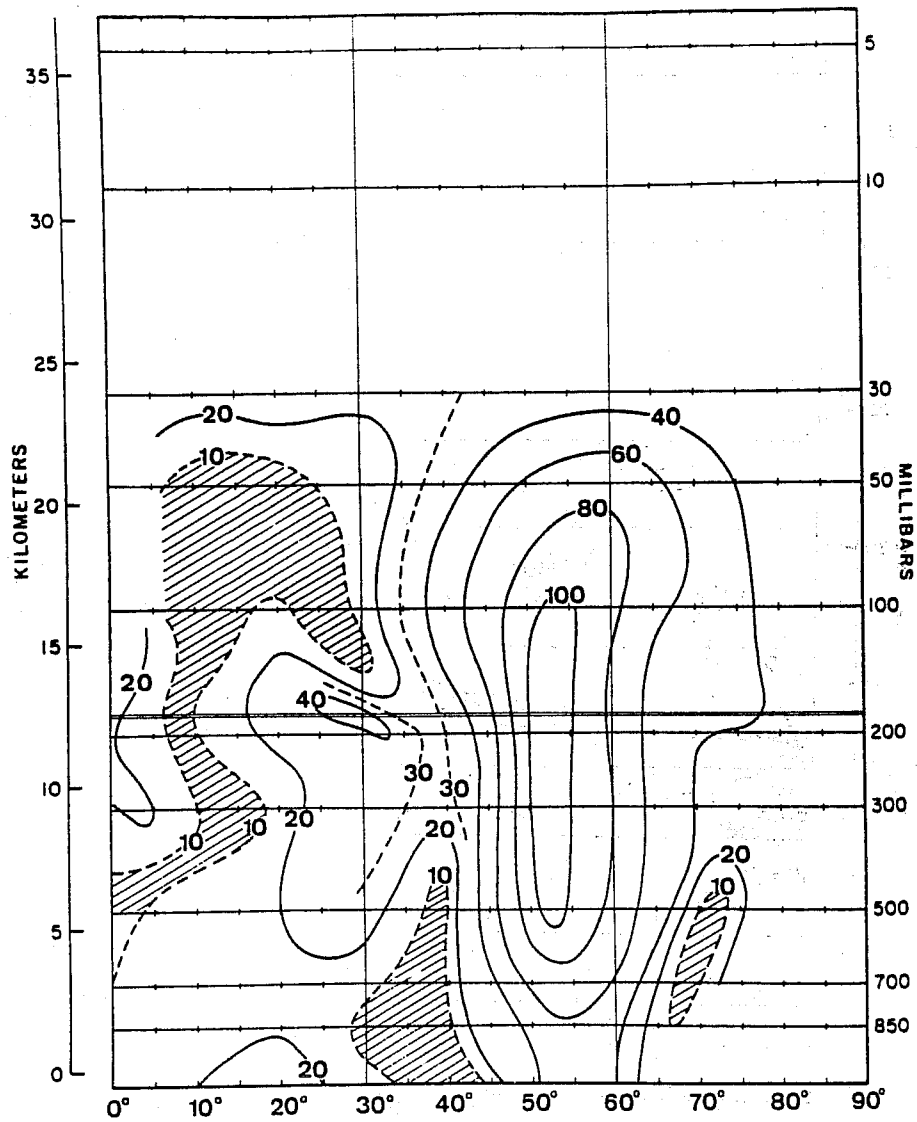

Fig. 17a. Latitude-height section of wavenumber 1 height amplitude in metres in January in the Southern Hemisphere; average of 1969-1973 (After Knittel, 1976).

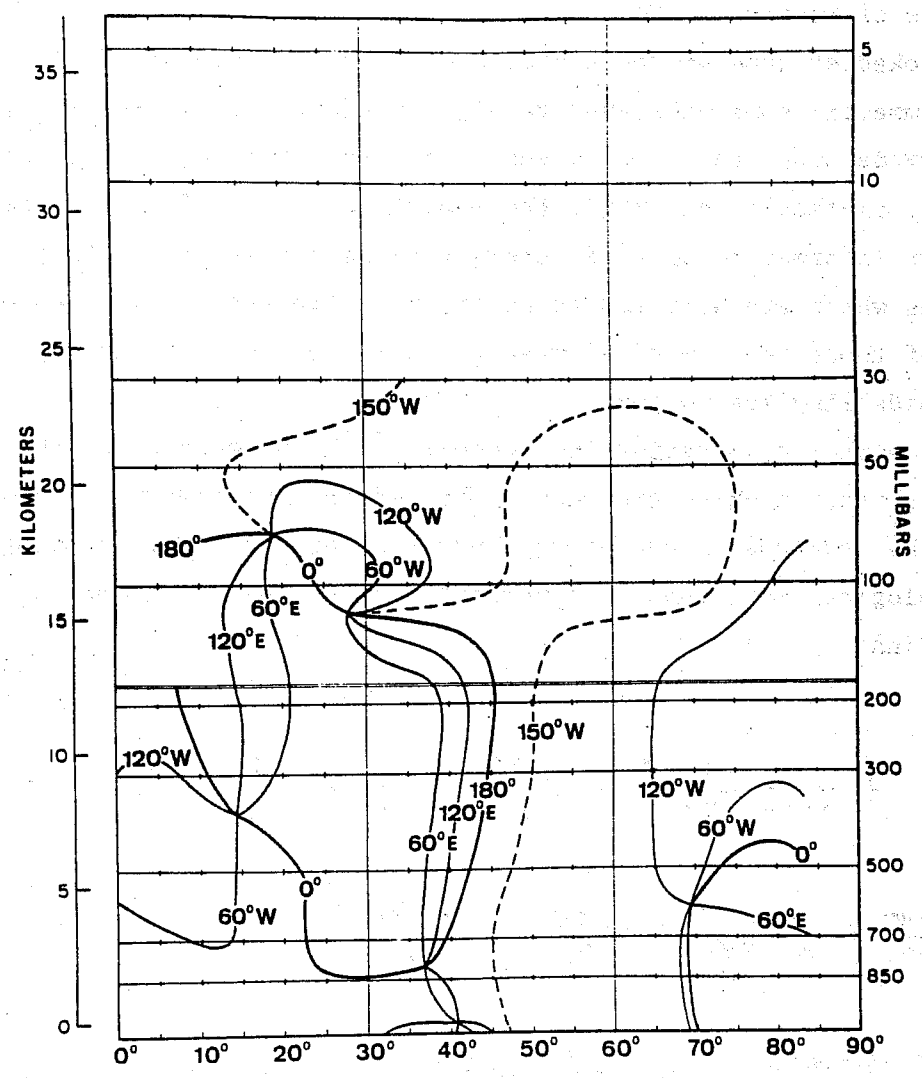

Fig. 17b. As in Fig. 17a but for the phase (longitude of ridge).

We see from Figs. 17 and 10 that in summer the height wave is confined to the troposphere and lower stratosphere where the zonal wind is westerly. We shall see later, when we analyze mathematical models of the forced waves, that even highly simplified models can account for the observed lack of significant standing wave energy in the region of easterlies of both hemispheres.

2.8 Energetics of Stationary Waves

Having looked at some of the features of the observed forced planetary waves, we will now summarize some published results on their energetics, i.e., on the way in which energy is supplied to the waves to maintain them against dissipative forces. It is remarkable that while the importance of the forced waves is well recognized, our information on their energetics is rather poor. Only those energy transformations which are believed to be the most important have been computed, and for some of those the numerical results could only be obtained by introducing rather crude modelling assumptions.

In order better to appreciate the results to be presented and the types of atmospheric circulation which are required to effect the energy transfers, we will first derive the stationary wave energy budget equations. Our starting point will be the meteorological equations in spherical coordinates, with pressure as the vertical coordinate:

$$\frac{\partial u}{\partial t} + \frac{u}{a\cos\varphi}\frac{\partial u}{\partial \lambda} + \frac{v}{a\cos\varphi}\frac{\partial u\cos\varphi}{\partial \varphi} + \omega\frac{\partial u}{\partial p} = -\frac{1}{a\cos\varphi}\frac{\partial \phi}{\partial \lambda} + fv + F^{(u)} \tag{1.1}$$

$$\frac{\partial v}{\partial t} + \frac{u}{a\cos\varphi}\frac{\partial v}{\partial \lambda} + \frac{v}{a}\frac{\partial v}{\partial \varphi} + \omega\frac{\partial v}{\partial p} + \frac{u^2\tan\varphi}{a} = -\frac{1}{a}\frac{\partial \phi}{\partial \varphi} - fu + F^{(v)} \tag{1.2}$$

$$\frac{\partial T}{\partial t} + \frac{u}{a\cos\varphi}\frac{\partial T}{\partial \lambda} + \frac{v}{a}\frac{\partial T}{\partial \varphi} + \omega\left(\frac{\partial T}{\partial p} - K\frac{T}{p}\right) + \omega\left(\frac{\partial T_0}{\partial p} - K\frac{T_0}{p}\right) = \frac{\dot{H}}{c_p} \tag{1.3}$$

$$\frac{1}{a\cos\varphi}\left(\frac{\partial u}{\partial \lambda} + \frac{\partial v\cos\varphi}{\partial \varphi}\right) + \frac{\partial \omega}{\partial p} = 0 \tag{1.4}$$

$$T = -\frac{p}{R}\frac{\partial \phi}{\partial p}. \tag{1.5}$$

In (1.3) T_o is the area-average (on constant p surfaces) of the temperature and T is the deviation of the temperature from T_o. Following Holton (1975), the term $\kappa T/p$ in (1.3) will be neglected in comparison to $\kappa T_o/p$.

The functions u, v, ω, ϕ, T, $F^{(u)}$, $F^{(v)}$ and $\dot{H}$ are expressed as a sum of a zonally averaged part denoted by a subscript Z and a deviation therefrom, denoted by a subscript E, i.e.,

$$(\ ) = ( )_Z + ( )_E \tag{1.6}$$

where

$$( )_Z = \frac{1}{2\pi} \int_0^{2\pi} ( ) \, d\lambda . \tag{1.7}$$

If we substitute expressions of the form (1.6) in (1.1) - (1.4) and then apply the averaging operator (1.7) we obtain the following eddy equations:

$$\frac{\bar{D} u_E}{Dt} - \left(2\Omega + \frac{u_Z}{a\cos\varphi}\right) \sin\varphi \, v_E - \frac{v_Z u_E \tan\varphi}{a} + v_E \frac{\partial u_Z}{\partial y} + \omega_E \frac{\partial u_Z}{\partial p} + \frac{\partial \phi_E}{\partial x} =$$

$$F_E^{(u)} - \mathcal{F}_E^{(u)} \tag{1.8}$$

$$\frac{\bar{D} v_E}{Dt} + \left(2\Omega + \frac{u_Z}{a\cos\varphi}\right) \sin\varphi \, u_E + \frac{u_Z u_E \tan\varphi}{a} + v_E \frac{\partial v_Z}{\partial y} + \omega_E \frac{\partial v_Z}{\partial p} + \frac{\partial \phi_E}{\partial y} =$$

$$F_E^{(v)} - \mathcal{F}_E^{(v)} \tag{1.9}$$

$$\frac{\bar{D} T_E}{Dt} + v_E \frac{\partial T_Z}{\partial y} + S\omega_E = \frac{\dot{H}}{c_p} - \mathcal{H}_E \tag{1.10}$$

$$\frac{1}{a\cos\varphi} \left(\frac{\partial u_E}{\partial \lambda} + \frac{\partial v_E \cos\varphi}{\partial \varphi} \right) + \frac{\partial \omega_E}{\partial p} = 0 \tag{1.11}$$

where

$$\mathcal{F}_E^{(u)} = \frac{\partial}{\partial x}\left(u_E^2\right) + \frac{1}{\cos^2\varphi} \frac{\partial}{\partial y} \left\{ \left[v_E u_E - (v_E u_E)_Z \right] \cos^2\varphi \right\}$$

$$+ \frac{\partial}{\partial p} \left[\omega_E u_E - (\omega_E u_E)_Z \right] \tag{1.12}$$

$$\mathcal{F}_E^{(v)} = \frac{\partial}{\partial x}(u_E v_E) + \frac{1}{\cos\varphi}\frac{\partial}{\partial y}\left\{\left[v_E^2 - (v_E)_z^2\right]\cos\varphi\right\}$$

$$+ \left[u_E^2 - (u_E^2)_z\right]\frac{\tan\varphi}{a} + \frac{\partial}{\partial p}\left[\omega_E v_E - (\omega_E v_E)_z\right] \qquad (1.13)$$

$$\mathcal{H}_E = \frac{\partial}{\partial x}(u_E T_E) + \frac{1}{\cos\varphi}\frac{\partial}{\partial y}\left\{\left[v_E T_E - (v_E T_E)_z\right]\cos\varphi\right\}$$

$$+ \frac{\partial}{\partial p}\left[\omega_E T_E - (\omega_E T_E)_z\right] \qquad (1.14)$$

$$S = \kappa\frac{T_0}{p} - \frac{\partial T_0}{\partial p}$$

$$\frac{\bar{D}}{Dt} = \frac{\partial}{\partial t} + u_z\frac{\partial}{\partial x} + v_z\frac{\partial}{\partial y} + \omega_z\frac{\partial}{\partial p} \qquad (1.15)$$

$$\frac{\partial}{\partial x} = \frac{1}{a\cos\varphi}\frac{\partial}{\partial\lambda}$$

$$\frac{\partial}{\partial y} = \frac{1}{a}\frac{\partial}{\partial\varphi} .$$

We now write the eddy variables as a sum of a stationary part and a transient part, i.e.,

$$(\ )_E = (\ )_S + (\ )_T \qquad (1.16)$$

where

$$(\ )_S = \frac{1}{\tau}\int_{t-\tau/2}^{t+\tau/2}(\ )_E\,dt .$$

The kinetic and available potential energies associated with the stationary waves are then

$$K_s = \int_V \frac{u_s^2 + v_s^2}{2} \rho \, dV \tag{1.17a}$$

$$A_s = \frac{R}{2} \int_V \frac{T_s^2}{p_S} \rho \, dV \, . \tag{1.17b}$$

To obtain the energy budget equations for K_S we multiply (1.7) and (1.8) by u_s and v_s respectively, integrate over time and over the mass of the atmosphere and add the two equations. The equation for A_S is obtained by multiplying (1.9) by RT_s/pS and by integrating over the mass and over time. Since our purpose here is to provide some background for the "observational" results to be presented subsequently, we will simplify the equations in a way similar to that of Holopainen (1970) whose results we want to discuss. Thus we neglect the energy transformations which arise from the following terms: the vertical advection of momentum, the mean meridional circulation, the terms $\omega_E T_E$ in (1.14) and the transient part of u_Z. The simplified energy equations are (see Holopainen, 1970 for further details)

$$C(A_S, K_S) + C(K_Z, K_S) - C(K_S, K_T) - D_S + CB(K_Z, K_S) = 0 \tag{1.17}$$

$$G(A_S) + C(A_Z, A_S) - C(A_S, A_T) - C(A_S, K_S) = 0 \tag{1.18}$$

where the subscripts S, T, Z refer to the energy of the stationary waves, transient waves and zonal flow, respectively. The symbol $C(\alpha,\beta)$ represents a conversion of energy from α to β. The approximate expressions for the transformations are

$$(A_s, K_s) = -\int \frac{R T_s \omega_s}{p} \, dm = -\int \omega_s \alpha_s \, dm \quad ; \quad dm = \rho \, dV \tag{1.19}$$

$$(K_z, K_s) = -\int u_s v_s \cos\varphi \, \frac{\partial}{\partial y}\left(\frac{u_z}{\cos\varphi}\right) dm \tag{1.20}$$

$$(K_S, K_T) = \int \left\{ u_s \left[\frac{\partial}{\partial x}(u_T^2) + \frac{1}{\cos^2\varphi} \frac{\partial}{\partial y}(u_T v_T \cos^2\varphi) \right]_S \right. \tag{1.21}$$

$$\left. + v_s \left[\frac{\partial}{\partial x}(u_T v_T) + \frac{1}{\cos\varphi} \frac{\partial}{\partial y}(v_T^2 \cos\varphi) + \frac{u_T^2 \tan\varphi}{a} \right]_S \right\} dm \tag{1.22}$$

$$D_s = -\int \vec{V}_s \cdot \vec{F}_s \, dm \tag{1.23}$$

$$CB(K_z, K_s) = -\frac{1}{g}\int \phi_s u_z \frac{\partial}{\partial x} p_g \, dA \tag{1.24}$$

evaluated at the average surface pressure

$$G(A_s) = \int \frac{R}{pS} \cdot \dot{H}_s T_s \, dm = \int \frac{\dot{H}_s \alpha_s}{S} \, dm \tag{1.25}$$

$$C(A_z, A_s) = -\int \frac{R}{pS} v_s T_s \frac{\partial T_z}{\partial y} \, dm \tag{1.26}$$

$$C(A_s, A_T) = \int \frac{R}{pS} T_s \nabla \cdot (\vec{V}_T T_T)_s \, dm . \tag{1.27}$$

The results obtained by Holopainen (1970) for these energy transformations are summarized in Fig. 18. The arrows represent the direction of the energy flow and the dashed lines indicate that the number was obtained as a residual to balance the inflow and outflow of energy in a given box.

To obtain the dissipation of K_S Holopainen assumed that it takes place entirely in the planetary boundary layer and that it can be written in the form

$$D = C V_g^2 \tag{1.28}$$

where C is a constant and $\vec{V}_g$ is the geostrophic wind. C was estimated from information on the mean annual rate of energy dissipation ($2.3 Wm^{-2}$) published in a review of energetics by Oort (1964) and the mean annual value of V_g^2 at 850 mb north of 15°N from Crutcher's (1959) data; the resulting value was $C = 2.4 \times 10^{-2} Wm^{-4} s^2$. D_S was then obtained from the relationship (1.28) with V_g^2 replaced by $(V_{gS})^2$. As can be seen from Fig. 18 the order of magnitude of the dissipation of K_S thus

obtained is one tenth that of the mean annual dissipation of kinetic energy.

The exchange of kinetic energy between the zonal flow and the standing waves due to the deflecting effects of mountains, $CB(K_Z,K_S)$, was obtained by noting that CB is proportional to the integral of u_Z and the mountain torque created by the pressure difference on opposite sides of mountains. The mountain torque values were taken from Yeh and Chu (1958). We note from Fig. 18 that this source of kinetic energy for the standing waves is an order of magnitude smaller than the $C(A_S,K_S)$ conversion.

The main source of kinetic energy for the waves is the available potential energy of the waves themselves (Fig. 18). As can be seen from (1.19) this conversion of energy is a result of the fact that on the average the warm air within the wave rises and the cold air subsides. While Holopainen obtained this term as a residual in the energy budget, Murakami (1963) computed it explicitly using a vertical motion field obtained by integrating the mass continuity equation vertically. The difficulties inherent in this approach are well known and were reflected in his results. Depending on whether he used the boundary condition $\omega = 0$ at $p = 1000$ mb or 100 mb he obtained for $C(A_S,K_S)$ values of 0.65 Wm^{-2} or 0.31 Wm^{-2} for mean annual conditions. So the sign of the energy conversion does not seem to be in doubt but its value is rather uncertain.

The other two conversions affecting K_S are $C(K_Z,K_S)$ and $C(K_S,K_T)$, both of which can be evaluated from the horizontal component of the wind field. Holopainen used Crutcher's (1959) wind statistics. The results shown in Fig. 18 indicate that in general the standing eddies lose kinetic energy to the zonal flow and to the transient eddies. The only exception is $C(K_S,K_T)$ which is negative in summer, but the value is quite small and so presumably the sign could be wrong. Note that in winter and for the annual mean conditions the drain of K_S by the transient eddies is of the same order of magnitude as the boundary layer dissipation.

We have seen that the standing waves convert their potential energy to kinetic energy. Let us now look at how they maintain their level of potential energy in the face of this conversion. In other words, the eddy vertical motion field is such that there is adiabatic compression (warming) in the cold areas and adiabatic expansion (cooling) in the warm regions which naturally works to reduce the eddy horizontal temperature gradient. To maintain the latter at a steady state level other physical processes must be active, operating in an opposite sense. As seen from Fig. 18, in winter the most important source of A_S is $C(A_Z,A_S)$, involving the

meridional advection of temperature by the standing waves themselves. The north-south temperature gradient of the zonal flow is thus seen to be the main energy source for the standing waves. The same applies to the mean annual flow. In summer $C(A_Z,A_S)$ is extremely small and negative.
The sign of the result should not be too surprising if we recall that in the summer the midlatitude standing waves slope the east with height, implying that they are transporting heat southward, i.e., increasing the meridional temperature gradient, hence A_Z in that region.

As for $C(A_S,A_T)$ we see from Holopainen's results (based on vertically integrated sensible heat transports) that the transient eddies, through their advection of their own temperature field, tend to warm the cold areas and cool the warm areas of the standing waves, thus reducing the standing eddy temperature variance (A_S).

Finally, we turn to the generation of A_S. For winter and summer Holopainen calculated this generation as a residual necessary to balance the A_S budget. It is difficult to ascertain the accuracy of the resulting $G(A_S)$ but at least we can say that it agrees rather well with similar calculations made by Brown (1964) with different data sets. Holopainen found (see Fig. 18) that in winter $G(A_S) = 0.62 Wm^{-2}$, the negative sign implying that on the average the warm regions of the stationary waves are cooled and the cool regions are heated diabatically by the stationary sources. Brown obtained $G(A_S) = -0.74$, -0.65 and -1.2 Wm^{-2} for January 1959, 1962 and 1963 respectively.

Both Holopainen and Brown's results indicate that in summer $G(A_S)$ is positive. The former found $G(A_S) = 0.43 Wm^{-2}$ and the latter obtained $G(A_S) = 0.24$ and 0.21 Wm^{-2} for July 1961 and 1962.

So we see that according to the above results the energy cycle responsible for the maintenance of the stationary waves is fundamentally different in summer and winter. In winter the energy source for the waves is the meridional temperature gradient of the zonal flow; the stationary heat sources are reported to drain energy from the waves, although they may be largely responsible for the existence of the waves in the first place. In summer the energy cycle is computed to be a more direct one in the sense that the stationary heat sources and sinks maintain the available potential energy of the waves which is then converted to eddy kinetic energy, which is in turn dissipated in the boundary layer.

We conclude by stressing the tentative nature of these results. As Holopainen himself pointed out, many simplifying assumptions had to be made to estimate some of the conversions and hence the numbers quoted above must be considered rough first estimates.

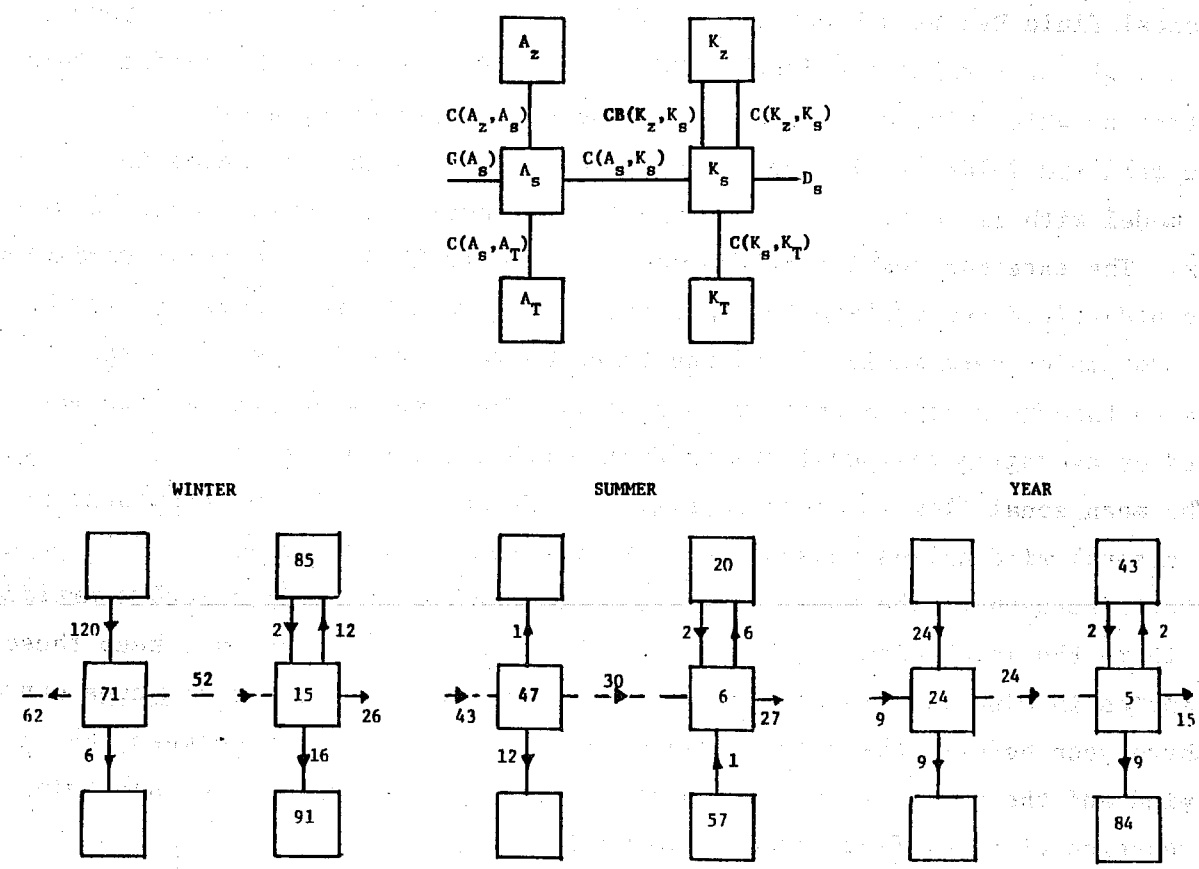

Fig. 18. Upper part: energy processes affecting the stationary disturbances. Lower part: numerical values of the energy balance of the stationary disturbances for normal winter, normal summer and for mean conditions over several years over the Northern Hemisphere (15°N - 90°N; 100 mb - 1000 mb). Dashed lines denote processes which have been evaluated purely as residuals. Units for energy: 10^4 J m^{-2}; for energy change: 10^{-2} W m^{-2} (Redrawn from Holopainen, 1970).

2.9 Stationary Waves in a General Circulation Model

A number of general circulation models (GCMs) have been developed to investigate various aspects of climate. The stationary waves found in these models when their output is averaged over an extended period of time have been discussed, for example, by Kasahara and Washington (1971), Kasahara et al. (1973) and Williams (1976) at the National Center for Atmospheric Research (NCAR) and by Manabe and Terpstra (1974) and Hayashi and Golder (1977) at the Geophysical Fluid Dynamics Laboratory (GFDL). In this section we will present just a few of the results obtained at GFDL and NCAR to indicate in general terms the extent to which GCMs can reproduce the observed stationary waves.

Hayashi and Golder (1977) analyzed the disturbances that appeared in a global model with 11 levels in the vertical and a horizontal grid spacing of 2.4 degrees. The external forcing of the model was controlled by the solar radiation and the prescribed sea surface temperature, both of which had a seasonal variation. Mountains were included and the temperature at the land surface was calculated through a heat balance requirement. The results presented here were obtained by averaging the model states from October through March.

The mean zonal flow is shown in Fig. 19. We note that in the troposphere the mean zonal wind agrees reasonably well with the observed state. In the lower stratosphere the model fails to reproduce the observed relative minimum and at 10 mb the model winds are too strong by a factor 2. We should keep these deficiencies in mind when we compare the computed and observed forced waves since, as we have seen before, there is evidence showing a relationship between the mean zonal wind and the structure of the forced waves. We will return to this point in our discussion of simplified forced wave models.

Fig. 20 compares the model and observed structures of stationary zonal wavenumber 1. We see that the computed amplitude is too large by a factor of more than 2 near 10 mb. The explanation for this is not clear at this time. In the troposphere the maximum amplitude near 300 mb is roughly 25% larger than that of the seven-year average flow for January published by van Loon et al. (1973). The model wave slopes westward with height in mid latitudes as observed. Between 30°N and 80°N the wave tilts from the southwest to the northeast; this agrees with observations from about 30°N to 50°N but north of 50°N the observed tilt is in the opposite direction.

Hayashi and Golder point out that even when the year to year fluctuations in the observations are taken into account, the conclusion still holds that the model

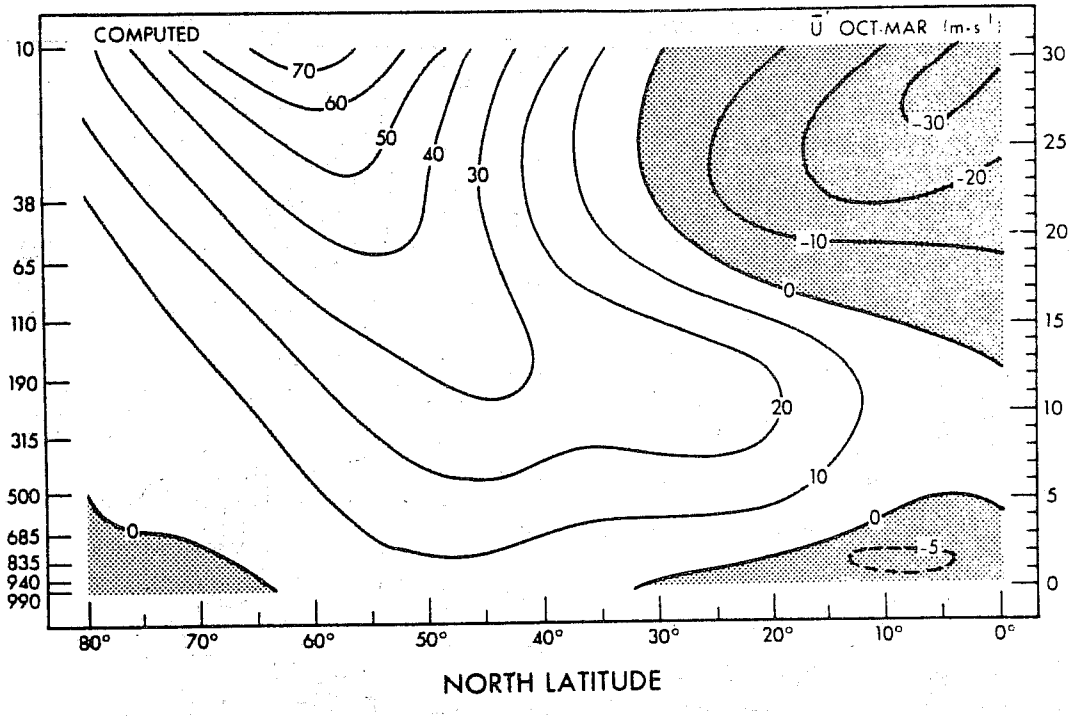

Fig. 19a. Latitude-height section (pressure (mb) left, height (km) right) of the mean zonal wind of the numerical model during the period October-March (After Hayashi and Golder, 1977).

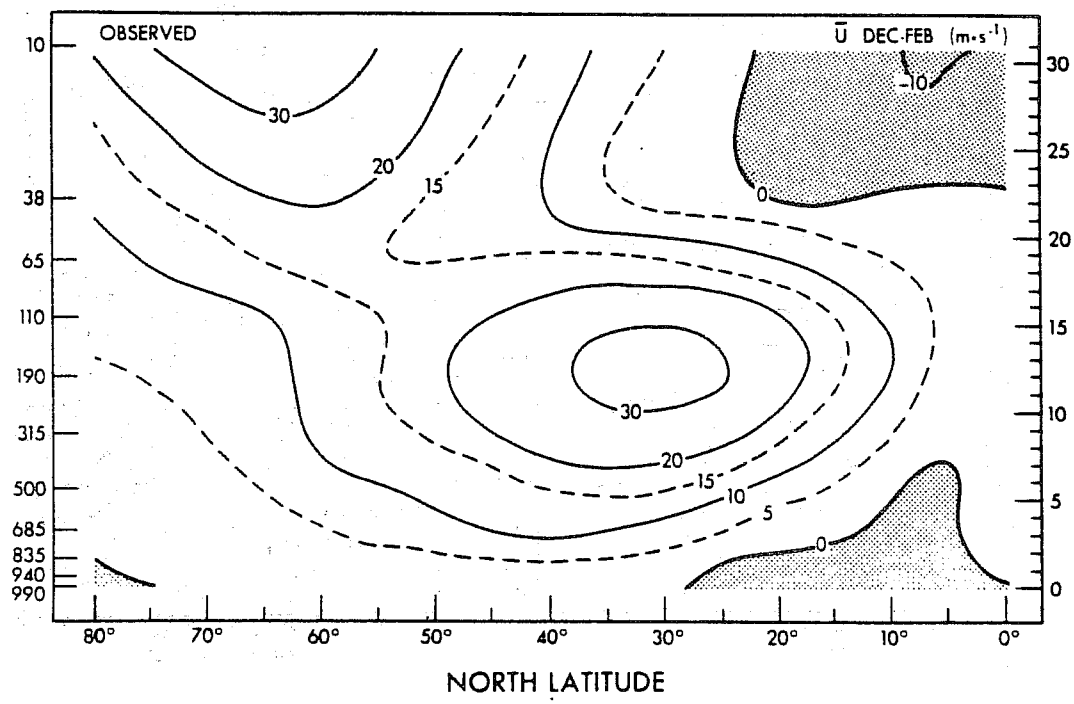

Fig. 19b. Latitude-height section of the mean zonal wind in the atmosphere during the period December-February (After Hayashi and Golder, 1977; original diagram from Newell et al., 1970).

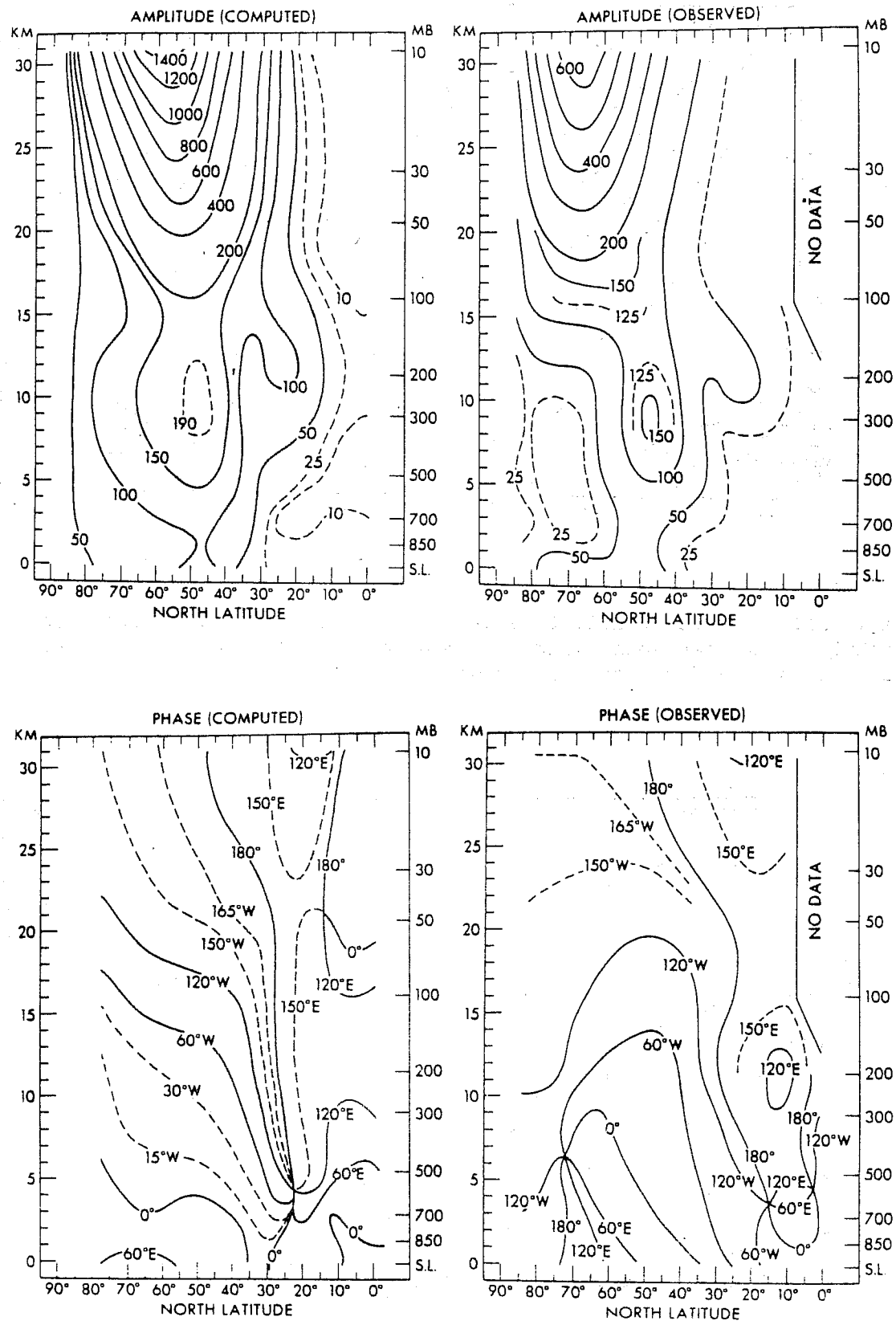

Fig. 20. Top: latitude-height section of the amplitude in metres of stationary geopotential height wavenumber 1 in January; left, model wave (After Hayashi and Golder, 1977), right, observed wave (After van Loon et al., 1973). Bottom: phase of the wave, same format as at the top.

stationary waves are too strong (and the transient ultra-long waves too weak). It is nevertheless interesting to compare the model wave structure with the observed one for January 1958 (Fig. 3). We notice that now the model wave in the upper troposphere is weaker than the observed one. Recall that the model results apply to the six-month average October through March whereas the observations apply to a single month when the wave is at or close to its peak intensity. Even here, however, the intensity of the model wave at 10 mb is much too large and the observed phase tilt in the horizontal, from southeast to northwest near 55°N, 200 mb, is not reproduced by the model.

Fig. 21 shows the normalized amplitudes at 50°N of the geopotential, temperature and vertical motion for the model standing wavenumber 1, as well as the phase relationships between the variables. We see that at least in the troposphere the southward moving air is cold and is subsiding. From the energetics point of view this means that at 50°N zonal available potential energy is being converted to stationary wave available potential energy and the latter to stationary wave kinetic energy.

Hayashi and Golder found that zonal wavenumber 1 in their model has a positive conversion $C(A_Z,A_S)$ almost everywhere over the northern hemisphere up to 10 mb. The zonal integral of $\dot{H}_S\alpha_S/S$, which appears in the expression for $G(A_S)$, is generally positive except near the ground between 35°N and 60°N where it is negative. In other words the diabatic heating in the mid-troposphere, resulting mainly from moist convective heating, tends to take place in warm air and generates A_S; in the lower troposphere the heating is due mainly to sensible heat flux from the surface and tends to occur in cold air, thus destroying A_S. The net effect appears to be a positive $G(A_S)$, at least as far as can be ascertained by inspection of their meridional cross-section of the zonally averaged product $\dot{H}_S\alpha_S/S$ (their Fig. 5.9a).

In short the model energetics agree with Holopainen's calculations in so far as the zonal available potential energy is the main source of energy for the winter standing waves. As for the role of diabatic heating the agreement is far less obvious. Holopainen and Brown found that the diabatic heating destroys A_S in the atmosphere while it seems to be a source of A_S in the model if mass-integrated effects are considered. It remains to be seen whether these results are related to the fact that the model standing wavenumber 1 is more intense than normally observed in the atmosphere.

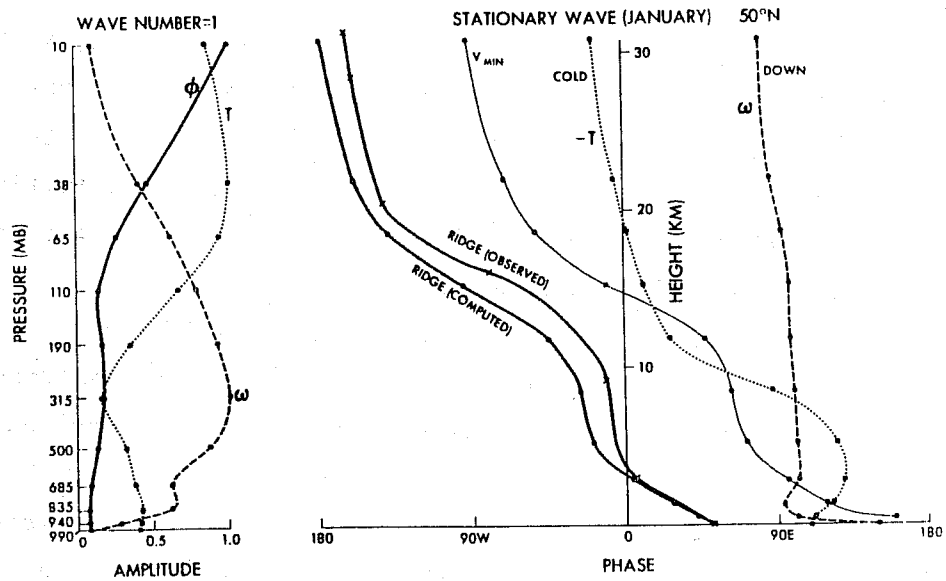

Fig. 21. Normalized amplitude (left) and phase (right) of stationary wavenumber 1 as functions of height at 50°N. The observed phase line (ridge) is from Muench (1965) (After Hayashi and Golder, 1977).

Let us now look at the vertical structure of zonal wavenumbers 1 and 2 of the height field along 60°N (Fig. 22) published by Kasahara et al. (1973) for the NCAR model. This particular model has 12 layers in the vertical, each 3 km deep. The horizontal resolution is 5 degrees in longitude and latitude (coarser than the GFDL model just discussed). The earth's orography is included and the sea surface temperature is specified. We see from Fig. 22 that the model succeeds in reproducing the intensity of the observed wave 1 above 18 km but that the wave is too far to the west. The importance of the earth's orography in determining the amplitude of this wave in the stratosphere is evident. As for wave number 2 the model has a reasonable amplitude at about 20 km but it fails to reproduce the observed growth with height; the phase of the wave does not agree well with the observations from van Loon et al. (1973).

Some of the discrepancies between GCM stationary waves and the observed ones can be seen from Fig. 23. The figure compares the variance at 500 mb, 50°N in the stationary waves, transient planetary waves and smaller scale transient waves in the GFDL model (Hayashi and Golder, 1977), the NCAR model (Kasahara et al., 1973) and observations. We see that (at least for that coordinate) the GFDL standing waves are too intense and the NCAR ones too weak when compared with observations. It seems also that for both models the ratio of standing wave to transient wave variance is too high.

Contribution to standing waves by topography. Since it is possible to integrate GCMs with and without the earth's orography it is possible to compare the two integrations to determine the role of topography. Such comparisons by Kasahara and Washington (1971) seem to show that the earth's orography plays a secondary role compared to diabatic heating in the troposphere. From Kasahara et al. (1973) we find that in the stratosphere, on the other hand, the circulation is significantly modified when the earth's topography is removed from the model. In particular the Aleutian anticyclone which is reproduced reasonably well by the model with topography is absent in the model without orography. This seems to be a consequence of the weakening of wavenumber 1 (see Fig. 22) when the mountains are removed.

The effects of mountains at 45°N, 500 mb and 1000 mb in the GFDL model of Manabe and Terpstra (1974) can be seen from Fig. 24. The effect of topography is seen to be rather important at both levels.

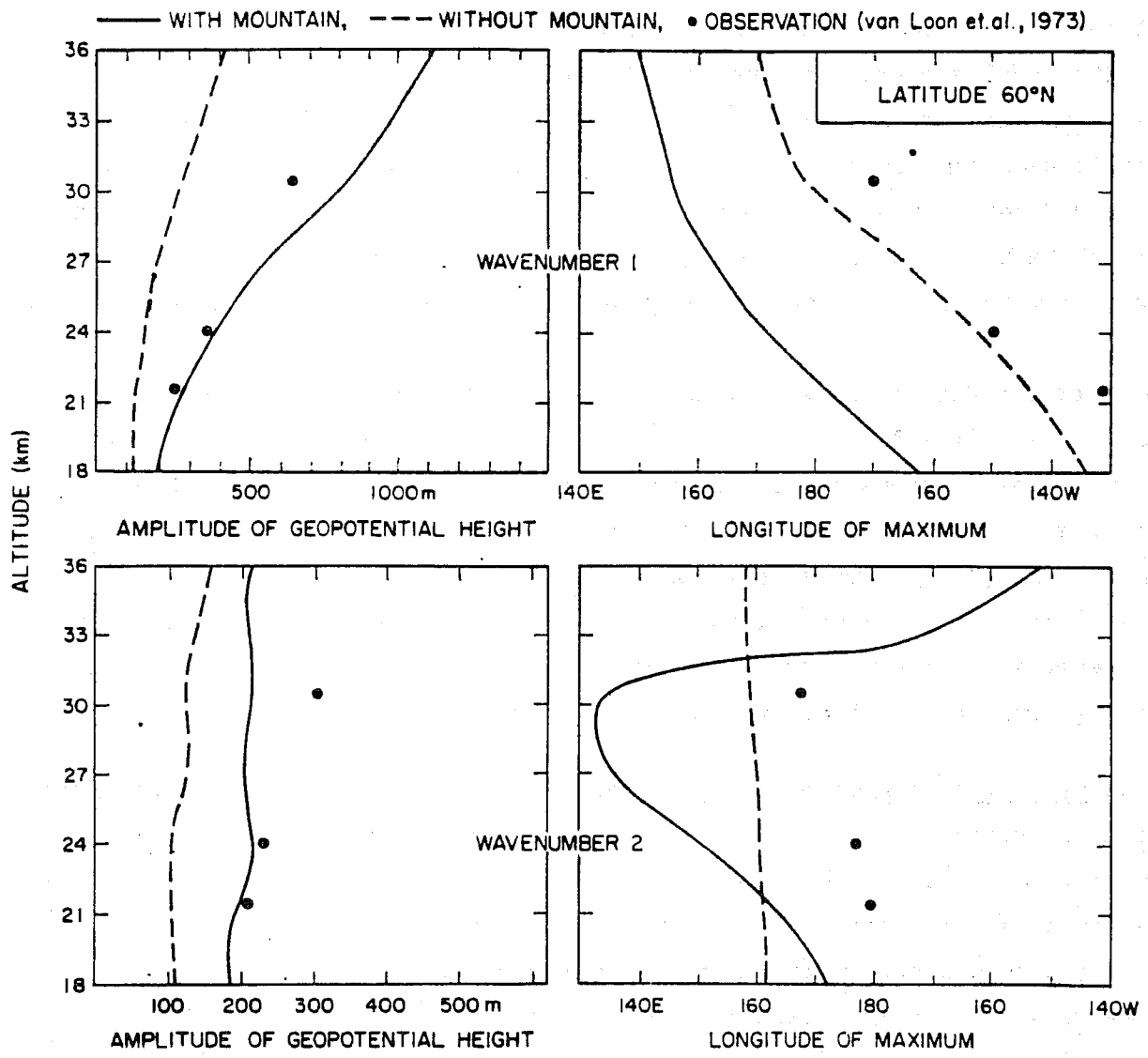

Fig. 22. Vertical profiles of geopotential height amplitude (left) and phase (right) for wavenumber 1 (top) and wavenumber 2 (bottom) at 60°N (After Kasahara et al., 1973).

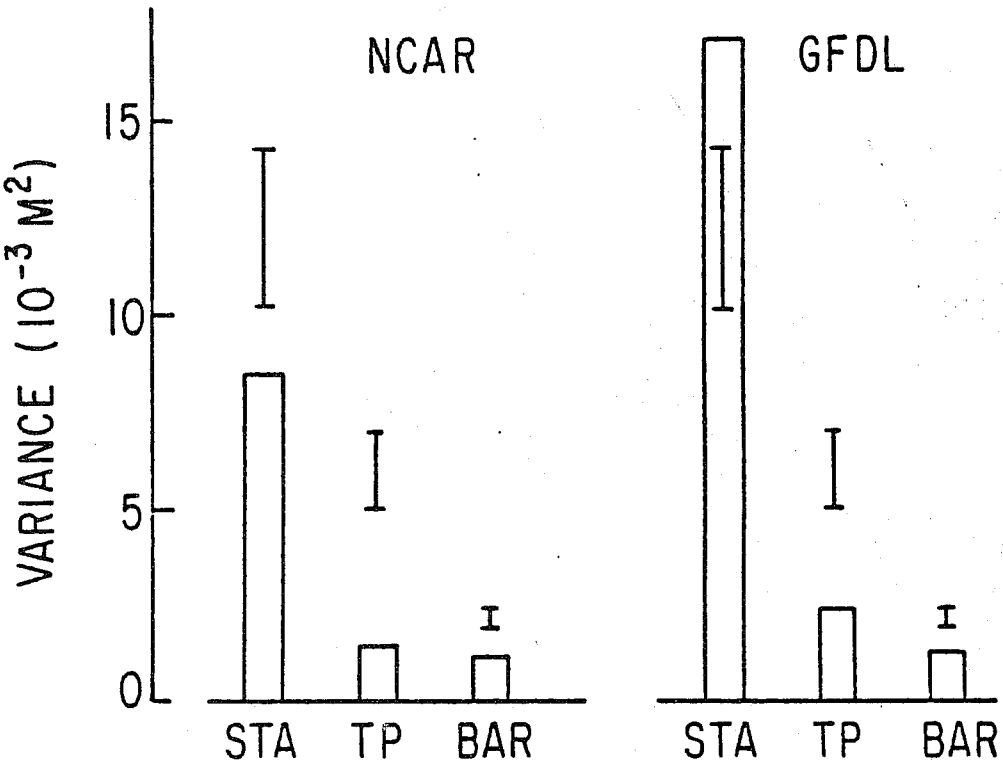

Fig. 23. Geopotential height variance at 500 mb, 50°N for the stationary waves (STA), the transient planetary waves (TP), i.e., variations of 1 to 3 weeks and zonal wavenumbers 1 - 3, and "baroclinic waves (BAR), i.e., higher frequency disturbances with zonal wavenumbers 4 - 8 in two general circulation models. Vertical lines show the range of values for four observed winters (After Pratt, 1979).

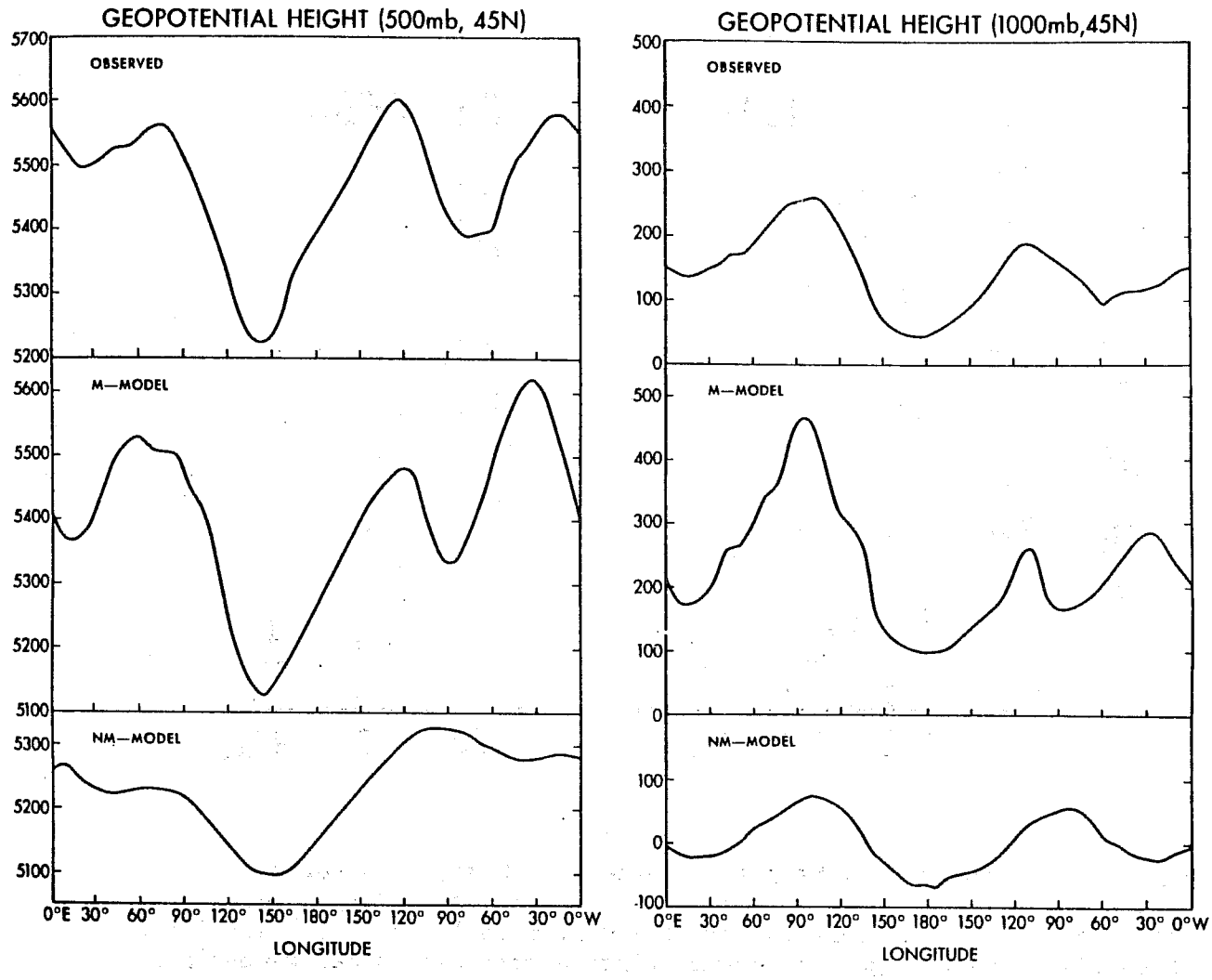

Fig. 24. Time-mean geopotential height (gpm) as a function of longitude at 500 and 1000 mb. Top, observed as provided by Oort and Rasmusson; middle, model with topography; bottom, model without topography (After Manabe and Terpstra, 1974).

In closing it should be pointed out that the effects of topography and diabatic heating are not strictly separable, as already noted by Manabe and Terpstra. The topography alters the distribution of precipitation and diabatic heating so that when mountains are removed from a model the heat sources are to some extent simultaneously modified.

APPENDIX

List of Symbols

a	mean radius of the earth
c_p	specific heat of dry air at constant pressure
dA	element of area
dm	element of mass
dV	element of volume
$\partial(\ )/\partial x$	$\partial(\ )/a\cos\varphi\partial\lambda$
$\partial(\ )/\partial y$	$\partial(\ )/a\partial\varphi$
f	Coriolis parameter
g	acceleration of gravity
n	zonal wavenumber
p	pressure
t	time
u	zonal wind component
v	meridional wind component
w	vertical wind component in height coordinates
A	available potential energy
$\vec{F}$	friction force, with zonal and meridional components $F^{(u)}, F^{(v)}$
$\dot{H}$	diabatic heating per unit mass per unit time
K	kinetic energy
R	gas constant for dry air
S	static stability parameter, $\kappa T_o/p - \partial T_o/\partial p$
T	deviation of the temperature from its area average
T_o	area average of T on a constant pressure surface
α	specific volume
λ	longitude
φ	latitude
ϕ	geopotential
ρ	density
ω	dp/dt
κ	R/c_p
τ	averaging period
$(\ )_Z$	zonal average of $(\ )$, $\frac{1}{2\pi}\int_0^{2\pi}(\ )d\lambda$
$(\ )_E$	$(\ ) - (\ )_Z$; eddy part of $(\ )$
$(\ )_S$	time average of $(\ )_E$, i.e., standing eddy part of $(\ )$

REFERENCES

Avery, S., 1978: The tropospheric forcing and vertical propagation of stationary planetary waves in the atmosphere. Ph.D. thesis, University of Illinois at Urbana-Champaign. Available from University Microfilm, Ann Arbor, Michigan.

Brown, J.A., Jr., 1964: A diagnostic study of tropospheric diabatic heating and the generation of available potential energy. Tellus, 16, 371-388.

Craddock, J.M. and C.R. Flood, 1969: Eigenvectors for representing the 500 mb geopotential surface over the Northern Hemisphere. Quart. J. Roy. Meteor. Soc., 95, 576-593.

Crutcher, H., 1959: Upper wind statistics charts of the Northern Hemisphere. Office of the Chief of the U.S. Naval Operations.

Hayashi, Y. and D.G. Golder, 1977: Space-time spectral analysis of mid-latitude disturbances appearing in a GFDL General Circulation Model. J. Atmos. Sci., 34, 237-262.

Holopainen, E.O., 1970: An observational study of the energy balance of the stationary disturbances in the atmosphere. Quart. J. Roy. Meteor. Soc., 96, 626-644.

Holton, J.R., 1975: The dynamic meteorology of the stratosphere and mesosphere. Meteor. Monogr., No. 37, 218 pp.

Hirota, I. and Y. Sato, 1969: Periodic variation of the winter stratospheric circulation and intermittent vertical propagation of planetary waves. J. Meteor. Soc. Japan, 47, 390-402.

Kasahara, A. and W.M. Washington, 1971: General circulation experiments with a six-layer NCAR model, including orography, cloudiness, and surface temperature calculations. J. Atmos. Sci., 28, 657-701.

Kasahara, A., T. Sasamori and W.M. Washington, 1973: Simulated experiments with a 12-layer stratospheric global circulation model. I. Dynamical effects of the earth's orography and thermal influence of continentality. J. Atmos. Sci., 30, 1229-1251.

Knittel, J., 1976: Ein beitrag zur klimatologie der stratosphäre der südhalbkugel. Meteor. Aband., Neue Folge, Serie A Monogr. Vol. 2, No. 1, 112 pp. plus appendices.

Manabe, S. and T.B. Terpstra, 1974: The effects of mountains on the general circulation of the atmosphere as identified by numerical experiments. J. Atmos. Sci., 31, 3-42.

Muench, H.S., 1965: On the dynamics of the winter stratosphere circulation. J. Atmos. Sci., 22, 349-360.

Muench, H.S., 1967: On the structure and behavior of the planetary waves in winter. Proceedings of the (seventh) Stanstead Seminar on the middle atmosphere. Publication in meteorology No. 90, McGill University, 1-7.

Murakami, T., 1963: On the maintenance of kinetic energy of the large-scale stationary disturbances in the atmosphere. Final Report on Plan. Circ. Proj., Massachusetts Institute of Technology, Dept. of Meteorology, 42 pp.

Newell, R.E., D.G. Vincent, T.G. Dopplick, D. Ferruzza and J.W. Kidson, 1970: The energy balance of the global atmosphere. Global Circulation of the Atmosphere. G.A. Corby, Ed., Roy. Meteor. Soc., 42-90.

Newell, R.E., J.W. Kidson, D.G. Vincent and G.J. Boer, 1972: The general circulation of the tropical atmosphere and interactions with extra-tropical latitudes, Vol. 1, M.I.T. Press, 258 pp.

Oort, A.H., 1964: On estimates of the atmospheric energy cycle. Mon. Wea. Rev., 92, 483-493.

Pratt, R.W., 1979: A space-time spectral comparison of the NCAR and GFDL general circulation models of the atmosphere. J. Atmos. Sci., 36, in press for Sept. issue.

Saltzman, 1968: Surface boundary effects on the general circulation and macroclimate: A review of the theory of the quasi-stationary perturbations in the atmosphere. Meteor. Monogr., No. 30, 4-19.

Saltzman, B. and M. Sankar-Rao, 1963: A diagnostic study of the mean state of the atmosphere. J. Atmos. Sci., 20, 438-447.

Simmons, A., 1978: Some effects of meridional shear and spherical geometry on long stratospheric waves. Quart. J. Roy. Meteor. Soc., 96, 626-644.

van Loon, H., R.L. Jenne and K. Labitzke, 1973: Zonal harmonic standing waves. J. Geophys. Res., 78, 4463-4471.

Williams, J., 1976: Zonal harmonic standing waves in the NCAR global circulation model. Mon. Wea. Rev., 104, 249-259.

Yeh Tu-Cheng and Chu Pao-Chen, 1958: Some fundamental problems of the general circulation of the atmosphere. (in Chinese, English summary) Institute of Geophysics and Meteorology, Academia Sinica.

FORCED WAVES IN A MIDDLE LATITUDE BETA PLANE MODEL

Jacques Derome
Department of Meteorology
McGill University
Montreal

FORCED WAVES IN A MIDDLE LATITUDE BETA-PLANE MODEL

1. The Model Equations

As a first approach to the problem of modelling forced stationary waves we will use a quasi-geostrophic model on a Beta plane. The geometry of this model leaves much to be desired but most of the basic physics of the problem is retained and as we shall see a wealth of important results can be extracted from the model.

Our model equations will be

$$\frac{\partial}{\partial t}\nabla^2\psi + \vec{V}\cdot(\nabla^2\psi + f) = \frac{f_o}{\rho_o}\frac{\partial}{\partial Z}(\rho_o w) \tag{1}$$

$$\frac{\partial}{\partial t}\frac{\partial\psi}{\partial Z} + \vec{V}\cdot\nabla\frac{\partial\psi}{\partial Z} + \frac{N^2}{f_o}w = \frac{\kappa}{Hf_o}\dot{H} \tag{2}$$

where $Z = -H\ln(p/p_s)$

$\vec{V} = k\times\nabla\psi$

$\rho_o = \rho_s\exp(-Z/H)$

and the other symbols are as defined in appendix A. In (2) we used $\partial\phi/\partial Z = f_o\partial\psi/\partial Z$. Eliminating w between (1) and (2) we obtain the potential vorticity equation

$$\frac{\partial q}{\partial t} + \vec{V}\cdot\nabla q = \frac{f_o}{\rho_o}\frac{\partial}{\partial Z}\left(\frac{\rho_o \kappa}{N^2 H}\dot{H}\right). \tag{3}$$

In much of our discussion we will be concerned with the stationary wave propagation away from the energy source region, i.e., we will work with the equation for adiabatic flow

$$\frac{\partial q}{\partial t} + \vec{V}\cdot\nabla q = 0. \tag{4a}$$

In the above q, the potential vorticity is given by

$$q = \nabla^2\psi + \frac{f_o^2}{\rho_o}\frac{\partial}{\partial Z}\left(\frac{\rho_o}{N^2}\frac{\partial\psi}{\partial Z}\right) + f_o + \beta y. \tag{4b}$$

To simplify the problem we shall treat the problems of horizontal and vertical propagation of forced waves separately.

2. Horizontal Propagation

In this section we examine the problem of a wave which is forced at some latitude y_F through some unspecified steady mechanism and which propagates away from the forcing. For simplicity we will use a barotropic model so that

the influence of the forcing can only propagate horizontally. In this case the governing equation for adiabatic inviscid flow is

$$\frac{\partial q}{\partial t} + \vec{V} \cdot \nabla q = 0 \tag{5a}$$

with

$$q = \nabla^2 \psi + f_0 + \beta y . \tag{5b}$$

We express variables as a sum of a zonally averaged part, denoted by an overbar, and a deviation from the zonal part, denoted by a prime; thus

$$q = \bar{q}(y,t) + q'(x,y,t) \tag{6}$$

where

$$\bar{q} = -\frac{\partial \bar{u}}{\partial y} + f_0 + \beta y \quad ; \quad q' = \nabla^2 \psi' .$$

Substituting (6) into (5a) and averaging zonally, we get

$$\frac{\partial \bar{q}}{\partial t} = -\frac{\partial}{\partial y} \overline{v'q'} . \tag{7}$$

Subtracting (7) from (5a) and neglecting products of primed quantities we get the linearized potential vorticity equation

$$\frac{\partial q'}{\partial t} + \bar{u} \frac{\partial q'}{\partial x} + v' \frac{\partial \bar{q}}{\partial y} = 0 . \tag{8}$$

It should be kept in mind that our discussion now is restricted to small amplitude perturbations.

If we multiply (8) by q' and then integrate zonally we get

$$\frac{\partial}{\partial t} \frac{\overline{(q')^2}}{2} = -\frac{\partial \bar{q}}{\partial y} \overline{v'q'} . \tag{9}$$

We find that <u>if the disturbance is steady</u>, i.e. if $\partial \overline{(q')^2}/\partial t = 0$ (the wave need not be stationary; it can be propagating along the x-axis, as long as it is not growing or decaying in amplitude), then

$$\overline{v'q'} = 0 \tag{10}$$

($\partial \bar{q}/\partial y$ will be assumed positive because of the strong contribution of β). Thus if the disturbance is steady in a latitude band the right-hand side of (7) vanishes and we find that

$$\frac{\partial \bar{q}}{\partial t} = 0 . \tag{11}$$

In short, a steady disturbance will not change the potential vorticity of the zonal flow ($\partial^2\bar{u}/\partial t\partial y = 0$).

Now by using the definition of q' we can rewrite $\overline{v'q'}$ as

$$\overline{v'q'} = -\frac{\partial}{\partial y}(\overline{u'v'}) \tag{12}$$

so that (9b) takes the form

$$\frac{\partial}{\partial t}\frac{\overline{(q')^2}}{2} = -\frac{\partial \bar{q}}{\partial y}\frac{\partial}{\partial y}(\overline{u'v'}) \tag{13}$$

and we find the important result that for a steady disturbance

$$\frac{\partial}{\partial y}(\overline{u'v'}) = 0 \tag{14a}$$

or

$$\overline{u'v'} = C \tag{14b}$$

where C is independent of y; that is the zonally averaged wave momentum flux $\overline{u'v'}$ is independent of latitude. It is easily seen then that if the fluid is bounded by a rigid wall at some latitude $y = y_B$, $\overline{u'v'}$ will be zero at the wall because v' = 0 there, and by (14) $\overline{u'v'}$ will be zero at all latitudes between the wall and the forcing. In the case of a pure harmonic wave in x the ridge and trough lines of the stream function will have no tilt in the north-south direction.

As shown by Eliassen and Palm (1961)[1] the momentum flux by a steady wave is related to the wave energy flux $\overline{v'\phi'}$. To see this we start with the linearized first equation of motion

$$\frac{\partial u'}{\partial t} + \bar{u}\frac{\partial u'}{\partial x} + v'\frac{\partial \bar{u}}{\partial y} = -\frac{\partial \phi'}{\partial x} + fv'.$$

For a wave disturbance $u' = \hat{u}(y)\exp ik(x-ct)$ we get

$$(\bar{u}-c)\frac{\partial u'}{\partial x} + v'\frac{\partial \bar{u}}{\partial y} = -\frac{\partial \phi'}{\partial x} + fv'.$$

Multiplying both sides by ψ' and averaging over x we get

$$F_H = \overline{v'\phi'} = -(\bar{u}-c)\overline{u'v'}. \tag{15}$$

We see that for a stationary wave (c = 0) in a westerly current the wave energy flux is southward ($\overline{v'\phi'}$ negative) when the momentum flux is northward

---

[1] But see appendix B for a different interpretation.

($\overline{u'v'}$ positive), and vice versa.

We found in (14) that $\overline{u'v'}$ is independent of y so we have

$$\overline{v'\phi'} = (\bar{u}-c)\,C \tag{16}$$

and the flux of energy is seen to be proportional to $(\bar{u}-c)$.

Let us now solve the linearized barotropic vorticity equation for the simple case $\bar{u}$ = constant. We have

$$\frac{\partial}{\partial t}\nabla^2\psi' + \bar{u}\frac{\partial}{\partial x}\nabla^2\psi' + \beta\frac{\partial\psi'}{\partial x} = 0 . \tag{17}$$

At y_F we force a stationary wave by imposing

$$\psi'(y_F) = \psi_F \cos kx . \tag{18}$$

Substituting a solution

$$\psi' = \frac{1}{2}\left[\Psi(y)\,e^{ikx} + \Psi^*(y)\,e^{-ikx}\right], \quad k>0 \tag{19}$$

where the asterisk denotes a complex conjugate, into (16) we get

$$\frac{d^2\Psi}{dy^2} + \left(\frac{\beta}{\bar{u}} - k^2\right)\Psi = 0 . \tag{20}$$

If $\beta/\bar{u}-k^2$ is negative, i.e. $l^2 = k^2-\beta/\bar{u} > 0$, then

$$\Psi = Ae^{ly} + Be^{-ly} .$$

We consider a domain extending from y_F southward to $y = -\infty$. To have a bounded solution at $-\infty$ we must set

$$B = 0$$

and the amplitude A is determined from the boundary condition (18). For convenience we set the origin at the forcing latitude ($y_F = 0$) and get

$$\psi' = \psi_F e^{ly}\cos kx . \tag{21}$$

The amplitude of the wave is seen to decay exponentially away from the source (in negative y region) and it has no phase tilt in the north-south direction. We recall from (15) that this implies that the wave energy flux is identically zero. Solutions of this type are said to be "trapped". They apply to

(i) All zonal wave numbers k when $\bar{u} < 0$ (easterlies)

(ii) "Short" waves, $k^2 > \beta/\bar{u}$, when $\bar{u} > 0$.

The other possibility to be examined is $\beta/\bar{u}-k^2 = \mu^2 > 0$. For this case to be applicable, the mean zonal flow must be westerly and the zonal wavenumber must be sufficiently small. The solution to (19) is then

$$\Psi = A e^{i\mu y} + B e^{-i\mu y}, \quad \mu > 0. \tag{22}$$

In this case both parts of the solution are bounded at $-\infty$ and we must invoke another boundary condition. We will use the Somerfeld radiation condition, which states that at $-\infty$ there can be no flux of energy towards the source at $y = 0$. Thus we require $\overline{v'\phi'}$ to be negative (southward flux of energy) as $y \to -\infty$. Since here $\bar{u} > 0$ and $c = 0$, (15) implies that we take $\overline{u'v'} > 0$ as $y \to -\infty$.

If we substitute (21) into (18) to obtain ψ' and then compute $\overline{u'v'}$ we obtain

$$\overline{u'v'} = \tfrac{1}{2}\mu k \left(|B|^2 - |A|^2 \right).$$

We see that the "B part" of the solution (22) contributes a positive momentum flux, but the "A part" contributes a negative momentum flux, i.e. it is a solution which propagates energy northward to the source. We must therefore set $A = 0$ and get, using (17),

$$\psi' = \psi_F \cos(kx - \mu y). \tag{23}$$

Note that ψ' has an amplitude which is independent of y, so that the effect of the forcing is felt at great distances away from the forcing latitude. The phase lines tilt from the south-west to the north-east and hence the wave energy flux is southward. A solution of this type is called a "propagating wave".

3. Vertical Propagation

To examine the problem of the vertical propagation of a disturbance forced in the lower atmosphere by a steady forcing we will use a Beta plane model bounded by rigid walls at $y = 0$ and $y = D$. The disturbance will be forced by prescribing a vertical velocity at the lower boundary of the form

$$w'(x, y, z = 0, t) = w_F \sin ly \cos k(x - ct) \tag{24}$$

where

$$l = \frac{n\pi}{D}$$

with n a positive integer. The flow will be assumed adiabatic and inviscid. The mean zonal flow will be taken to be a function of Z only. In such a model there is no horizontal propagation of energy and so the mechanism of vertical propagation can be isolated.

Our model equation is

$$\frac{\partial q}{\partial t} + \vec{V} \cdot \nabla q = 0 \tag{25a}$$

with

$$q = \nabla^2 \psi + \frac{f_0^2}{\rho_0} \frac{\partial}{\partial z} \left(\frac{\rho_0}{N^2} \frac{\partial \psi}{\partial z} \right) + f_0 + \beta y \tag{25b}$$

$$\vec{V} = k \times \nabla \psi . \tag{25c}$$

The zonally averaged part of (25a) is

$$\frac{\partial \bar{q}}{\partial t} = - \frac{\partial}{\partial y} \left(\overline{v' q'} \right) \tag{26a}$$

where

$$\bar{q} = \frac{f_0^2}{\rho_0} \frac{\partial}{\partial z} \left(\frac{\rho_0}{N^2} \frac{\partial \bar{\psi}}{\partial z} \right) + f_0 + \beta y \tag{26b}$$

$$q' = \nabla^2 \psi' + \frac{f_0^2}{\rho_0} \frac{\partial}{\partial z} \left(\frac{\rho_0}{N^2} \frac{\partial \psi'}{\partial z} \right) . \tag{26c}$$

The linearized perturbation form of (25a) is

$$\frac{\partial q'}{\partial t} + \bar{u} \frac{\partial q'}{\partial x} + v' \frac{\partial \bar{q}}{\partial y} = 0. \tag{27}$$

Multiplying by q' and averaging zonally we get

$$\frac{\partial}{\partial t} \frac{\overline{(q')^2}}{2} = - \frac{\partial \bar{q}}{\partial y} \overline{v' q'} \tag{28}$$

which is identical to (9) of the previous section, except for the definition of $\bar{q}$ and q'. Again we find that for a steady disturbance

$$\overline{v' q'} = 0 . \tag{29}$$

Substituting for q' from (26c) we get

$$\overline{v' q'} = - \frac{\partial}{\partial y} \left(\overline{u' v'} \right) + \frac{f_0^2}{\rho_0} \frac{\partial}{\partial z} \left(\frac{\rho_0}{N^2} v' \frac{\partial \psi'}{\partial z} \right) = 0 . \tag{30}$$

Because of the type of forcing we are using and the form of (27), the stream-function can be written as

$$\psi' = \mathcal{R}_e \left[\Psi(z) e^{ik(x - ct)} \right] \sin ly$$

for which the momentum flux $\overline{u'v'}$ is zero. Thus (30) yields

$$\frac{\partial}{\partial z}\left(\frac{\rho_0}{N^2} v' \frac{\partial \psi'}{\partial z}\right) = 0. \tag{31}$$

We will now show that the quantity in brackets is related to the vertical wave energy flux. First we note that if we multiply the linearized adiabatic versions of (1) and (2), i.e.

$$\frac{\partial}{\partial t}\nabla^2\psi' + \bar{u}\frac{\partial}{\partial x}\nabla^2\psi' + \frac{\partial \bar{q}}{\partial y} v' = \frac{f_0}{\rho_0}\frac{\partial}{\partial z}(\rho_0 w') \tag{32a}$$

$$\frac{\partial}{\partial t}\frac{\partial \psi'}{\partial z} + \bar{u}\frac{\partial}{\partial x}\frac{\partial \psi'}{\partial z} - v'\frac{\partial \bar{u}}{\partial z} + \frac{N^2}{f_0} w' = 0 \tag{32b}$$

by $-\rho_0\psi'$ and $(f_0^2\rho_0/N^2)\,\partial\psi'/\partial Z$, respectively, add and integrate over the volume between levels Z_1 and Z_2, we obtain the energy equation

$$\frac{d}{dt}\int_V \left[\frac{1}{2}|\nabla\psi'|^2 + \frac{1}{2}\frac{f_0^2}{N^2}\left(\frac{\partial\psi'}{\partial z}\right)^2\right]\rho_0 dV = \int_V \frac{f_0^2}{N^2} v'\frac{\partial\psi'}{\partial z}\frac{\partial\bar{u}}{\partial z}\rho_0 dV - \left[\int_A f_0 w'\psi'\rho_0 dA\right]_{Z_1}^{Z_2} \tag{33}$$

where A is the horizontal area of the domain. The time rate of change of the perturbation kinetic plus potential energy is seen to be given by conversion of available potential energy from the zonal flow (first integral on the r.h.s.) plus the rate of flow of wave energy into the volume. So the vertical flux of wave energy zonally averaged for a fixed y is

$$F = f_0\rho_0\overline{w'\psi'}. \tag{34}$$

Now multiplying (32b) by ψ', using $\partial t = -c\partial/\partial x$ and averaging zonally we get

$$\overline{w'\psi'} = \frac{f_0}{N^2}(\bar{u}-c)\overline{\frac{\partial\psi'}{\partial x}\frac{\partial\psi'}{\partial z}}$$

i.e.,
$$F = f_0\rho_0\overline{w'\psi'} = \frac{\rho_0(\bar{u}-c)}{N^2}\cdot f_0^2\overline{\frac{\partial\psi'}{\partial x}\frac{\partial\psi'}{\partial z}} \tag{35a}$$

or
$$= \frac{\rho_0(\bar{u}-c)}{N^2}\cdot\frac{f_0 R}{H}\cdot\overline{v'T'}. \tag{35b}$$

We see that for a stationary wave in a westerly current the vertical flux of wave energy in our adiabatic inviscid model is upward ($\overline{w'\psi'} > 0$) when the

eddy heat transport is northward ($\overline{v'T'} > 0$) and it is downward when the wave heat transport is southward. Put another way, the flux of wave energy is upward when the wave tilts to the west with height and downward when the wave tilts to the east with height, when $\bar{u} > 0$. Now we found in (31) that for a steady wave $\rho_o N^{-2} \overline{v' \partial\psi'/\partial Z}$ is independent of Z; this combined with (35a) implies that

$$F = f_o \rho_o \overline{w'\psi'} = (\bar{u} - c) C \qquad (36)$$

where C is independent of Z. So the flux of wave energy in the vertical varies in proportion to $(\bar{u} - c)$.

We recall from (16) that a result similar to (36) was obtained for the case of pure horizontal propagation (see (16)). We note first that if at some level the vertical flux of energy is zero, as would be the case in a model with a rigid lid as an upper boundary then, assuming $(\bar{u} - c) \neq 0$, we find from (36) that $C = 0$ and so $F = 0$ at all levels and the phase lines of the stream function are vertical. We will see later that the boundary condition $\omega = dp/dt = 0$ at $p = 0$ in finite difference models is equivalent to a rigid lid upper boundary condition.

We note also from (36) that if $\bar{u}$ varies with height in such a way that $\bar{u} - c = 0$ at $Z = Z_c$, called the critical level, there can be no flux of wave energy across Z_c, as $F \to 0$ there. For stationary waves this is the level where the westerlies change to easterlies. Although our present analysis is valid strictly speaking only for small-amplitude inviscid adiabatic waves, it is nevertheless indicative of the reason why the mean monthly height waves in the summer stratospheric easterlies have such small amplitudes - the stationary wave energy generated in the troposphere cannot flow across the $\bar{u} = 0$ level.

Let us now obtain the solution to the linearized potential vorticity equation (27) subject to the lower boundary condition (24). As an upper boundary condition we will require that the wave energy density be bounded at infinity; if that condition does not yield useful information we will require that there be no flow of energy from ∞ towards the source at $Z = 0$. For simplicity here we will assume $\bar{u}$ = constant. Solutions for cases with $\bar{u}$ a function of Z can be found in Charney and Drazin (1961). We will also assume that the horizontally averaged temperature is a constant so that

$\rho_o^{-1}\partial\rho_o/\partial Z = -H^{-1}$ = constant, N = constant $\simeq 2 \times 10^{-2}$ s^{-1}.

The potential vorticity equation is then

$$\left(\frac{\partial}{\partial t} + \bar{u}\frac{\partial}{\partial x}\right)\left[\nabla^2\psi' + \frac{f_o^2}{\rho_o}\frac{\partial}{\partial z}\left(\frac{\rho_o}{N^2}\frac{\partial\psi'}{\partial z}\right)\right] + \beta\frac{\partial\psi'}{\partial x} = 0 . \tag{37}$$

Equations (24) and (32b) yield the lower boundary condition

$$\left(\frac{\partial}{\partial t} + \bar{u}\frac{\partial}{\partial x}\right)\frac{\partial\psi'}{\partial z} = -\frac{N^2}{f_o} w_F \sin ly \cos k(x-ct) . \tag{38}$$

Substituting a solution of the form

$$\psi'(x, y, z, t) = \frac{1}{2}\left[\Psi(z)e^{ik(x-ct)} + \Psi^*(z)e^{-ik(x-ct)}\right]\sin ly \tag{39}$$

into (37) we get

$$\frac{f_o^2}{\rho_o}\frac{\partial}{\partial z}\left(\frac{\rho_o}{N^2}\frac{\partial\Psi}{\partial z}\right) + \left(\frac{\beta}{\bar{u}-c} - K^2\right)\Psi = 0 \tag{40}$$

where $K^2 = k^2 + l^2$. This can be reduced to an equation with constant coefficients by the substitution

$$\Psi = \tilde{\Psi}(z)\, e^{z/2H} \tag{41}$$

in which case $\tilde{\Psi}$ satisfies

$$\frac{d^2\tilde{\Psi}}{dz^2} + \left[\frac{N^2}{f_o^2}\left(\frac{\beta}{\bar{u}-c} - K^2\right) - \frac{1}{4H^2}\right]\tilde{\Psi} = 0 . \tag{42}$$

We note that the wave kinetic energy density, $\rho_o\overline{(u'^2 + v'^2)}/2$, is proportional to $\rho_o|\Psi|^2$, hence to $|\tilde{\Psi}(Z)|^2$. We can therefore use $\tilde{\Psi}(Z)$ as a measure of the (square root of) wave kinetic energy density. Also, Ψ and $\tilde{\Psi}$ have the same phase so that the tilt (or lack of tilt) of $\tilde{\Psi}$ is indicative of the vertical propagation (or lack of it) by the wave.

To solve (42) let us first consider the possibility

$$-\left[\frac{N^2}{f_o^2}\left(\frac{\beta}{\bar{u}-c} - K^2\right) - \frac{1}{4H^2}\right] = r^2 > 0 \tag{43a}$$

that is

$$\bar{u}-c < 0 \quad \text{or} \quad \bar{u}-c > \frac{\beta}{K^2 + f_o^2/4H^2N^2} \tag{43b}$$

In this case the solution is

$$\tilde{\Psi} = A e^{-rz} . \qquad r > 0. \tag{44}$$

The other possible solution Bexp(rZ) must be rejected to have a bounded energy density at infinity. Using (38) and (39) and (41) we get

$$\psi' = \frac{N^2}{f_0}\,\frac{W_F}{k(\bar{u}-c)}\,\frac{1}{(r-1/2H)}\cdot e^{(1/2H - r)z}\sin k(x-ct)\sin ly. \tag{45}$$

We know from (44) that the energy density of the wave decays exponentially with height; the amplitude of ψ', on the other hand, as seen from (45) will grow or decay with height depending on whether or not the magnitude of r is less than $\frac{1}{2}H$. We also see from (45) that the phase lines of the stream function are vertical so the vertical wave energy flux is identically zero. The wave is therefore "trapped".

The other possibility in (42) is

$$\frac{N^2}{f_0^2}\left(\frac{\beta}{\bar{u}-c} - K^2\right) - \frac{1}{4H^2} = r^2 > 0 \tag{46a}$$

i.e.

$$0 < \bar{u} - c < \frac{\beta}{K^2 + f_0^2/4H^2N^2} \equiv u_c \tag{46b}$$

in which case the solution is

$$\tilde{\Psi} = Ae^{irz} + Be^{-irz}, \quad r > 0. \tag{47}$$

Using (39), (41) and (47) we can write the solution for ψ' as

$$\psi'(x,y,z,t) = \frac{1}{2}\left[Ae^{i(kx+rz-kct)} + Be^{i(kx-rz-kct)}\right]e^{z/2H}$$
$$+ \text{complex conjugate}. \tag{48}$$

The solution proportional to B slopes to the east with height, i.e. it has a downward energy flux at infinity and must be rejected by setting B = 0. Using the lower boundary condition (38) we get

$$\psi' = \frac{N^2}{f_0}\,\frac{W_F}{k(\bar{u}-c)}\,\frac{\sin ly}{(r^2+1/4H^2)}\,e^{z/2H}\left[r\cos(kx+rz-kct) - \frac{1}{2H}\sin(kx+rz-kct)\right]. \tag{49}$$

This solution slopes to the west with height, has an upward energy flux, has a constant energy density with height and has an amplitude which grows exponentially with height. It is a "propagating solution".

We can summarize the regions of applicability of solutions (45) and (49) by means of Fig. 1 which has been drawn for the case of stationary forcing, c = 0. It is clear from the figure that the conditions favorable to

the penetration of forced stationary waves into the upper atmosphere are weak westerly zonal winds and/or long wavelengths.

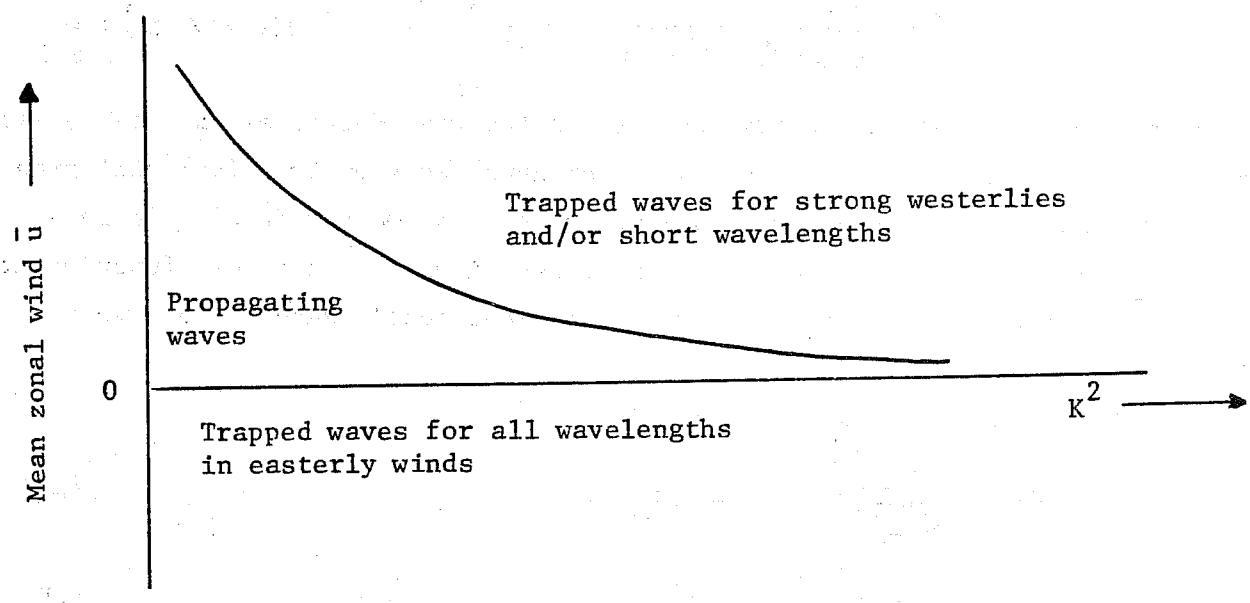

Fig. 1. Schematic diagram showing the separate regions where trapped and propagating solutions are obtained for the case of stationary forcing with $\bar{u}$ = constant. The curve is the plot of $\bar{u} = \beta/(K^2 + f^2/4H^2N^2)$.

Orographic Lifting. If we assume that the forcing of the stationary waves results from orographic lifting, we have

$$w = \vec{V} \cdot \nabla h_g \qquad z = h_g \tag{50}$$

where h_g is the height of the ground above some reference level. Linearizing (50) we get

$$w' = \bar{u} \frac{\partial}{\partial x} h_g \qquad z = 0 .$$

With

$$h_g = \hat{h}_g \sin kx \sin ly \tag{51}$$

we find from (24) that

$$w_F = \bar{u} k \hat{h}_g \tag{52}$$

and hence the stream function for the trapped, orographically forced waves is

$$\psi' = \hat{h}_g \frac{N^2}{f_o} \frac{1}{(r - 1/2H)} e^{(1/2H - r)z} \sin kx \sin ly \tag{53a}$$

and for the propagating waves it is

$$\psi' = \hat{h}_g \frac{N^2}{f_0} \frac{1}{(r^2 + 1/4H^2)} e^{z/2H} \left[r\cos(kx + rz) - \frac{1}{2H} \sin(kx + rz) \right] \sin ly \quad (53b)$$

with $$r = + \left| \frac{N^2}{f_0^2} \left(\frac{\beta}{\bar{u}} - K^2 \right) - \frac{1}{4H^2} \right|^{1/2}.$$

The amplitude of the mountain harmonic h_g in (51) is a function of the wavenumbers k and l, but for the purpose of the following discussion we will assume it is not.

From (51) and (53) we see that

(i) the trapped waves are either in phase with the orography or exactly half a wavelength out of phase, depending on the sign of $r-\frac{1}{2}H$. Now $r = \frac{1}{2}H$ at $K^2 = \beta/\bar{u}$; for "short" waves, i.e., $K^2 > \beta/\bar{u}$, the forced waves are out of phase with the topography. Because of that phase relationship the trapped waves do not exert a torque on the topography which is consistent with the fact that they have no vertical energy flux.

(ii) At $r = \frac{1}{2}H$, ($K^2 = \beta/\bar{u}$) the amplitude of the forced wave is singular and the present model breaks down.

(iii) At Z = 0 the sine part of the propagating stream function is out of phase with the topography and exerts no torque on the topography; the cosine part, on the other hand, leads to higher pressures on the west side of the mountain than on the east side and makes a contribution to the mountain torque.

The amplitude of the propagating stream function at Z = 0 was computed by Hirota (1971) as a function of $\bar{u}$ and the zonal wavelength $2\pi/k$ with all other parameters kept fixed; the meridional wavelength was assumed infinite so that K^2 was set equal to k^2. The results are shown in Fig. 2.

Charney and Dragin (1961) have shown that if the cartesian geometry of the present analysis is formally replaced by spherical geometry, then K^2 is replaced by $n(n+1)/a^2$ where a is the earth's radius and n is the degree of the spherical harmonic $P_n^m(\varphi)e^{im\lambda}$ which describes the horizontal structure of

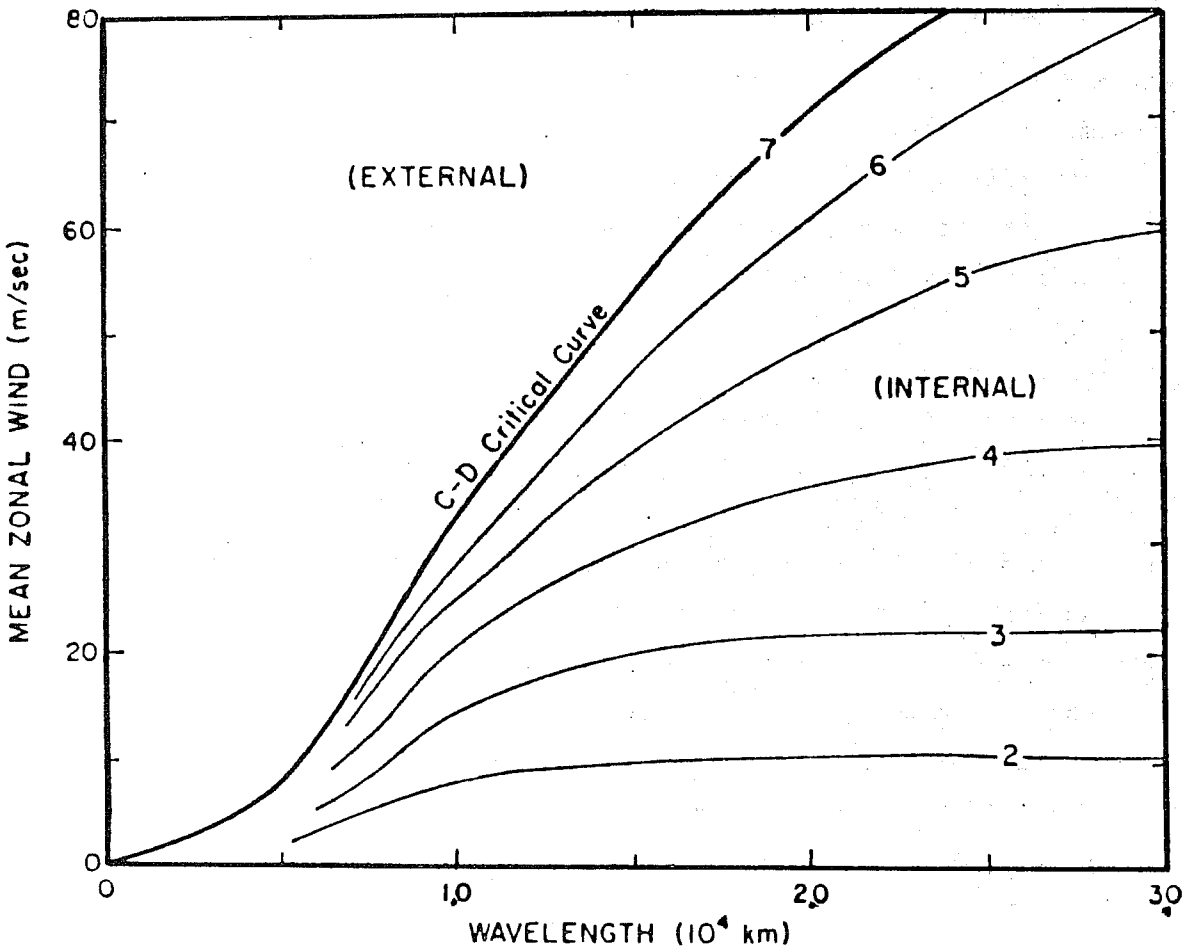

Fig. 2. The amplitude of the stationary stream function in units of 10^3 m^2s^{-1} forced by a sinusoidal mountain of amplitude 1.25 km, as a function of the mean zonal wind speed and wavelength.

the wave. They also state that the dominant harmonics of the earth's orography have $n > 3$. For $n > 3$ we get $L/2\pi < a/\sqrt{n(n+1)} = a/\sqrt{12}$ or $L < 11{,}500$ km. From Fig. 2 we see that some of the forced waves would propagate vertically only if $\bar{u} \lesssim 38\text{m s}^{-1}$.

4. Horizontal and Vertical Propagation

For the case where the wave can propagate horizontally as well as vertically and $\bar{u} = \bar{u}(y,Z)$ we can use equations (25) through (30) except for (26b), the definition of $\bar{q}$, which is now

$$\bar{q} = -\frac{\partial \bar{u}}{\partial y} + \frac{f_o^2}{\rho_o}\frac{\partial}{\partial z}\left(\frac{f_o^2}{N^2}\frac{\partial \bar{\psi}}{\partial z}\right) + f_o + \beta y . \tag{54}$$

To obtain the energy equation for the present problem we multiply (32a) and (32b) by $-\rho_o\psi'$ and $(f_o^2\rho_o/N^2)\partial\psi'/\partial Z$, respectively, add and integrate zonally. The result is

$$\frac{\partial}{\partial t}\left[\overline{\rho_o\frac{|\nabla\psi'|^2}{2} + \frac{f_o^2\rho_o}{2N^2}\left(\frac{\partial\psi'}{\partial z}\right)^2}\right] = -\rho_o\frac{\partial\bar{u}}{\partial y}\overline{u'v'} + \rho_o\frac{f_o^2}{N^2}\frac{\partial\bar{u}}{\partial z}\overline{v'\frac{\partial\psi'}{\partial z}}$$

$$-\rho_o\frac{\partial}{\partial y}\left(f_o\overline{v'_{ag}\psi'}\right) - \frac{\partial}{\partial z}\left(\rho_o f_o\overline{w'\psi'}\right) . \tag{55}$$

By the same procedure as in the previous sections we find, using the momentum and thermodynamic equations, that for a stationary wave

$$\hat{F}_H = \rho_o f_o\overline{v'_{ag}\psi'} = -\rho_o\bar{u}\,\overline{u'v'} \tag{56a}$$

$$\hat{F}_V = \rho_o f_o\overline{w'\psi'} = \rho_o\frac{f_o^2}{N^2}\bar{u}\,\overline{v'\frac{\partial\psi'}{\partial z}} . \tag{56b}$$

Substituting into (55) and using the fact that the wave is steady we obtain

$$\bar{u}\left[\frac{\partial}{\partial y}\left(-\rho_o\overline{u'v'}\right) + \frac{\partial}{\partial z}\left(\rho_o\frac{f_o^2}{N^2}\overline{v'\frac{\partial\psi'}{\partial z}}\right)\right] = 0 . \tag{57}$$

We can write, formally,

$$\vec{R} = \left(-\rho_o\overline{u'v'}\right)\vec{j} + \left(\rho_o\frac{f_o^2}{N^2}\overline{v'\frac{\partial\psi'}{\partial z}}\right)\vec{k} \tag{58}$$

$$\nabla = \vec{j}\frac{\partial}{\partial y} + \vec{k}\frac{\partial}{\partial z}$$

and, assuming $\bar{u} \neq 0$, (57) implies

$$\nabla\cdot\vec{R} = 0 . \tag{59}$$

Since $\vec{R}$ is nondivergent we can write it as

$$\vec{R} = \vec{i} \times \nabla \tilde{\psi} = \vec{t}\, \partial \tilde{\psi}/\partial n \tag{60}$$

where $\vec{i}$ is a unit vector pointing along the positive x axis, $\vec{t}$ is tangent to the $\tilde{\psi}$ contours and n is normal to them. Using (56) and (58) we see that the flux of wave energy $\vec{F} = \vec{j}\hat{F}_H + \vec{k}\hat{F}_V$ can be written as

$$\vec{F} = \bar{u}\, \vec{R}. \tag{61}$$

Equations (60) and (61) imply that the curves $\tilde{\psi}$ = constant are streamlines for the flow of wave energy in the y - Z plane. Fig. 3 illustrates the streamlines as dashed curves.

The flow of energy between two streamlines is given by

$$\int \vec{F}\, dn = \int \bar{u}\, \vec{R}\, \partial n = \vec{t} \int (\bar{u}\, \partial \tilde{\psi}/\partial n)\, dn$$
$$= \vec{t}\, \bar{u}_A\, \Delta \tilde{\psi} \tag{62}$$

where $\Delta\tilde{\psi}$ is the increment of $\tilde{\psi}$ from one streamline to the next and $\bar{u}_A$ is the average value of $\bar{u}$ along the path of integration. Since $\Delta\tilde{\psi}$ = constant for two neighboring streamlines we see that the flux of energy is proportional to $\bar{u}_A$.

From the definition of $\tilde{\psi}$ we see that the energy flows along each streamline in the same direction throughout the length of the streamline as long as $\bar{u} > 0$. Equations (61) and (62) imply that the flux goes to zero as we approach a line where $\bar{u} = 0$ so that the wave energy cannot cross that line, called a singular line because the steady perturbation potential vorticity equation used to obtain these results is singular at $\bar{u} = 0$. Note that for a steady wave $\psi' = \Psi(y,Z)\exp ik(x-ct)$, (27) leads to

$$\frac{\partial^2 \Psi}{\partial y^2} + \frac{f_0^2}{\rho_0} \frac{\partial}{\partial Z}\left(\frac{\rho_0}{N^2} \frac{\partial \Psi}{\partial Z}\right) + \left[\frac{1}{(\bar{u}-c)} \frac{\partial \bar{q}}{\partial y} - k^2\right] \Psi = 0 \tag{63}$$

so that the equation is singular if somewhere $\bar{u} = c$ with $\partial\bar{q}/\partial y \neq 0$. If such a situation arises (63) poses some important difficulties which we will now

discuss very briefly. A more detailed discussion can be found in Béland (1978) and the references therein.

The singular line. It will suffice here to deal with the barotropic version of (63) for a stationary wave, i.e.,

$$\frac{d^2\Psi}{dy^2} + \left[\frac{\beta - d^2\bar{u}/dy^2}{\bar{u}} - k^2\right]\Psi = 0 \qquad (64)$$

and we will assume that at some latitude $y = 0$ we have $\bar{u} = 0$ so that (64) is singular there. Two solutions to (64) can be obtained by the method of Frobenius. They are

$$\Psi_1 = y + \left(\frac{\bar{u}_c'' - \beta}{2\bar{u}_c'}\right)y^2 + \left[\frac{\bar{u}_c'''}{\bar{u}_c'} + \frac{\beta}{2\bar{u}_c'^2}(\beta - \bar{u}_c'') + k^2\right]\frac{y^3}{6} + \cdots$$

$$\Psi_2 = 1 + \left[\frac{\bar{u}_c'''}{2\bar{u}_c'} + \frac{\beta}{4\bar{u}_c'^2}(7\bar{u}_c'' - \beta) - \frac{\bar{u}_c''^2}{\bar{u}_c'^2} + \frac{k^2}{2}\right]y^2 + \cdots$$

$$+ \left(\frac{\bar{u}_c'' - \beta}{\bar{u}_c'}\right)\Psi_1 \ln|y|$$

where a prime on $\bar{u}$ indicates differentiation with respect to y and the subscript c means evaluation at the critical line. Note that Ψ_1 and Ψ_2 are bounded at $y = 0$ but $\partial\Psi_2/\partial y$, and hence u', is singular. The solution to (64) can be written as

$$\Psi^{\pm} = A^{\pm}\Psi_1 + B^{\pm}\Psi_2 \,. \qquad (65)$$

Of the four constants in (65) two can be determined by the boundary conditions at the northern and southern boundaries but the other two can only be found by reintroducing some of the terms (nonlinearities, dissipation, transience) which have been neglected in (64). In fact it is because these terms were neglected that we obtained a singular equation. It is clear that in a real physical system the flow would become nonlinear or dissipation would become important before the wave could reach an infinite amplitude in u' as obtained above.

The main difficulty here is that if nonlinear effects alone are reintroduced to determine the constants in (65), a different solution is obtained from that found when dissipative effects alone are reintroduced. Briefly, when

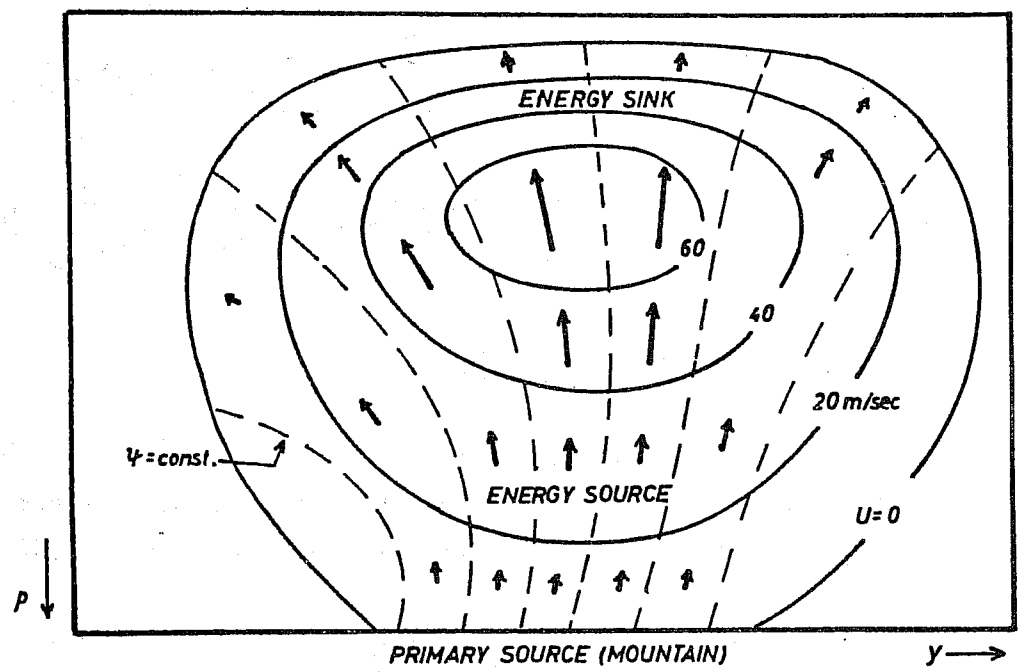

Fig. 3. Schematic diagram showing the wave energy flux (arrows) in relation to the mean zonal wind speed (solid lines). The dashed lines are streamlines for the energy flow. Note that while the energy source and sink regions can be interpreted as areas of energy exchange between the zonal flow and the wave, both are steady due to a compensating energy flux divergence or convergence; see text and appendix B for more details (After Eliassen and Palm, 1961).

viscous effects are invoked we find a Ψ solution which slopes from the north-east to the south-west north of the singular line, implying an energy flux southward towards the singularity; in the easterlies to the south there is no phase tilt and no energy flux. Thus at $y = 0$ the momentum flux $\overline{u'v'}$ is discontinuous, being positive for $y > 0$ and 0 for $y < 0$. In contrast when nonlinearities are invoked to close the problem the momentum flux appears to be zero both to the north and to the south of the singular line (i.e., no phase tilt in ψ'). There is then no flux of energy and the singular line appears to reflect back the energy that impinges on it from the source to the north. Of course it is possible to invoke both nonlinearities and dissipation simultaneously but then the resulting wave structure can be anything between the two extremes discussed above, depending on the relative magnitudes of the nonlinear and viscous terms. While the magnitude of the former is determined by the magnitude of the forcing, the magnitude of the dissipation terms appears more difficult to fix.

ACKNOWLEDGEMENT

I would like to thank T. Warn for proposing the use of the potential vorticity equation to obtain equations (14) and (30) in a concise manner.

REFERENCES

Béland, M., 1978: The evolution of a nonlinear Rossby Wave critical level: effects of viscosity. J. Atmos. Sci., 10, 1802-1815.

Charney, J.G. and P.G. Drazin, 1961: Propagation of planetary scale disturbances from the lower to the upper atmosphere. J. Geophys. Res., 66, 83-109.

Eliassen, A. and E. Palm, 1961: On the transfer of energy in stationary mountain waves. Geofys. Publ., 22, No. 3, 22 pp.

Hirota, I., 1971: Excitation of planetary Rossby waves in the winter stratosphere by periodic forcing. J. Meteor. Soc. Japan, 49, 439-449.

Holton, J.R., 1974: Forcing of mean flows by stationary waves. J. Atmos. Sci., 31, 942-945.

_____, 1975: The dynamic meteorology of the stratosphere and mesosphere. Meteor. Monogr., Vol. 15, No. 37, Amer. Meteor. Soc., 216 pp.

APPENDIX A

List of New Symbols

c	phase speed of a wave
f_o	value of Coriolis at centre of Beta plane
h_g	height of ground above some reference level
k	wavenumber in x
l	wavenumber in y
m	zonal wavenumber = $k\ a\cos\varphi_o$
n	degree of spherical harmonic
p_s	pressure at Z = 0
q	absolute potential vorticity
x	west-east coordinate on Beta plane
y	south-north coordinate on Beta plane
A	horizontal area of the Beta plane
D	width of the Beta plane
F	flux of energy
H	scale height = RT/g
$\dot{H}$	diabatic heating per unit mass per unit time
K	horizontal wavenumber, $(k^2 + l^2)^{\frac{1}{2}}$
N^2	square of buoyancy frequency = $(R/H)(dT_o/dZ + \kappa T_o/H)$
β	df/dy evaluated at centre of Beta plane
ψ	stream function
ψ_F	amplitude of ψ forcing
φ_o	latitude at centre of Beta plane
$\overline{(\ )}$	zonal average of ( )
$(\ )'$	$(\ ) - \overline{(\ )}$, eddy part of ( )

Appendix B

The Definition of Wave Energy Flux

The definition of wave energy flux used in these notes follows the classical one employed by Eliassen and Palm (1961). As pointed out by Holton (1974, 1975) it is possible to use a different definition and the purpose of this appendix is to show the relationship between the two. We will deal only with the horizontal propagation of wave energy but similar ideas apply to the more general problem of propagation in the y-Z plane.

Let us start with the x-momentum equation for the mean zonal flow and for the perturbation (linearized) as well as the linearized vorticity equation for nondivergent flow. They are

$$\frac{\partial \bar{u}}{\partial t} = -\frac{\partial}{\partial y}\overline{(u'v')} \tag{B1}$$

$$\frac{\partial u'}{\partial t} + \bar{u}\frac{\partial u'}{\partial x} + v'\frac{\partial \bar{u}}{\partial y} = -\frac{\partial \phi'}{\partial x} + fv' \tag{B2}$$

$$\frac{\partial}{\partial t}\nabla^2\psi' + \bar{u}\frac{\partial}{\partial x}\nabla^2\psi' + \left(\beta - \frac{\partial^2 \bar{u}}{\partial y^2}\right)\frac{\partial \psi'}{\partial x} = 0 \tag{B3}$$

where $u' = -\psi'_y$, $v' = \psi'_x$. Note that (B3) is identical to (8). We form the energy equations by (a) multiplying (B1) by $\bar{u}$ and (b) multiplying (B3) by $-\psi'$, integrating zonally and using (B2) to eliminate a term of the form $\psi'\partial^2\psi'/\partial t\partial y$. The point of the discussion here is that the resulting equations can be written in either of two equivalent forms. One is

$$\frac{\partial}{\partial t}\frac{\bar{u}^2}{2} = -\bar{u}\frac{\partial}{\partial y}\overline{(u'v')} \tag{B4a}$$

$$\frac{\partial}{\partial t}\overline{\left(\frac{u'^2 + v'^2}{2}\right)} + \frac{\partial}{\partial y}\left[\overline{v'\phi'} + \bar{u}\,\overline{u'v'}\right] = \bar{u}\frac{\partial}{\partial y}\overline{(u'v')}. \tag{B4b}$$

The other is

$$\frac{\partial}{\partial t}\left(\frac{\bar{u}^2}{2}\right) + \frac{\partial}{\partial y}\left(\bar{u}\,\overline{u'v'}\right) = \overline{u'v'}\frac{\partial \bar{u}}{\partial y} \tag{B5a}$$

$$\frac{\partial}{\partial t}\overline{\left(\frac{u'^2 + v'^2}{2}\right)} + \frac{\partial}{\partial y}\left(\overline{v'\phi'}\right) = -\overline{u'v'}\frac{\partial \bar{u}}{\partial y}. \tag{B5b}$$

It is easily verified that (B4) can be rewritten as (B5) or vice versa simply by differenciating a product; the two forms are thus obviously equivalent to each other. Note that by (16) and (14a) the term involving the square bracket in (B4b) is identically zero for a steady wave. Thus adding (B4a) and (B4b) or (B5a) and (B5b) we get that the total kinetic energy is conserved. Since we have assumed the wave to be steady we get $\partial\bar{u}/\partial t = 0$ whether we use system (B4) or (B5).

As mentioned above, in these notes we have followed Eliassen and Palm (1961) and used formulation (B5). Holton (1974, 1975) prefers formulation (B4) and calls $[\overline{v'\phi'} + \bar{u}\overline{u'v'}]$ the "total wave energy flux". For a steady wave the latter vanishes, as we have seen, and in fact each of the other terms in (B4) vanishes identically showing immediately that there is no wave-mean flow interaction.

The interpretation of (B5) requires that we call $\overline{v'\phi'}$ the wave energy flux and $\bar{u}\overline{u'v'}$ the flux of mean flow energy by the wave. By the Eliassen and Palm result obtained in (15) and (14a) the divergence of one just equals the convergence of the other. Thus we can interpret (B5) as follows for the case of a steady wave in a mean flow: if $\overline{u'v'}\partial\bar{u}/\partial y < 0$, indicating a transformation of mean flow energy to the wave, this is balanced by a divergence of wave energy flux to keep the wave steady. Simultaneously there is a convergence of mean flow energy flux to balance the transformation of energy to the wave so that the zonal flow remains steady.

MODELLING OF SMALL AMPLITUDE FORCED PLANETARY WAVES IN SPHERICAL GEOMETRY

Jacques Derome
Department of Meteorology
McGill University
Montreal

MODELLING OF SMALL AMPLITUDE FORCED PLANETARY WAVES IN SPHERICAL GEOMETRY

1. Some Effects of Spherical Geometry

We have seen that in a linearized Beta plane model steady quasi-geostrophic waves can propagate vertically only if the mean zonal wind $\bar{u}$ is westerly and less than some critical value u_c. We will now examine whether this result applies to models that use the more realistic spherical geometry. In this case the corresponding problem is one in which the basic state is in solid rotation, that is, $\bar{u}/a\cos\varphi$ is a constant. This type of comparison was first made by Dickinson (1968).

1.1 A Spherical Geometry Model

We consider a model of small amplitude stationary waves forced at the lower boundary. We look for solutions to the model and seek to determine whether they correspond to disturbances that propagate energy vertically or whether they are trapped near the forcing.

The linearized primitive equations for stationary disturbances are

$$\frac{\bar{u}}{a\cos\varphi}\frac{\partial u'}{\partial\lambda} = -\frac{1}{a\cos\varphi}\frac{\partial\phi'}{\partial\lambda} + v'\left[f - \frac{1}{\cos\varphi}\frac{\partial}{a\partial\varphi}(\bar{u}\cos\varphi)\right] \tag{1}$$

$$\frac{\bar{u}}{a\cos\varphi}\frac{\partial v'}{\partial\lambda} = -\frac{\partial\phi'}{a\partial\varphi} - u'\left(f + \frac{2\bar{u}\tan\varphi}{a}\right) \tag{2}$$

$$\frac{\bar{u}}{a\cos\varphi}\frac{\partial}{\partial\lambda}\frac{\partial\phi'}{\partial z} + \frac{v'}{a}\frac{\partial}{\partial\varphi}\frac{\partial\bar{\phi}}{\partial z} + N^2 w' = 0 \tag{3}$$

$$\frac{1}{a\cos\varphi}\left(\frac{\partial u'}{\partial\lambda} + \frac{1}{a}\frac{\partial v'\cos\varphi}{\partial\varphi}\right) + \frac{1}{\rho_0}\frac{\partial}{\partial z}(\rho_0 w') = 0. \tag{4}$$

We will look for solutions of the form

$$\{u', v', w', \phi'\} = \{u(\varphi,z), v(\varphi,z), w(\varphi,z), \phi(\varphi,z)\}\exp im\lambda \tag{5}$$

and we will take $\bar{\Omega} = \bar{u}/a\cos\varphi$ = constant. It is then possible from (1) and (2) to obtain expressions for u' and v' in terms of ϕ'. When these are substituted into (4) and w' is eliminated from the resulting equation by means of (3) we get

$$\mathcal{L}_\varphi \Phi' - 4a^2(\Omega+\bar{\Omega})^2 \frac{1}{\rho_0}\frac{\partial}{\partial z}\left(\frac{\rho_0}{N^2}\frac{\partial \Phi'}{\partial z}\right) = 0 \tag{6a}$$

where

$$\mathcal{L}_\varphi \Phi' = \frac{1}{\cos\varphi}\frac{\partial}{\partial\varphi}\left(\frac{\cos\varphi}{q^2-\sin^2\varphi}\frac{\partial \Phi'}{\partial\varphi}\right) - \frac{1}{q^2-\sin^2\varphi}\left(\frac{m}{q}\cdot\frac{q^2+\sin^2\varphi}{q^2-\sin^2\varphi} + \frac{m^2}{\cos^2\varphi}\right)\Phi' \tag{6b}$$

$$q = \frac{m\bar{\Omega}}{2(\Omega+\bar{\Omega})} . \tag{7}$$

If we then look for separated solutions

$$\Phi(\varphi, z) = \Phi(\varphi)\hat{Z}(z) \tag{8}$$

we get the horizontal and vertical structure equations

$$\mathcal{L}_\varphi \Phi + \epsilon \Phi = 0 \tag{9}$$

$$\frac{4a^2(\Omega+\bar{\Omega})^2}{\rho_0}\frac{d}{dz}\left(\frac{\rho_0}{N^2}\frac{d\hat{Z}}{dz}\right) + \epsilon\hat{Z} = 0 \tag{10}$$

where ϵ is the separation constant. Equation (9) is the Laplace tidal equation studied by Hough (1898) and in great detail by Longuet-Higgins (1968), hereafter refered to as LH. In their case the model was a homogeneous fluid at rest on which were superposed free small amplitude perturbations. For that problem the parameter q stood for $-\sigma/2\Omega$ where σ is the frequency of the oscillation whereas here it is related to the mean angular velocity of the zonal wind in which are embedded the stationary forced waves.

For a given mean zonal flow and boundary conditions $\Phi(-\pi/2) = \Phi(\pi/2) = 0$, (9) can be solved for the eigenvalue ϵ and the corresponding eigenfunction $\Phi(\varphi)$. For each zonal wave number m appearing in $\mathcal{L}_\varphi$ an infinite number of pairs ϵ,Φ can be found; we will denote them by ϵ_n^m, Φ_n^m. The $\Phi_n^m(\varphi)$ are called Hough functions.

As $\epsilon\to 0$ the solutions to the horizontal structure equation (9) can be grouped in two classes. Class 1 is composed of the gravity wave solutions, while the solutions of class 2 are the planetary waves (Rossby waves). As can be seen in LH, as $\epsilon\to 0$ the horizontal velocity vector of class 1 solutions is nearly irrotational while that of class 2 solutions is nearly nondivergent. It turns out that in that same limit the velocity potential of class 1 solutions and the stream function of class 2 solutions are described very

nearly by individual associated Legendre polynomials. In other words, as $\epsilon \to 0$

$$\left.\begin{aligned} \chi(\varphi) &\simeq P_n^m(\varphi) \\ \Psi(\varphi) &\simeq 0 \end{aligned}\right\} \text{Class 1 gravity waves}$$

and

$$\left.\begin{aligned} \chi(\varphi) &\simeq 0 \\ \Psi(\varphi) &\simeq P_n^m(\varphi) \end{aligned}\right\} \text{Class 2 Rossby waves}$$

where $\chi(\varphi)$ and $\Psi(\varphi)$ are the meridional dependence of the potential and stream functions respectively. Because we will be presenting a number of results in terms of the height field it is worth stressing that it is the stream function of Rossby waves that tends to the associated Legendre polynomial P_n^m, not the geopotential.

Let us now look at the significance of ϵ in the context of the vertical propagation or trapping of waves. For simplicity we will assume that the basic state is isothermal, in which case N^2 = constant. The solution to (10) then has the form

$$\hat{Z} \sim e^{z/2H} \, e^{\pm\sqrt{\frac{1}{4}-\epsilon S}\, z/H} \tag{11}$$

where $S = [NH/2a(\Omega+\bar{\Omega})]^2 = R^2\bar{T}/4a^2c_p(\Omega+\bar{\Omega})^2$. With $\bar{\Omega}<<\Omega$, $a = 6.37 \times 10^6$m, $\bar{T} = 250$K, $R = 287\ ms^{-2}K^{-1}$, $R/c_p = 0.286$ we get $S = 0.024$. We see from (11) that the mode will be trapped if $\epsilon<1/4S \simeq 10$, i.e., we have

$$\begin{aligned} \epsilon &\lesssim 10 \quad \text{vertically trapped wave} \\ \epsilon &\gtrsim 10 \quad \text{vertically propagating wave.} \end{aligned} \tag{12}$$

Equation (9) was solved by LH for a large number of different values of q, which here is a parameter related to the angular velocity of the mean zonal wind, i.e., $q = m\bar{\Omega}/2(\Omega+\bar{\Omega})$. Some of his results appear in Fig. 1 for zonal wave number 1. (The curves have been labelled according to the type of free modes to which they correspond in LH's problem). On the abscissa some values of $\bar{u}$ at 45°N for the corresponding values of q are also given. On the ordinate the vertical wavelength of the waves, computed with the help

of (11), appear for the propagating waves, i.e. $\varepsilon>10$. When $\varepsilon<10$ only the minus sign in (11) is to be used for energy boundedness at infinity. In that case the energy density decays exponentially with height but the amplitude of ϕ' can grow or decay with height, depending on which of the two exponents dominates in (11). When the negative exponent dominates the ϕ' wave decays exponentially with height and we can define a "penetration depth" as that height at which the wave amplitude has decreased by a factor e; the value of the penetration depth is shown in kilometres for $\varepsilon = -10$ and -100.

We see from Fig. 1 that for a fixed $\bar{\Omega}>0$ a number of different modes are possible (only a few are shown), each having its own value of ε, i.e. its own vertical scale. For example, with $u(45°) = 81\ ms^{-1}$ we find that the modes of the Rossby type with indices n = 1 and 2 have $\varepsilon>10$ and are thus propagating waves. As in the Beta plane models these waves slope to the west with height and as seen from (11) their amplitude grows as $\exp(Z/2H)$. The modes with $n>3$ have $\varepsilon<10$ and are thus trapped modes. All modes of the gravity type are propagating energy upward; their vertical wavelength is relatively small and, as can be verified in LH, gravity modes with such large values of ε are trapped horizontally near the equator. So again we find that as in the Beta plane model, for a fixed mean zonal westerly wind some modes are trapped and others propagate, the difference between the two being related to their horizontal structure. The fact that we find an infinite number of modes from the gravity wave branch which can propagate energy to infinity, which was not the case in the Beta plane model, is not a consequence of the spherical geometry but rather of our having used a primitive equation model.

If we now look at Fig. 1 for a fixed $\bar{\Omega}<0$ ($q<0$) we find that contrary to the Beta plane model we have not only trapped modes in the easterlies but also propagating modes ($\varepsilon>10$). Again this is not related to the spherical geometry but to the fact that we are using a primitive equation model. These propagating modes were also absent from a filtered model in spherical geometry presented by Dickinson (1968). With their large values of ε they tend to be trapped near the equator, except perhaps for the Kelvin wave which has a smaller ε for a given $\bar{u}(45°)$.

We will see in the sequel that there is at least one important difference between the present results and those of the Beta plane model which is directly related to the spherical geometry. Before doing so let us first look at the structure of a few of the geopotential eigenfunctions, or Hough

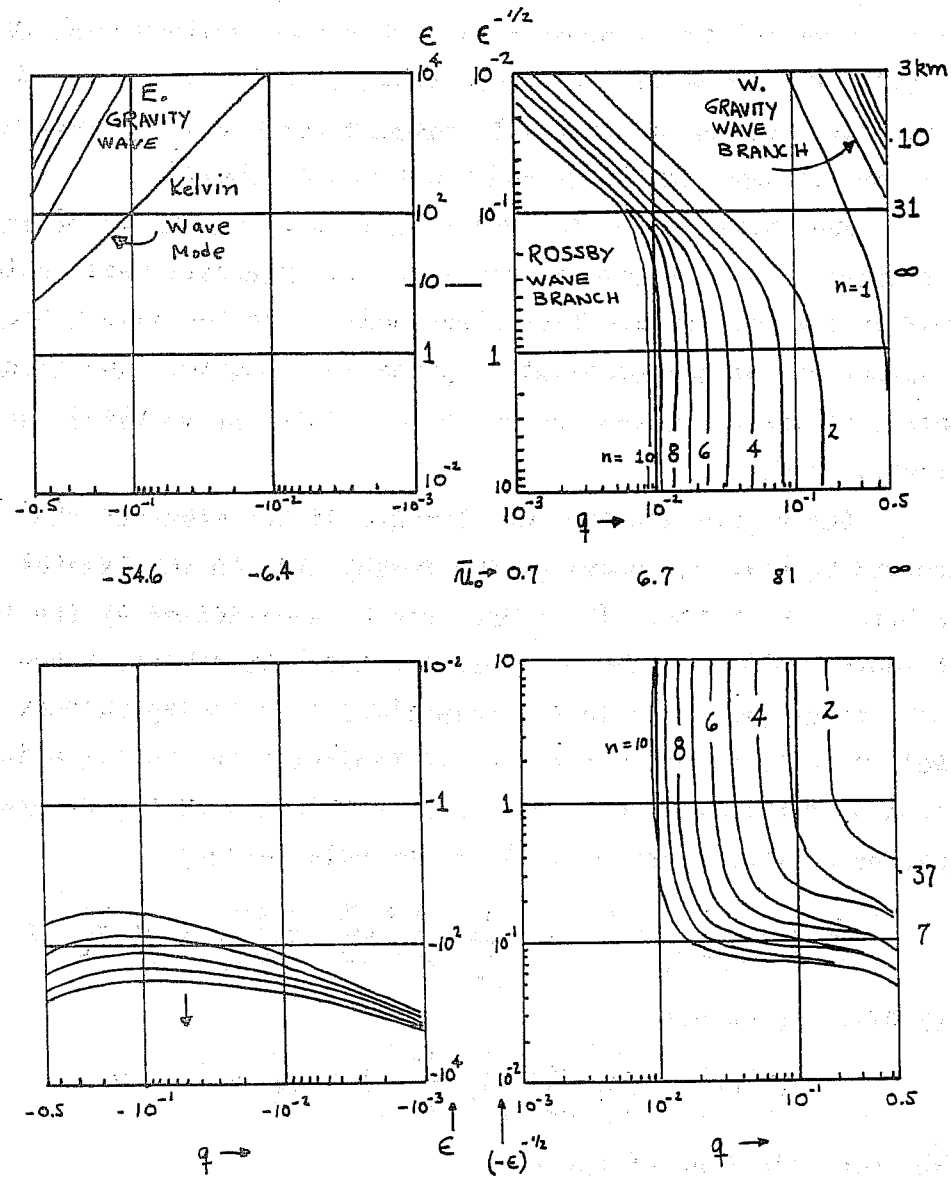

Fig. 1. $\epsilon^{-1/2}$ as a function of $q = m\bar{\Omega}/2(\bar{\Omega} + \Omega)$ for several horizontal modes denoted by the index n for zonal wavenumber 1. Some values of ϵ are also given, as well as a few corresponding values of the vertical wavelength for the propagating modes ($\epsilon \gtrsim 10$) and the "penetration depth" for some trapped modes (r. h. s. of diagram). $\bar{u}_o$ is the value of the mean zonal wind ($m\ s^{-1}$) at latitude 45° (Adapted from Longuet-Higgins, 1968, Figs. 2 and 17).

functions. In Fig. 2, adapted from LH, we show the Hough functions for the Rossby wave branch of Fig. 1, for zonal wave number m = 1. For a given ε only the first four meridional modes are shown as functions of latitude. The solutions were normalized so that all modes have the same amount of energy over the sphere. Let us fix our attention on a given mode, say n = 2. The figure shows how its structure changes as ε changes, i.e. (from Fig. 1) as $\bar{u}(45°)$ changes. Thus for ε = 1 (the wave is therefore trapped) the geopotential has a broad structure with a maximum amplitude near 60°. As $\bar{u}(45°)$ decreases in Fig. 1 the value of ε increases and when it passes 10 the wave becomes a vertically propagating mode. As this happens the geopotential wave amplitude maximum moves southward.

The above change in wave structure as the speed of the mean zonal wind changes is a feature of the spherical geometry model which was not found in the midlatitude Beta plane model. In the latter the horizontal structure of the geopotential is given by sinusoidal functions of y (latitude) which are independent of $\bar{u}$. Only the vertical structure is affected by $\bar{u}$.

Let us now compare the strength of the westerly wind $\bar{u}$ which is required to trap the modes of the Rossby type in the present model versus the Beta plane model. The comparison is complicated by the fact that the latitudinal width of the Beta plane channel is arbitrary and that width is an important parameter in the comparison. Following Charney and Drazin (1961) we will formally replace the Laplacian in the linearized Beta plane potential vorticity equation by its spherical geometry counterpart. The equation is (see equation (37) of preceding notes)

$$\left(\frac{\partial}{\partial t} + \bar{u}\frac{\partial}{\partial x}\right)\left[\nabla^2\psi' + \frac{f_0^2}{\rho_0}\frac{\partial}{\partial z}\left(\frac{\rho_0}{N^2}\frac{\partial \psi'}{\partial z}\right)\right] + \beta\frac{\partial \psi'}{\partial x} = 0. \qquad (13)$$

With $\partial/\partial t = 0$ we get

$$\nabla^2\psi' + \frac{f_0^2}{\rho_0}\frac{\partial}{\partial z}\left(\frac{\rho_0}{N^2}\frac{\partial \psi'}{\partial z}\right) + \frac{\beta}{\bar{u}}\psi' = 0 \qquad (14)$$

which has solutions of the form

$$\psi' = \Psi(z)\, P_n^m(\varphi)\, e^{im\lambda}$$

with the vertical structure equation

$$\frac{f_0^2}{\rho_0}\frac{\partial}{\partial z}\left(\frac{\rho_0}{N^2}\frac{\partial \Psi}{\partial z}\right) + \left[\frac{\beta}{\bar{u}} - \frac{n(n+1)}{a^2}\right]\Psi = 0. \qquad (15)$$

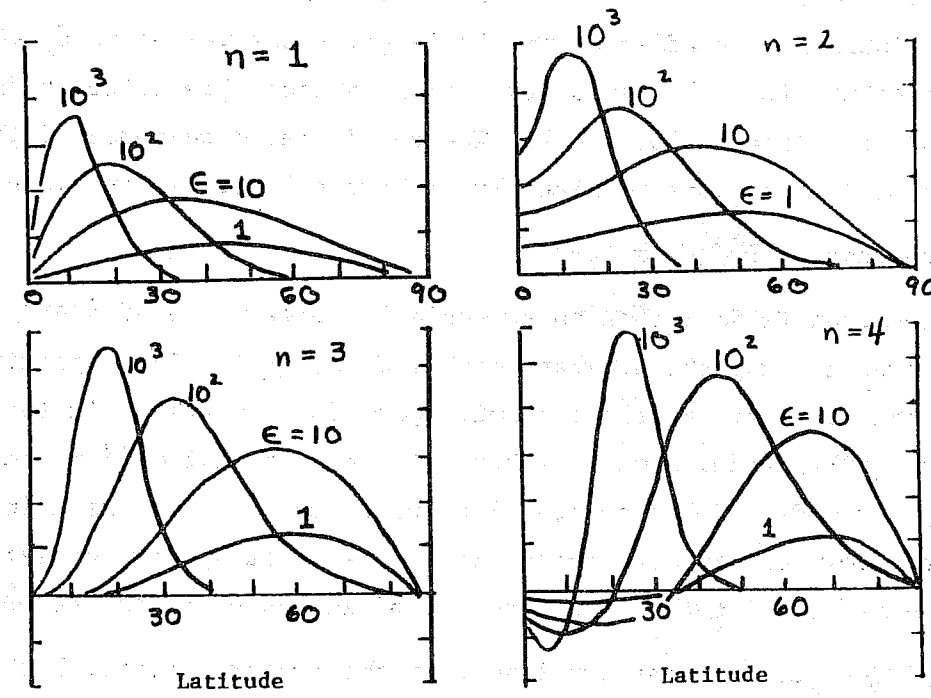

Fig. 2. Horizontal structure of the height field (Hough functions) for zonal wavenumber 1, n = 1-4, for different values of the eigenvalue ε (Adapted from Longuet-Higgins, 1968, Fig. 10).

Thus K^2, the square of the horizontal wavenumber, in the original equation (equation (40) of preceding lecture) has been replaced by $n(n+1)/a^2$. Proceeding as before we find that the waves are trapped for $\bar{u}<0$ and for

$$\bar{u} > \frac{\beta}{n(n+1)/a^2 + f_0^2/4H^2N^2} = u_c \,. \qquad (16)$$

The values of u_c for a few values of n are shown in Table 1 in the column "Beta plane analogue".

We have seen that in the spherical geometry model trapping occurs when $\varepsilon \lesssim 10$. From LH's Table 5 with $\varepsilon = 10$ we obtain the corresponding value of q and hence $\bar{u}(45°)$ which just traps the various modes. The results are given in Table 1. In addition the Table gives the values of $\bar{u}_c$ obtained by Dickinson (1968) for a filtered model on a sphere. The latter model can also be found in Holton (1975, p.46). The meridional dependence of the stream function in that case is given by prolate spheroidal wave functions $K_n^m(\varphi)$, which tend to $P_n^m(\varphi)$ as $\varepsilon \to 0$.

We see from Table 1 that an exceedingly large value of $\bar{u}(45°) = 1583$ ms^{-1} is required to trap the gravest Hough mode $H_1^1(\varphi)$. The approximations provided by the other two models are quite poor in this case. In the Beta plane analogue (BPA) model a much weaker value of $\bar{u} = 94.6$ ms^{-1} is required. As expected, for modes with a shorter horizontal scale, i.e., as n increases, the BPA model provides a better approximation, especially for the larger values of n - m (recall that n - m = number of zeroes of P_n^m in the open interval $-\pi/2<\varphi<\pi/2$). We can conclude from the comparison that both spherical models, which account for the full variation of the Coriolis parameter with latitude, allow waves to propagate through stronger westerlies than the Beta plane analogue model in which f is kept constant except in the advection of planetary vorticity.

TABLE 1

The westerly zonal wind in ms^{-1} at 45°N beyond which stationary forced modes of the Rossby type are trapped near the forcing. (Adapted in part from Dickinson, 1968).

Zonal wave number m	Two-dimensional index n	P.E. model on sphere	Dickinson's approximate model	Beta plane analogue
1	1	1583.0	400.6	94.6
1	2	77.2	83.2	60.0
1	3	43.2	44.8	38.7
1	4	27.0	28.8	26.3
2	2	144.9	125.0	60.0
2	3	49.2	50.2	38.7
2	4	29.6	30.0	26.3
3	3	62.4	59.3	38.7
3	4	31.9		26.3
4	4	35.5		26.3
5	5	23.1		18.8

2. Some Effects of Horizontal Shear in the Basic State

To appreciate how horizontal variations in $\bar{u}$ affect the propagation of stationary forced planetary waves we will first return to the Beta plane formulation. Subsequently we will present numerical results obtained by Simmons (1978) using a spherical geometry model with various meridional profiles of $\bar{u}$.

When $\bar{u} = \bar{u}(y,Z)$ the inviscid Beta plane potential vorticity equation (above the region of diabatic heating) for a perturbation stream function of the form

$$\psi'(x,y,z) = Re\, \Psi(y,z)\, e^{ikx}$$

is

$$\frac{1}{\rho_0}\frac{\partial}{\partial z}\left(\frac{\rho_0 f_0^2}{N^2}\frac{\partial \Psi}{\partial z}\right) + \frac{\partial^2 \Psi}{\partial y^2} + \left(\frac{1}{\bar{u}}\frac{\partial Q}{\partial y} - k^2\right)\Psi = 0 \qquad (17)$$

where

$$\frac{\partial Q}{\partial y} = \beta - \frac{\partial^2 \bar{u}}{\partial y^2} - \frac{1}{\rho_0}\frac{\partial}{\partial z}\left(\frac{\rho_0 f_0^2}{N^2}\frac{\partial \bar{u}}{\partial z}\right) \qquad (18)$$

is the meridional gradient of the basic state potential vorticity. We note again that if $\bar{u} = 0$ where $\partial Q/\partial y \neq 0$, (17) is singular and it is seen that in that case the shear (horizontal or vertical) can lead to possibly complex and interesting effects on the wave solution.

Let us now look at the effect of the term $\partial^2\bar{u}/\partial y^2$ on the wave propagation. Following Simmons (1974) we let

$$\bar{u}(y,z) = Y(y)\,\hat{z}(z)\,u_0 \qquad (19)$$

$$\beta = \beta_0 Y(y) + \text{correction} \qquad (20)$$

with $Y = 0$ at the southern and northern walls of the Beta plane. As he has shown, a good approximation to the wave solution Ψ can be obtained at large heights for typical $\bar{u}$ profiles $Y(y)$ by keeping only the first term on the right-hand side of (20). With this approximation (17) takes the form

$$\frac{1}{\rho_0}\frac{\partial}{\partial z}\left(\frac{\rho_0 f_0^2}{N^2}\frac{\partial \Psi}{\partial z}\right) + \frac{\partial^2 \Psi}{\partial y^2} + \left[\frac{\beta_0}{u_0 \hat{z}} - \frac{1}{Y}\frac{\partial^2 Y}{\partial y^2} - \frac{1}{\hat{z}}\frac{1}{\rho_0}\frac{d}{dz}\left(\frac{\rho_0 f_0^2}{N^2}\frac{d\hat{z}}{dz}\right) - k^2\right]\Psi = 0. \qquad (21)$$

Contrary to (17) this equation is separable. The horizontal and vertical structure equations are found by letting

$$\Psi(y,z) = \Psi_H(y)\,\Psi_V(z). \qquad (22)$$

They are

$$\frac{d^2\Psi_H}{dy^2} - \left(\frac{1}{Y}\frac{d^2Y}{dy^2} + k^2 - \epsilon\right)\Psi_H = 0 \tag{23}$$

$$\frac{1}{\rho_0}\frac{d}{dz}\left(\frac{\rho_0 f_0^2}{N^2}\frac{d\Psi_V}{dz}\right) + \left[\frac{\beta_0}{\bar{u}_0}\frac{1}{\hat{z}} - \frac{1}{\hat{z}}\frac{1}{\rho_0}\frac{d}{dz}\left(\frac{\rho_0 f_0^2}{N^2}\frac{d\hat{z}}{dz}\right) + \epsilon\right]\Psi_V = 0. \tag{24}$$

By inspection of (23) we see that

$$\Psi_H(y) = Y$$

$$\epsilon = k^2$$

is a solution. In other words for that solution the meridional structure of the wave is the same as that of $\bar{u}$.

In Charney and Dragin's (1961) Beta-plane model where $\bar{u}$ is independent of latitude, the vertical structure equation is

$$\frac{1}{\rho_0}\frac{d}{dz}\left(\frac{\rho_0 f_0^2}{N^2}\frac{d\Psi_V}{dz}\right) + \left[\frac{\beta}{\bar{u}(z)} - \frac{1}{\bar{u}}\frac{1}{\rho_0}\frac{d}{dz}\left(\frac{\rho_0 f_0^2}{N^2}\frac{d\bar{u}}{dz}\right) - (k^2+l^2)\right]\Psi_V = 0 \tag{25}$$

where l^2 is the meridional wavenumber of ψ'. By comparison of (24) and (25) we see that the effect of the horizontal shear in $\bar{u}$ is to reduce the wavenumber in the vertical structure equation from $k^2 + l^2$ to k^2. This clearly leads to an enhancement of the penetration of the waves forced from below. The same conclusion was reached by Rutherford (1969) who had also approximated the β term as above. It was Simmons (1974) who discussed the accuracy of the approximation. We note finally that the result that the wave amplitude tends to be a maximum at the latitude where $\bar{u}$ is a maximum is in agreement with observations in the lower stratosphere (Hirota and Sato, 1969). It does not quite agree, on the other hand, with observations of the middle mesosphere ($Z \approx 60$ km) by Hirota and Barnett; at that altitude the observed wave amplitude maximum is north of the mean zonal wind maximum. We will return to this point when we discuss results obtained by Simmons (1978) with a spherical geometry model.

The singular line. We will now present some results due to Simmons (1974)

on the horizontal and vertical propagation of forced waves in a zonal flow containing a singular line (where $\bar{u} = 0$). The $\bar{u}$ profile is independent of height but varies with y on the Beta plane as shown in Fig. 3. At the lower boundary $Z = Z_o$ the ψ' wave is forced by specifying $\psi'(Z_o)$ to have the same meridional profile as $\bar{u}$ in $0 < y/L < 2$. For $y < 0$ he set $\psi'(Z_o) = 0$. The meridional cross section of the ψ' amplitude for zonal wave number 2 is shown in the upper part of Fig. 4.

To reveal the influence of the singular line the wave structure was recomputed, this time with a rigid wall at $y = 0$, in which case the singular line is effectively removed from the problem. The result is shown in the lower part of Fig. 4. It is clear that for $y > 0$ the results are quite similar. For both models, it should be noted, the solution was obtained analytically. In the model with a singular line the solutions north and south of the singularity were connected by invoking viscous effects rather than nonlinear effects. The results obtained with a barotropic model in the preceding set of notes (see also Dickinson, 1968) indicate that wave energy should be absorbed at the singular line. The singular line, acting as a sink of energy for the forced wave, should lead to an attenuation of the wave amplitude with height in comparison to the case without singular line. As can be seen from Fig. 4 this effect here is quite small. From Simmon's (1974) discussion it seems that the difference between his results and those predicted by Dickinson is due to the fact that the separation constant appearing in the horizontal and vertical structure equations is not real as assumed by Dickinson.

The above comparison may well give the impression that in forced wave problems the troublesome singular line can safely be replaced by a rigid wall if one is interested only in the region of mean westerlies. Matters are not so simple, however, as seen from Fig. 5. In this case the stream function phase is also shown as well as the wave momentum flux. We see that the momentum flux north of the singular line is positive, indicating a flux of energy towards the singular line. In agreement with the above the wave tilts westward with decreasing latitude, in qualitative agreement with observations. The solution of a model with a rigid wall at $y = 0$ is not shown but we can safely expect that the reflection at the wall would lead to a zero momentum flux at and near the wall with the necessary north-south orientation of the phase lines. It is possible that in the region of maximum wave amplitude the

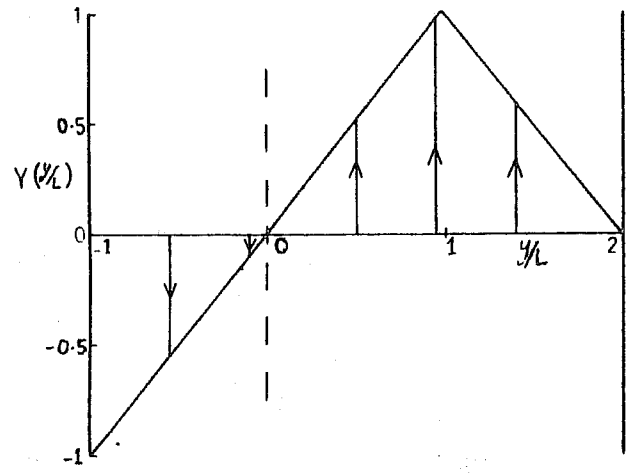

Fig. 3. The latitudinal dependence of the mean zonal wind profile used to obtain the wave structures shown in Fig. 4 (After Simmons, 1974).

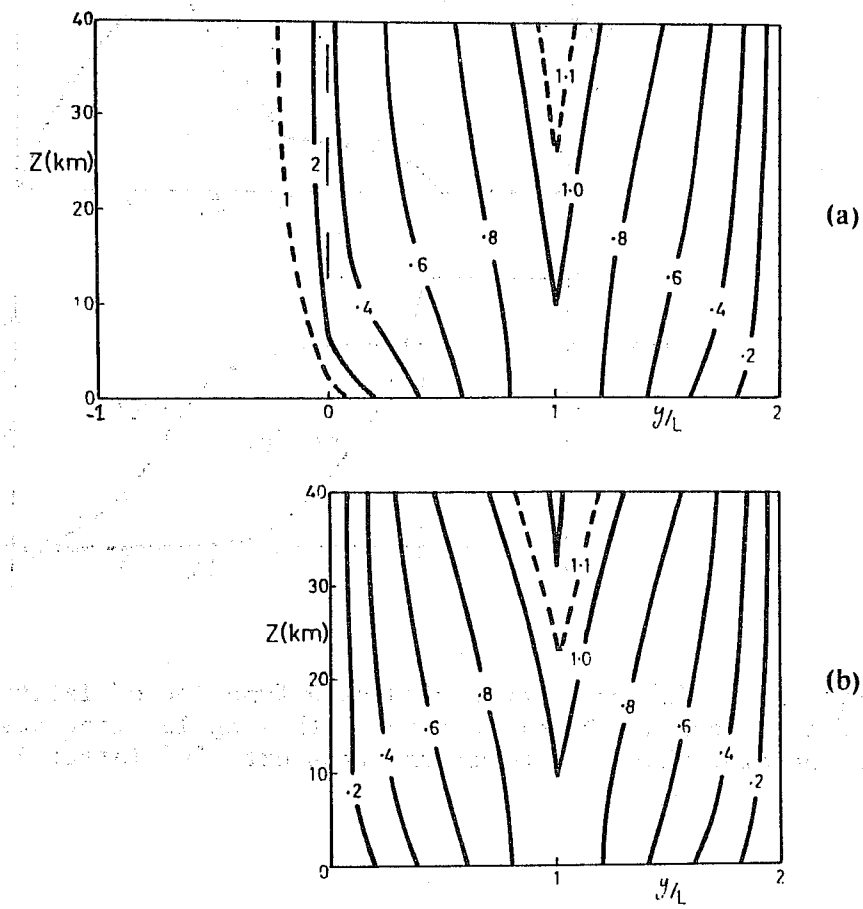

Fig. 4. Latitude-height section of the amplitudes of zonal wavenumber 2 disturbances. Upper: with wall at y = -L and singular line absorbtion. Lower: with wall at y = 0, without singular line absorbtion (After Simmons, 1974).

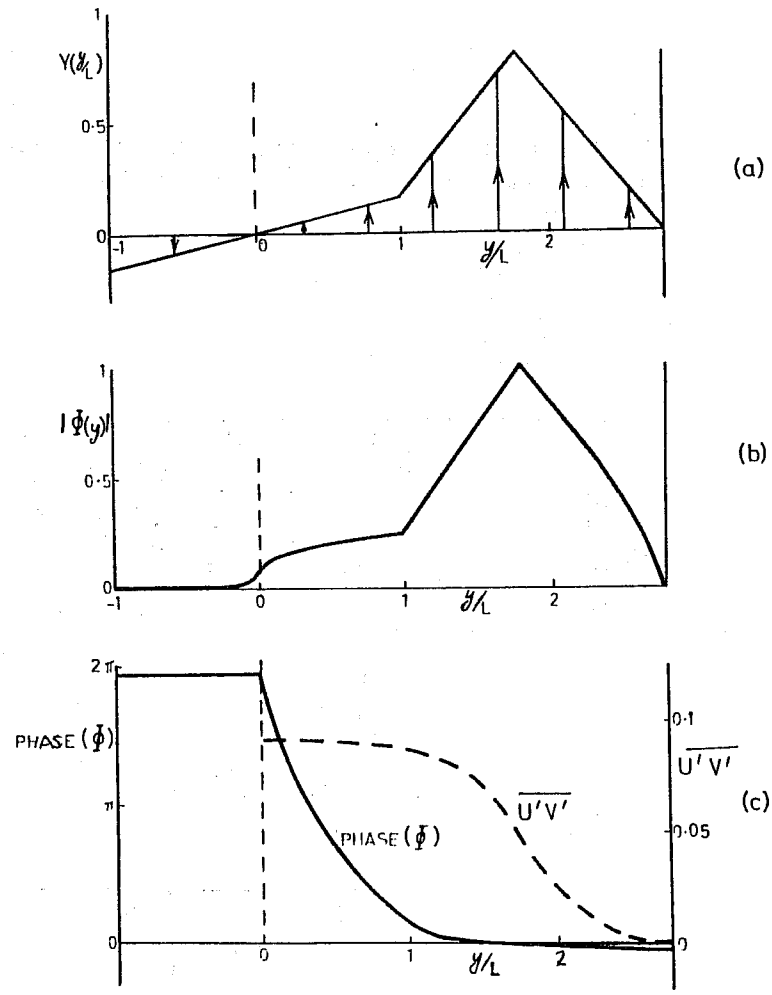

Fig. 5. (a) Mean zonal wind as a function of latitude. (b) Amplitude of a typical height disturbance with singular line absorbtion. (c) Corresponding phase and momentum transport u'v' (After Simmons, 1974).

wave structures with and without a wall at y = 0 would be in reasonable agreement both in amplitude and phase since even the model with singular line shows no wave tilt there. Near the singular line, however, the wall would lead to a different solution.

When numerical methods (finite differences or expansion in basis functions) are used to solve the singular potential vorticity equation it is not clear how the singularity is to be handled. It has been customary (c.f. Matsuno, 1970; Beaudoin and Derome, 1976; Schoeberl and Geller, 1977; Simmons, 1978) to remove the singularity by introducing some dissipation. This leads to wave energy absorption at the singular line and to the north-east to south-west phase tilt of the wave in the mean westerly region. This phase tilt is in qualitative agreement with observations but it is not clear how to formulate the dissipation to obtain quantitative agreement. It is possible that the nonlinear terms play a significant role near the singular line and that they must be considered if quantitative agreement with observations is to be achieved. Finally we note that according to calculations by Schoeberl and Geller (1976), simply locating the singularity between two grid points without introducing dissipative effects leads to a wave reflection at the singular line (at least in the barotropic vorticity equation).

$\bar{u} = \bar{u}(\varphi)$, spherical geometry. To get some further insight on the effect of horizontal shear in the mean zonal flow on forced waves, we can turn to some results obtained by Simmons (1978). He used a primitive equation model in spherical coordinates (see (1) through (4)) in which the mean zonal velocity $\bar{u}$ is a function of latitude only. Such a model has separated solutions. For an isothermal basic state the vertical structure equation is simple and can be solved analytically. The horizontal structure of the solution was obtained by expanding the dependent variables in terms of associated Legendre polynomials. When a singular line (latitude) was present the series were found to converge only if dissipation was included and so a bi-harmonic diffusion of vorticity, divergence and temperature was introduced.

Simmons computed the wave structures for a number of zonal wind profiles, some of which are shown in Fig. 6. The broad jet represented by the solid line in Fig. 6(a) is given by

$$\bar{u} = u_{max} \sin 2\varphi$$

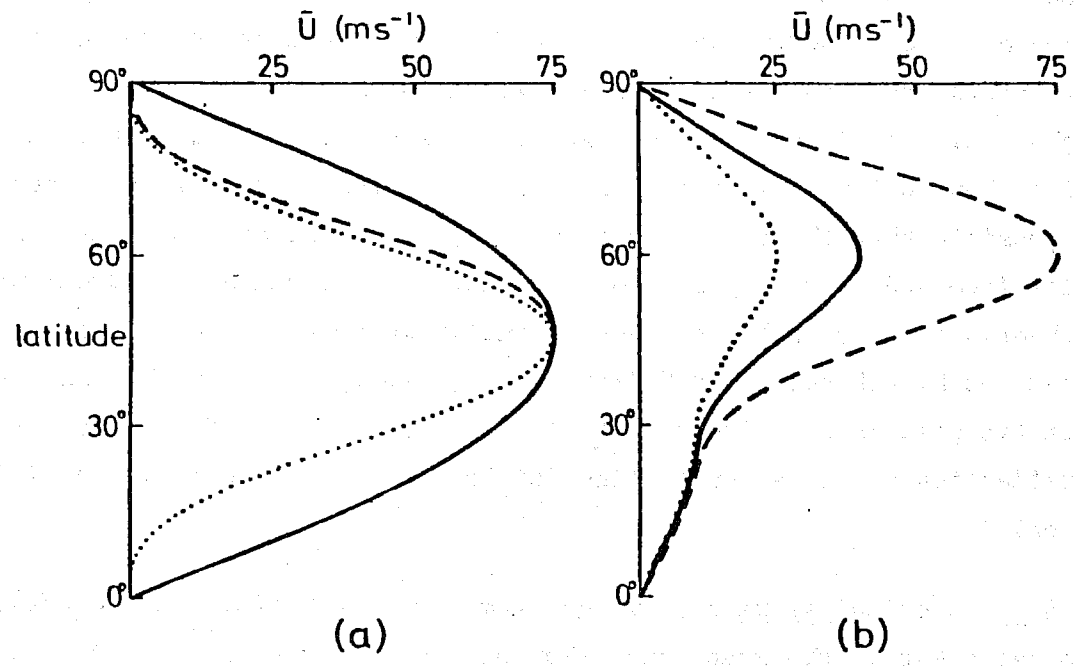

Fig. 6. Some mean zonal wind profiles taken to be representative of (a) the upper stratosphere and lower mesosphere and (b) the lower stratosphere. Winds are easterly in the Southern Hemisphere (After Simmons, 1978).

with southern hemisphere easterlies of similar strength to the winter northern hemisphere westerlies. For the profiles of Fig. 6(b) the southern hemisphere has broad easterlies with maximum strength of 10 to 12 ms^{-1}.

In the sequel we will discuss only that horizontal mode which has the greatest penetration in the vertical. Fig. 7 illustrates the horizontal structure of that mode when the solid curve of Fig. 6(a) is used for $\bar{u}(\varphi)$. It is particularly interesting to note that while the geopotential wave amplitude is concentrated in the high latitudes (maximum at 58°N) the eddy velocity reaches a maximum at 10°N, with a secondary maximum at the pole. The large value of $\vec{V}'$ at 10°N reflects the quasi-geostrophic nature of the flow and the decrease of the Coriolis parameter with decreasing latitude.

If we follow the dashed line in Fig. 7 we find that the wave tilts westward by about 135 degrees from 80°N to 20°N. This is in good agreement with observations by Hirota and Barnett (1977) of mean monthly wave number one (in temperature) in winter at an altitude of about 62 km. The fact that the maximum in the wave amplitude lies to the north of the jet maximum is also in agreement with observations by Belmont et al. (1975) discussed by Hirota and Barnett.

The horizontal phase tilt and the accompanying southward wave energy flux is clearly a consequence of the viscous critical layer. In his analytical Beta plane study Simmons (1974) had found that the wave absorption at the critical latitude did not affect significantly the vertical penetration of the wave. Here the results are quite different in that Simmons found the wave to be significantly attenuated in the vertical by its loss of energy in the viscous critical layer.

When the sharper jets of Fig. 6(b) were used (typical of lower stratosphere) Simmons found that, as demonstrated by Matsuno (1970) and himself in 1974, the wave amplitude maximum tends to be collocated with the jet maximum, especially for strong jets. It was found, however, that the horizontal tilt of the wave was much too large. Simmons believes that this may be due to the neglect of the vertical curvature in $\bar{u}$ which reduces the latitudinal gradient of mean potential vorticity in middle latitudes, and acts to reduce the southward energy propagation. This tentative explanation could be verified by generalizing the model to allow for vertical shear in the mean zonal flow.

3. Propagation through Horizontal and Vertical Shear

Matsuno (1970) has studied the propagation of stationary small ampli-

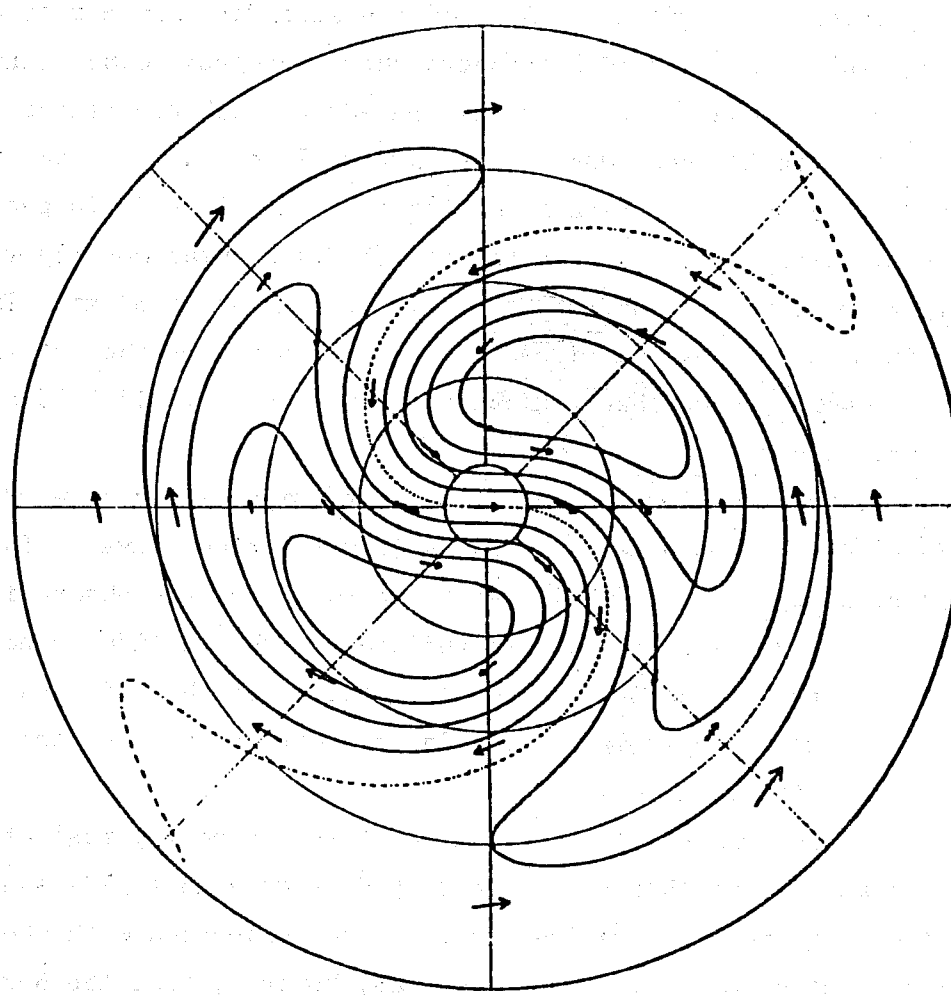

Fig. 7. Perturbation velocities and geopotential for a zonal wavenumber 1 disturbance to the zonal flow given by the solid curve in Fig. 6(a). This is the mode with the greatest penetration in the vertical. Note that the velocity maximum occurs at 10°N. The contour interval is 0.2 of the maximum value and the zero contour is dashed. (After Simmons, 1978).

tude forced waves in a background flow varying in latitude and height. He started from the vorticity and thermodynamic equations in spherical coordinates written as

$$\left(\frac{\partial}{\partial t}+\bar{\Omega}\frac{\partial}{\partial\lambda}\right)\zeta' + v'\frac{1}{a}\frac{\partial}{\partial\varphi}\left(f+\bar{\zeta}\right) = 2\Omega\sin\varphi\,\frac{1}{\rho_0}\frac{\partial}{\partial z}\left(\rho_0 w'\right) \tag{26}$$

$$\left(\frac{\partial}{\partial t}+\bar{\Omega}\frac{\partial}{\partial\lambda}\right)\frac{\partial\phi'}{\partial z} - 2\Omega\sin\varphi\,(a\cos\varphi)\frac{\partial\bar{\Omega}}{\partial z}v' + N^2 w' = 0 \tag{27}$$

where $Z = -H\ln(p/p_s)$, $w = dZ/dt$ and the other symbols are as defined in the appendix. The vertical advection terms in the original momentum equations have been neglected and $\bar{\zeta}$ has been neglected with respect to $2\Omega\sin\varphi$ both on the right-hand side of (26) and in the middle term of (27). The latitudinal gradient of $\bar{\zeta}$, on the other hand, is kept in (26). In order to obtain a potential vorticity equation in terms of the geopotential ϕ' Matsuno evaluated u', v', and ζ' geostrophically (keeping the latitudinal dependence of f) except in the advection of planetary vorticity where he found it necessary to add a higher order correction to v' to have an energetically consistent equation. Thus in the term $v'\partial f/a\partial\varphi$ he used

$$v' = \frac{1}{2\Omega\sin\varphi}\left[\frac{1}{a\cos\varphi}\frac{\partial\phi'}{\partial\lambda} + \bar{\Omega}\frac{\partial u'}{\partial\lambda}\right] \tag{28}$$

where

$$u' = -\frac{1}{2\Omega\sin\varphi}\frac{1}{a}\frac{\partial\phi'}{\partial\varphi}. \tag{29}$$

The first term on the right-hand side of (28) is of course the geostrophic part of v' and the origin of the second term can easily be seen from inspection of (1), the steady linearized u' momentum equation.

Elimination of w' between the vorticity and thermodynamic equations then yields the potential vorticity equation

$$\bar{\Omega}\frac{\partial}{\partial\lambda}\left[\frac{\sin^2\varphi}{\cos\varphi}\frac{\partial}{\partial\varphi}\left(\frac{\cos\varphi}{\sin^2\varphi}\frac{\partial\phi'}{\partial\varphi}\right) + \frac{1}{\cos^2\varphi}\frac{\partial^2\phi'}{\partial\lambda^2} + 4\Omega^2a^2\sin^2\varphi\,\frac{1}{\rho_0}\frac{\partial}{\partial z}\left(\frac{\rho_0}{N^2}\frac{\partial\phi'}{\partial z}\right)\right]$$
$$+ \frac{\partial\bar{q}}{\partial\varphi}\frac{1}{\cos\varphi}\frac{\partial\phi'}{\partial\lambda} = 0 \tag{30}$$

where $\partial\bar{q}/\partial\varphi$ is the latitudinal gradient of mean potential vorticity, i.e.,

$$\frac{\partial\bar{q}}{\partial\varphi} = \left[2(\Omega+\bar{\Omega}) - \frac{\partial^2\bar{\Omega}}{\partial\varphi^2} + 3\tan\varphi\frac{\partial\bar{\Omega}}{\partial\varphi} - 4\Omega^2a^2\sin^2\varphi\,\frac{1}{\rho_0}\frac{\partial}{\partial z}\left(\frac{\rho_0}{N^2}\frac{\partial\bar{\Omega}}{\partial z}\right)\right]\cos\varphi. \tag{31}$$

We note that in the case where $\bar{\Omega}$ = constant (30) can be written as

$$\frac{1}{\cos\varphi}\frac{\partial}{\partial\varphi}\left(\frac{\cos\varphi}{\sin^2\varphi}\frac{\partial\phi'}{\partial\varphi}\right) + \frac{2(\Omega+\bar{\Omega})}{\bar{\Omega}}\frac{1}{\sin^2\varphi}\phi' - \frac{m^2}{\cos^2\varphi}\frac{1}{\sin^2\varphi}\phi'$$

$$+ 4\Omega^2 a^2 \frac{1}{\rho_0}\frac{\partial}{\partial z}\left(\frac{\rho_0}{N^2}\frac{\partial\phi'}{\partial z}\right) = 0 . \qquad (32)$$

By comparison with (6), the ϕ' equation obtained from a primitive equation model, we see that (32) can be obtained from (6) by neglecting $m\bar{\Omega}/2\Omega\sin\varphi$ in comparison to 1. It is clear then that for a given $\bar{\Omega}$ the validity of (32) will break down near the equator. As an example, if $\bar{\Omega}$ is such that $\bar{u}(45°) = 75\ ms^{-1}$ we get $\bar{\Omega}/2\Omega\sin45° = 0.16$ and $\bar{\Omega}/2\Omega\sin\varphi = 1$ at 6.6°N. In the problem actually discussed by Matsuno the breakdown of his equation near the equator is probably not a serious problem since, as we will see, very little wave energy reaches the tropics.

Let us return to the potential vorticity equation (30), in which the latitude and height variations of $\bar{\Omega}$ are retained. If we let

$$\phi' = \mathcal{R}e\, e^{z/2H}\sum_{m=1}^{\infty}\Psi_m(\varphi,z)e^{im\lambda}$$

then each zonal harmonic satisfies

$$\frac{\sin^2\varphi}{\cos\varphi}\frac{\partial}{\partial\varphi}\left(\frac{\cos\varphi}{\sin^2\varphi}\frac{\partial\Psi_m}{\partial\varphi}\right) + l^2\sin^2\varphi\frac{\partial^2\Psi_m}{\partial z^2} + Q_m\Psi_m = 0 \qquad (33)$$

in which

$$l = \frac{2\Omega}{N}a \simeq 46\,km \quad \text{for } N = 2\times10^{-2}s^{-1}$$

$$Q_m = \frac{1}{\bar{\Omega}\cos\varphi}\frac{\partial\bar{q}}{\partial\varphi} - \frac{l^2\sin^2\varphi}{4H^2} - \frac{m^2}{\cos^2\varphi} \qquad (34)$$

Q_m is the index of refraction squared for the anisotropic wave propagation in the φ and Z directions governed by (33).

Because of the division by $\bar{\Omega}$ in (34), equation (33) is singular along any line where $\bar{u} = 0$. Matsuno removed the singularity by introducing two damping mechanisms: a Rayleigh friction in the momentum equations and a Newtonian cooling in the thermodynamic equation. Thus the terms $-\alpha_M\zeta'$ and $-\alpha_T\partial\phi'/\partial Z$ were added to the right-hand sides of (26) and (27) with α_M and α_T

constants. In addition α_M was taken equal to $\alpha_T = \alpha$, with the net result that in the definition of Q_m the factor $1/\bar{\Omega}$ was replaced by $1/(\bar{\Omega}-i\alpha/m)$. A value of $\alpha = 5\times10^{-7}s^{-1} = 1/23.4$ days was used. It should be clear that the new term will play an important role near the singular line where $\bar{\Omega}$ is small, and that it will be unimportant in regions where $|\bar{\Omega}|>>\alpha/m$.

Boundary conditions.

a) At the lower boundary Matsuno specified the observed amplitude and phase of the zonal harmonics in the geopotential at Z = 5 km, for January 1967.

b) At the pole the geometry imposes the condition $\Psi_m = 0$.

c) At the equator the condition $\Psi_m = 0$ was used on the grounds that the singular line further north would prevent the wave energy from reaching the equator, the energy source being concentrated north of the singular line.

d) At the top of the model, located at 65 km, a radiation condition was used.

With these boundary conditions Matsuno solved (33) using finite differences of second order with increments of $\Delta\varphi = 5$ degrees and $\Delta Z = 2.5$ km. The mean zonal wind used to compute Q_m is shown in Fig. 8. It is an idealized distribution of $\bar{u}$ which retains only the main features of the observed distribution in winter. The vertical shear was forced to zero at the top of the model to make it possible to use the radiation upper boundary condition.

In Fig. 9 we have the cross-section of the quantity Q_c, defined by

$$Q_m = Q_c - m^2/\cos^2\varphi \qquad (35)$$

where Q_m is the index of refraction squared for wave number m (see (33) and (34)). It plays an important role in the propagation equation and it will be useful to keep its distribution in mind when interpreting Matsuno's results. The structure of Q_m in (35) can be imagined from Fig. 9 if we note that $1/\cos^2\varphi = 4.0$, 8.6, 38.3 and ∞ at $\varphi = 60°$, 70°, 80° and 90°, respectively. Thus Q_m is negative near the pole for all values of m.

The computed wave structures Ψ_m obtained by Matsuno for zonal wave numbers 1 and 2 are shown in Fig. 10. Recall from the definition of Ψ_m given above (33) that $|\Psi| \propto \rho_o^{1/2}|\phi'|$ so that $|\Psi|$ is proportional to the square root

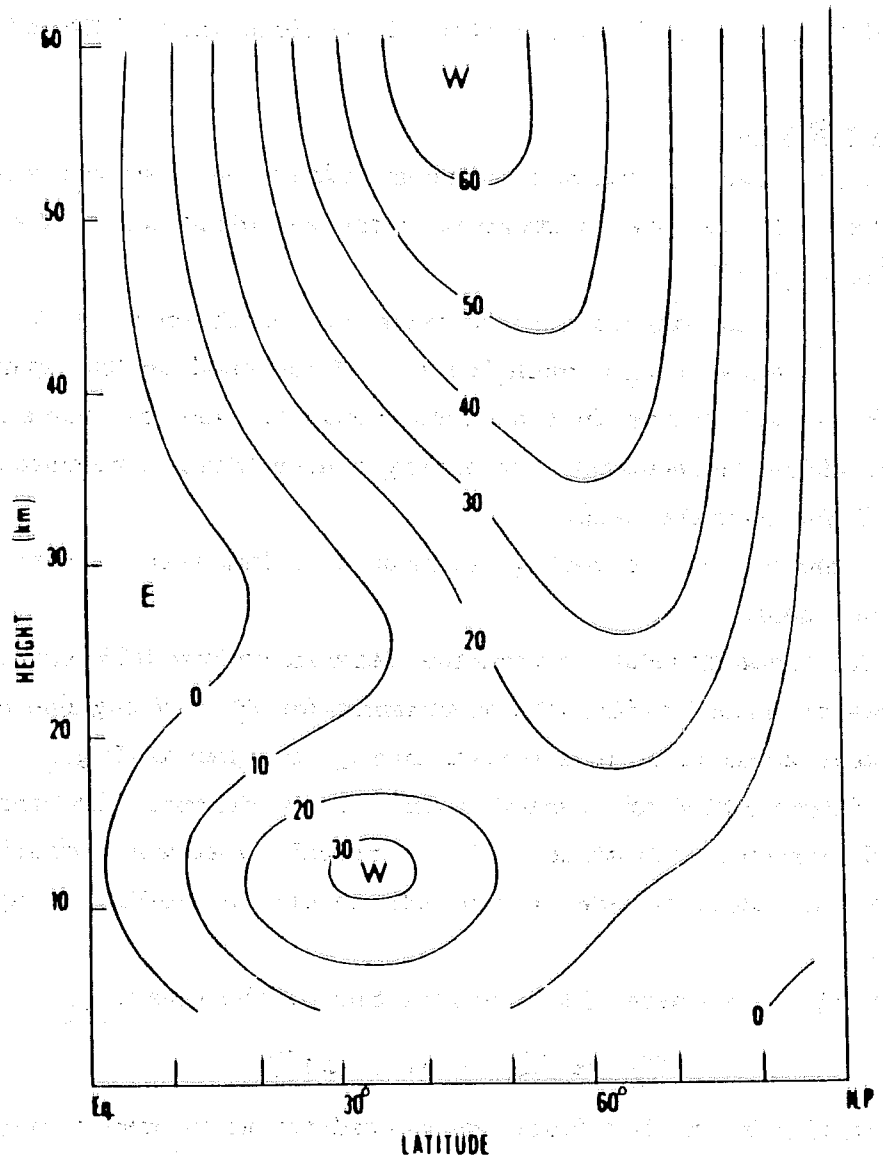

Fig. 8. Latitude-height section of the mean zonal wind (m s^{-1}) (After Matsuno, 1970).

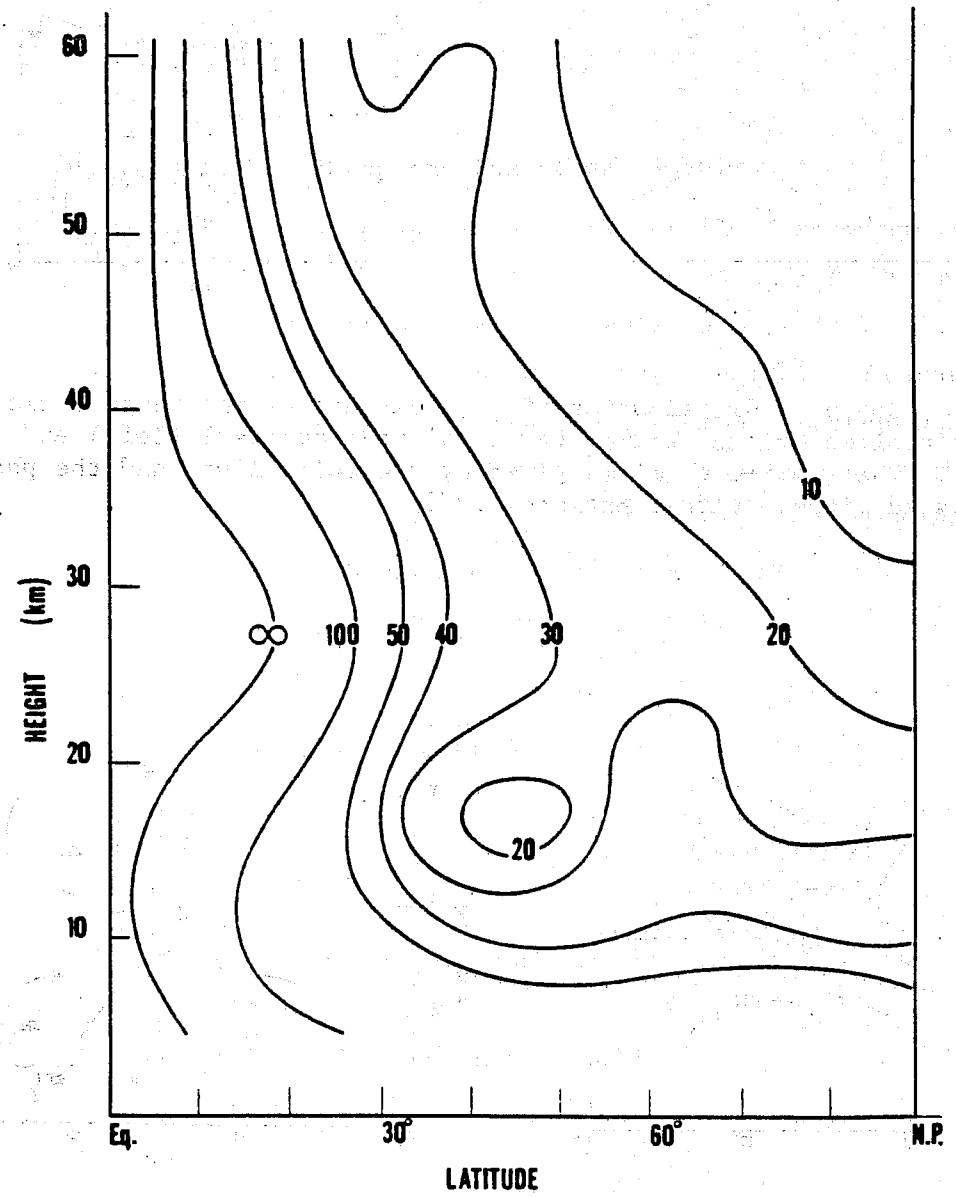

Fig. 9. The function Q_m defined by (34), for m = 0 (after Matsuno, 1970).

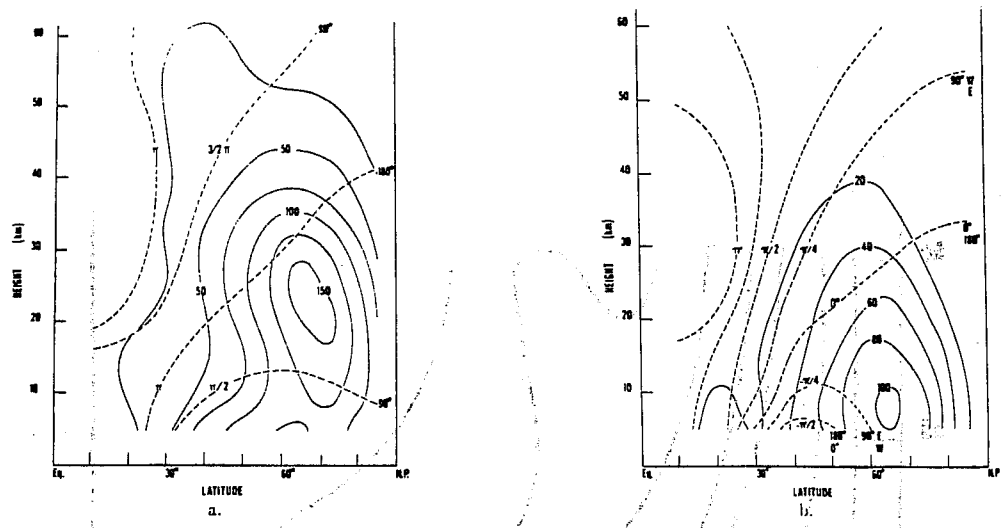

Fig. 10. Computed distribution of $|\Psi|$, defined as the geopotential height multiplied by $\exp(-Z/2H)$, for zonal wavenumbers 1 (left) and 2 (right). The amplitude (m) is given by the solid lines and the phase by the dashed lines. (After Matsuno, 1970).

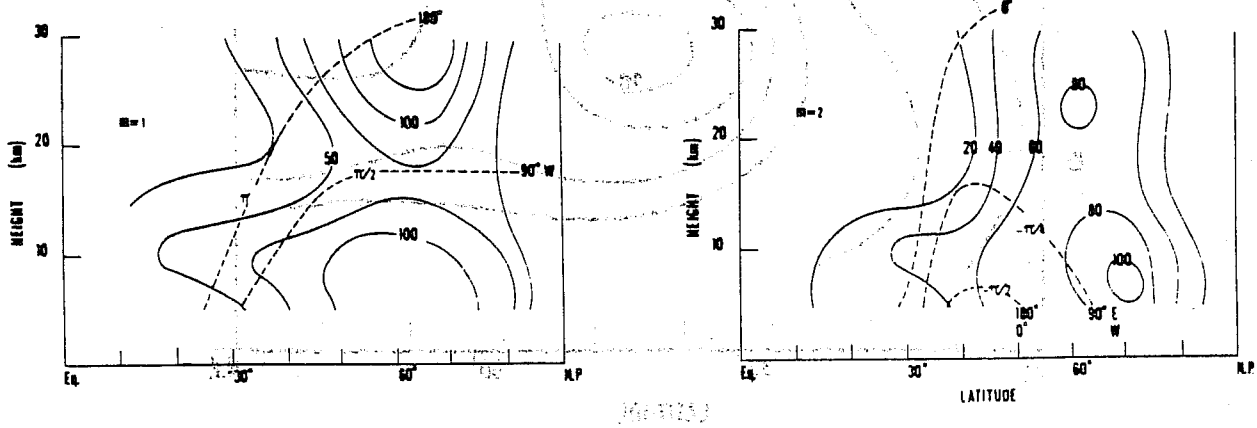

Fig. 11. The observed distributions of amplitude and phase of Ψ for zonal wavenumbers m = 1 and 2 (After Matsuno, 1970).

of energy density. The observed distribution of Ψ below 30 km is shown in Fig. 11.

The computed phase distribution is in reasonable agreement with observations, showing in particular the westward tilt with height indicative of an upward flux of energy. Over most of the domain the horizontal phase tilt is from north-east to south-west which implies a southward propagation of energy. The magnitude and direction of the energy flux were in fact computed by Matsuno and are given in Fig. 12 in vectorial form for the m = 1 wave. It seems that the energy flows around the area of small Q_o in the lower stratosphere, going mainly to the north of it.

Returning to Fig. 10 we see that the computed wave m = 1 has an energy density which increases with height in the lower stratosphere near 70°N. This seems to be a manifestation of some reflection taking place at the upper levels since a purely propagating mode without dissipation would have a constant energy density - dissipation should in fact lead to a decay of energy density away from the source. Matsuno was thus led to propose the schematic picture shown in Fig. 13 as an explanation for the computed amplitude maximum in the stratosphere. The small values of $\partial\bar{q}/\partial\varphi$ in the middle latitudes above the tropospheric jet and the large values of $\bar{u}$ in the upper levels lead to low values of Q_1 in those regions. The low Q_1 regions act as barriers to wave propagation and hence the wave is trapped in a cavity bounded by the above regions and the pole, where Q_1 is negative. When wave energy is injected from below multiple reflections on the "boundaries" of the cavity can take place and a standing wave is set up. Clearly the boundaries are not perfect reflectors since otherwise the net energy flux would vanish; in addition the model has dissipation, a feature which for simplicity was not included in the schematic picture of Fig. 13.

In closing our brief discussion of Matsuno's results, we should point out that while his model reproduced the major features of the observed forced harmonics m = 1 and 2, a number of deficiencies can also be noted. For example, as he himself remarked, the computed m = 2 wave decays too quickly with height, and in that respect Simmon's (1974) model was somewhat more successful. As pointed out by Schoeberl, Geller and Avery (1979) the wave solution is sensitive to the mean zonal wind profile so that Matsuno's use of an idealized $\bar{u}$ distribution may preclude a detailed comparison of his wave structures with observations. Finally it should be kept in mind that very little is known about the amount of wave energy that is actually absorbed

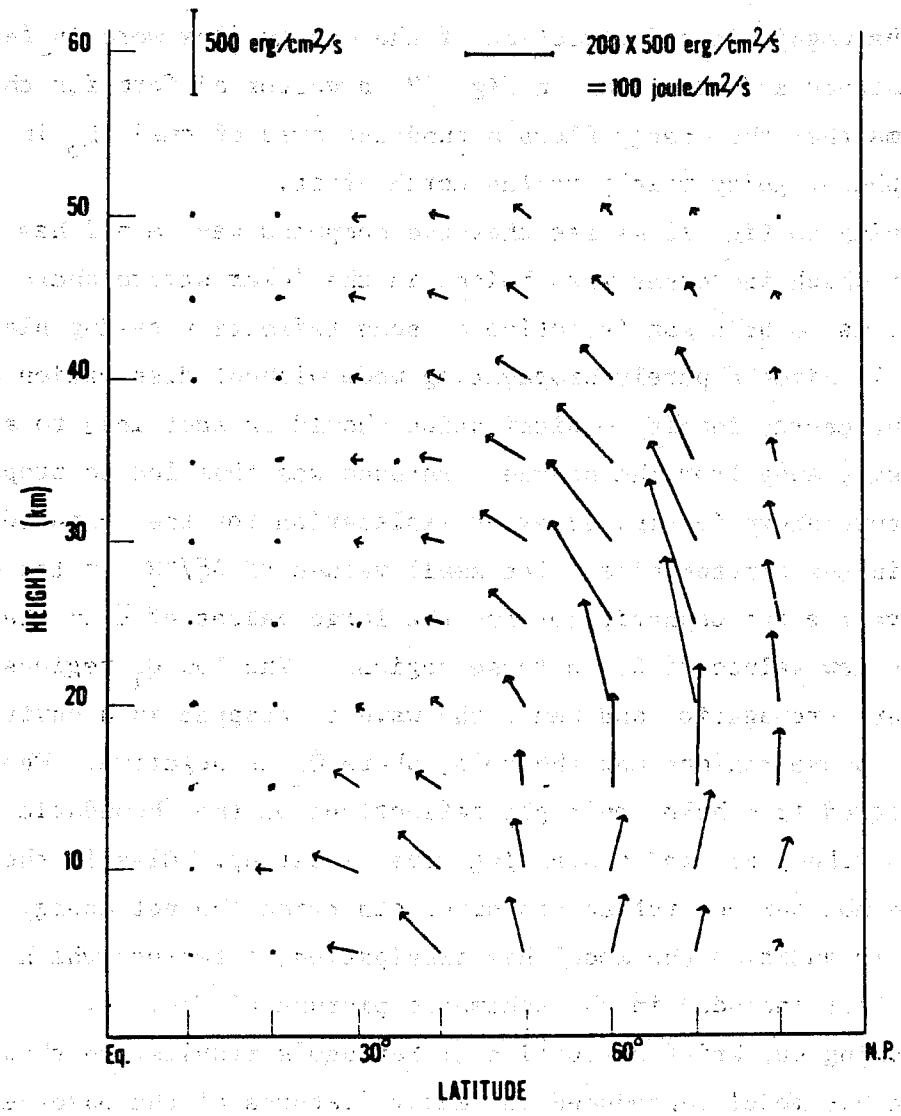

Fig. 12. Computed distribution of energy flow in the meridional plane for zonal wavenumber 1 shown in Fig. 10 (After Matsuno, 1970).

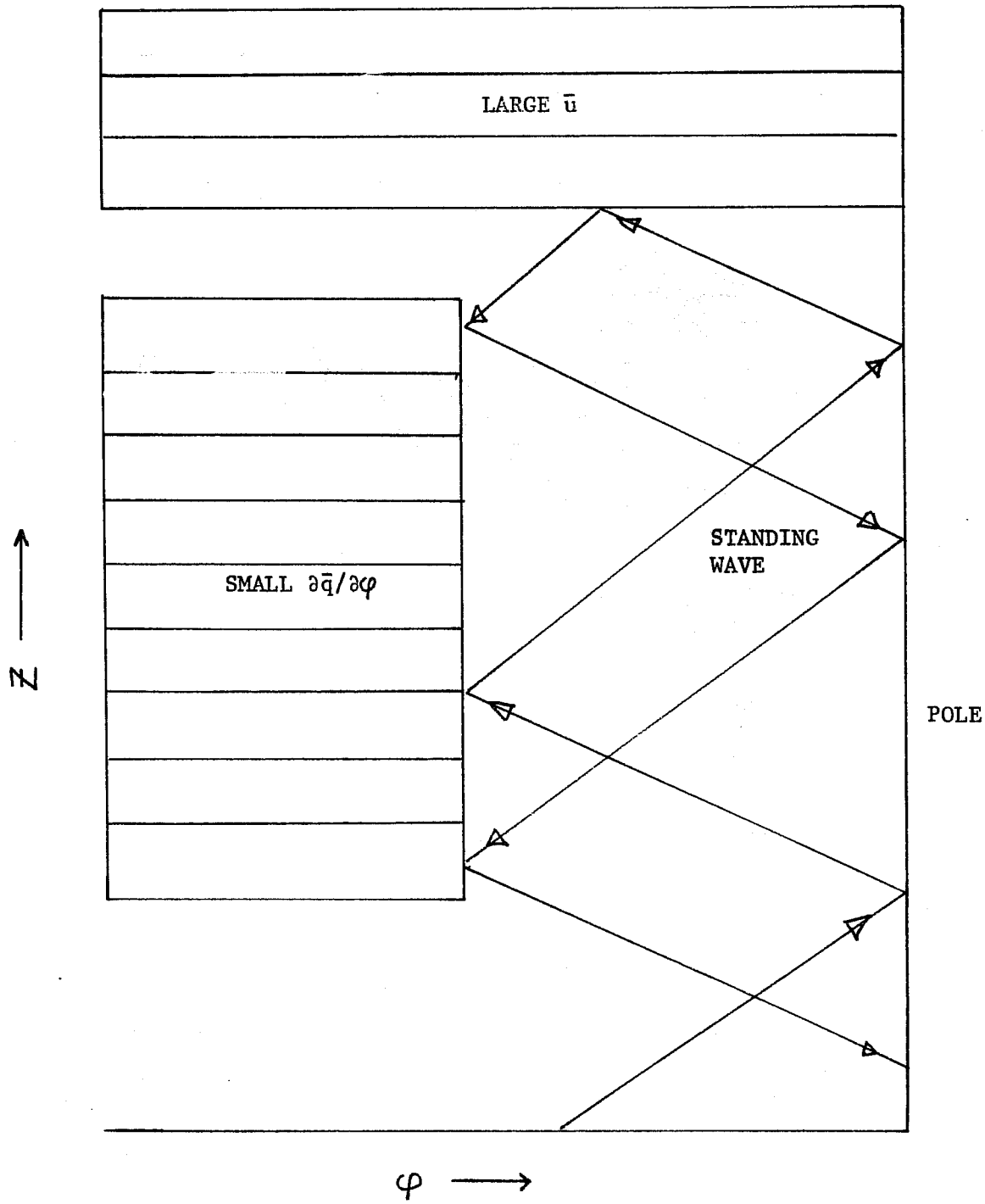

Fig. 13. Schematic representation of the distribution of barriers (hatched) and the resultant wave propagation (Redrawn from Matsuno, 1970).

at the singular line. It is possible that Matsuno's dissipation mechanisms overestimated the energy loss by the wave at the $\bar{u} = 0$ line, in which case the vertical penetration of the waves would have been reduced.

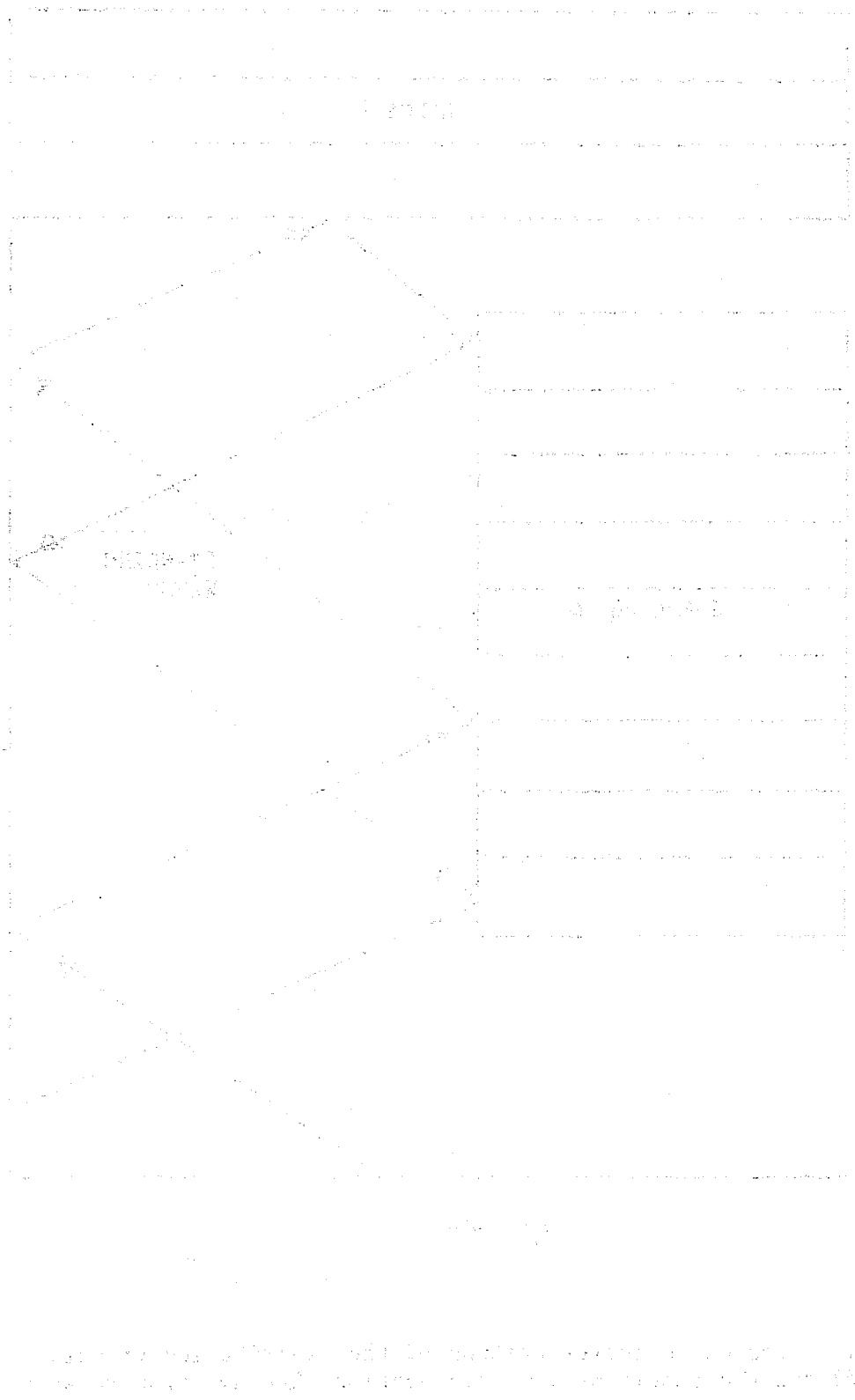

REFERENCES

Beaudoin, C. and J. Derome, 1976: On the modelling of stationary planetary waves. Atmosphere, 14, 245-253.

Belmont, A.D., D.G. Dartt and G.D. Nastrom, 1975: Variations of stratospheric zonal winds, 20-65 km, 1961-1971. J. Appl. Met., 14, 585-594.

Charney, J.G. and P.G. Drazin, 1961: Propagation of planetary-scale disturbances from the lower into the upper atmosphere. J. Geophys. Res., 66, 83-109.

Dickinson, R.E., 1968: On the exact and approximate linear theory of vertically propagating planetary Rossby waves forced at a spherical lower boundary. Mon. Wea. Rev., 96, 405-415.

Hirota, I. and J.J. Barnett, 1977: Planetary waves in the winter mesosphere - preliminary analysis of Nimbus 6 PMR results. Quart. J. Roy. Meteor. Soc., 103, 487-498.

Hirota, I. and Y. Sato, 1969: Periodic variation of the winter circulation and intermittent vertical propagation of planetary waves. J. Meteor. Soc. Japan, 47, 390-402.

Hough, S.S., 1898: On the application of harmonic analysis to the dynamical theory of the tides. II. On the general integration of Laplace's tidal equations. Phil. Trans. Roy. Soc. London, A 191, 139-185.

Longuet-Higgins, M.S., 1968: The eigenfunctions of Laplace's tidal equations over a sphere. Phil. Trans. Roy. Soc. London, A 262, 511-607.

Matsuno, T., 1970: Vertical propagation of stationary planetary waves in the winter Northern Hemisphere. J. Atmos. Sci., 27, 871-883.

Rutherford, I.D., 1969: The vertical propagation of geostrophic waves in a low-order spectral model. Ph.D. thesis, McGill University, Publ. Meteor., No. 92, 122 pp.

Schoeberl, M.R. and M.A. Geller, 1976: The propagation of planetary-scale waves into the upper atmosphere. Aeronomy report No. 70, University of Illinois, Urbana, 269 pp.

____, and ____, 1977: A calculation of the structure of stationary planetary waves in winter. J. Atmos. Sci., 34, 1235-1255.

____, and ____, and S.K. Avery, 1979: The structure of stationary planetary waves in winter: a correction. J. Atmos. Sci., 36, 365-369.

Simmons, A.J., 1974: Planetary scale disturbances in the polar winter stratosphere. Quart. J. Roy. Meteor. Soc., 100, 76-108.

_____, 1978: Some effects of meridional shear and spherical geometry on long stratospheric waves. Quart. J. Roy. Meteor. Soc., 104, 595-614.

APPENDIX

List of New Symbols

q	$m\bar{\Omega}/2(\Omega + \bar{\Omega})$
H_n^m	Hough function
S	$[NH/2a(\Omega + \bar{\Omega})]^2$
α	coefficient of Rayleigh friction and Newtonian cooling in Matsuno's model
ϵ	separation constant
ζ	relative vorticity
χ	potential function
Ω	earth's rotation rate
$\bar{\Omega}$	angular speed of the mean zonal wind = $\bar{u}/a \cos\varphi$
$\overline{(\ )}$	zonal average of ( ), except for $\bar{\Omega}$

THE UPPER BOUNDARY CONDITION IN NUMERICAL MODELS OF FORCED PLANETARY WAVES

Jacques Derome
Department of Meteorology
McGill University
Montreal

THE UPPER BOUNDARY CONDITION IN NUMERICAL MODELS OF FORCED PLANETARY WAVES

1. Introduction

In our discussion of forced wave models we have so far used the classical Somerfeld radiation condition at the upper boundary. In numerical weather prediction and general circulation models, on the other hand, the most frequently used boundary condition at the top of the model is either $\omega \equiv dp/dt = 0$ at $p = 0$ or $d\sigma/dt = 0$ at $\sigma = 0$, where σ = (pressure)/(surface pressure), depending on whether the pressure p or σ is used as the vertical coordinate. We will now look at the differences that arise in the wave structures of a simple model when the boundary condition $\omega(p = 0) = 0$ is used rather than the radiation condition. We will again be concerned with stationary waves forced at the lower boundary. The presentation will be based mainly on papers by Kirkwood and Derome (1977) and Desmarais and Derome (1978); closely related studies can be found in Nakamura (1976) and Bates (1977).

The approach will be to have two numerical models: the first, or reference model, employs the radiation condition at Z = 125 km while the second model uses the upper boundary condition $\omega = 0$ at $p = 0$. Both are Beta plane models in which the mean zonal wind $\bar{u}$ is a function of pressure only. Stationary waves are forced in the two models by specifying the vertical velocity at the lower boundary and the wave structures are then compared to reveal the influence of the upper boundary condition.

2. Model Equations

Our linearized Beta plane vorticity and thermodynamic equations for stationary forced waves with $\bar{u} = \bar{u}(p)$ are

$$\bar{u}\frac{\partial}{\partial x}\nabla^2\psi' + \beta\frac{\partial\psi'}{\partial x} - f_o\frac{\partial\omega'}{\partial p} = 0 \qquad (1)$$

$$\bar{u}\frac{\partial}{\partial x}\frac{\partial\psi'}{\partial p} - \frac{d\bar{u}}{dp}\frac{\partial\psi'}{\partial x} + \frac{\sigma}{f_o}\omega' = -\alpha_R\frac{\partial\psi'}{\partial p} \qquad (2)$$

where $\alpha_R(p)$ is a Newtonian cooling coefficient and the other symbols have their usual meaning. The horizontally averaged temperature in the basic state, T_o, is taken to be independent of pressure, in which case the static stability parameter $\sigma = \sigma_s(p_s/p)^2$ where $\sigma_s = R^2T_o/p_s^2c_p$, p_s = 1000 mb, T_o = 239K.

2.1 P model

In order to simulate conditions in several numerical weather prediction models we use finite differences in the vertical, with equal Δp increments, to solve (1) and (2). The discretization follows the lines of the standard two-level model.

The upper boundary condition is

$$\omega'(x, y, p = 0) = 0 \tag{3a}$$

and the lower boundary forcing is specified by

$$\omega'(x, y, p = p_s) = D \exp(ikx) \cos ly \tag{3b}$$

where k and l are the specified zonal and meridional wavenumbers and D is a constant, arbitrarily set equal to 10^{-9} N $m^{-2}s^{-1}$. The Beta plane is centered at 55°N and k and l are chosen such that the horizontal wavelengths ($2\pi/k$, $2\pi/l$) are equal to the length of the latitude circle at 55°N and 160 degrees of latitude respectively. Our choice for these parameters is based on the fact that we are interested in the largest horizontal scales, which are the most likely to propagate vertically and be affected by the upper boundary condition.

Equations (1) and (2) then have solutions of the form

$$\psi'(x, y, p) = \Psi(p) \exp(ikx) \cos ly \tag{4a}$$

$$\omega'(x, y, p) = \Omega(p) \exp(ikx) \cos ly . \tag{4b}$$

2.2 Reference Model

In the special case where $\bar{u}$ = constant > 0, $\alpha_R = 0$, (1) and (2) have solutions which are proportional to $\exp(Z/2 \pm i\mu Z)$, where μ is a positive constant if $\bar{u}$ is sufficiently small (propagating solution), and $Z = H\ln(p_s/p)$. Such solutions have a constant wavelength in Z whereas if p is chosen as the vertical coordinate they are found to oscillate faster and faster as $p \to 0$. Because we wish to use the radiation upper boundary condition at a high altitude we will use Z as the vertical coordinate in the reference finite difference model, so as to have a uniform vertical resolution, at least in the case of pure propagation. For all cases to be discussed we will use 200 levels between Z = 0 and Z = 125 km so that ΔZ = 0.625 km.

The potential vorticity equation obtained from (1) and (2) leads to the

following vertical structure equation when solutions of the form (4a) are considered:

$$\frac{1}{\rho_0}\frac{d}{dz}\left(\rho_0 \frac{d\Psi}{dz}\right) + \left[\frac{N^2}{f_0^2}\left(\frac{\beta}{\bar{u}} - K^2\right) - \frac{1}{\bar{u}}\frac{1}{\rho_0}\frac{d}{dz}\left(\rho_0 \frac{d\bar{u}}{dz}\right)\right]\Psi$$

$$- \frac{i}{\bar{u}\rho_0}\frac{d}{dz}\left(\rho_0 \frac{\alpha_R}{k}\frac{d\Psi}{dz}\right) = 0 \qquad (5)$$

where $\rho_0 = \rho_s \exp(-Z/H)$, $N^2 = g^2/c_p T_0 = \sigma_s p_s^2/H^2$ is the square of the Brunt-Vaisala frequency and $K^2 = k^2 + l^2$.

Equation (5) is solved subject to the same lower boundary forcing as the P model but at Z = 125 km a radiation condition is used as follows. Above 125 km the flow is assumed adiabatic and the vertical shear of the mean flow is assumed to vanish. Under these conditions (5) has the analytic solution

$$\Psi(z) = Be^{m_1 z} + Ce^{m_2 z} \qquad (6)$$

where

$$\left\{\begin{matrix} m_1 \\ m_2 \end{matrix}\right\} = 1/2H \pm \sqrt{\tfrac{1}{4} - \gamma}\,/H \qquad (7a)$$

$$\gamma = (N^2/f_0^2) H^2 (\beta/\bar{u} - K^2). \qquad (7b)$$

As we have seen earlier, vertical energy propagation is possible only when $\gamma > 1/4$. When that condition holds the solution which propagates energy upward is chosen by setting C = 0 in (6). This results in the boundary condition

$$\frac{d\Psi}{dz} - m_1\Psi = 0 \qquad \text{at} \quad z = 125\ km. \qquad (8a)$$

If $\gamma < 1/4$ we have trapped solutions and energy boundedness at infinity requires that B = 0, which leads to the boundary condition

$$\frac{d\Psi}{dz} - m_2\Psi = 0 \qquad \text{at} \quad z = 125\ km. \qquad (8b)$$

3. Model Behaviour with Simple Basic States

Let us first compare the solutions of our two models when $\bar{u}$ = constant = 20m s^{-1}, $\alpha_R \equiv 0$. In this case we have $\gamma > 1/4$ and the solution is of the propagating type when the Somerfeld radiation condition is employed.

The wave structure computed using the reference model is shown in Fig. 1. The "amplitude" curves shown in sections 3, 4 and 5 refer to the function $|\tilde{\Psi}| = \exp(-Z/2H)|\psi|$, unless otherwise stated. $|\tilde{\Psi}|$ is proportional to the square root of the wave energy density and should be independent of Z in the case of pure propagation. As expected the solution of the reference model shown in Fig. 1 agrees well with the analytic solution of (5). The energy density remains constant and the wave tilts to the west with height (vertical wavelength ≈ 70 km).

The analytic solution to (5) with the present parameters may be written as

$$\Psi(p) = \hat{B}\,(p/p_s)^{\Gamma_1} + \hat{C}\,(p/p_s)^{\Gamma_2} \qquad (9)$$

with

$$\Gamma_1 = -\tfrac{1}{2} - (\tfrac{1}{4} - \gamma)^{1/2}$$

$$\Gamma_2 = -\tfrac{1}{2} + (\tfrac{1}{4} - \gamma)^{1/2}.$$

Applying the boundary condition $\omega' = 0$ at some pressure p_T is equivalent (from the thermodynamic equation) to requiring

$$p_T^2 \left(\frac{d\Psi}{dp}\right)_{p_T} = 0. \qquad (10)$$

Substituting (9) into (10) we get

$$\hat{B}\Gamma_1 \left(\frac{p_T}{p_s}\right)^{\frac{1}{2} - (1/4 - \gamma)^{1/2}} + \hat{C}\Gamma_2 \left(\frac{p_T}{p_s}\right)^{1/2 + (1/4 - \gamma)^{1/2}} = 0. \qquad (11)$$

If we take the limit $p_T \to 0$ we find that both terms tend to zero when $\gamma > 0$ so that the boundary condition $\omega'(p = 0) = 0$ in this case yields no information. Recall from (6) and (7) that $\gamma > 0$ for all propagating modes and also for the deeper external (trapped) modes.

Although the upper boundary condition $\omega'(p = 0) = 0$ does not yield a unique analytic solution, this boundary condition was imposed in the numerical formulation of the P model to demonstrate its effect. It is evident that for $\gamma > 0$ the finite-difference P model would be required to find an approximate solution to a problem for which no unique analytic solution exists.

The numerical sclutions of the P model with 101 and 11 levels are shown in Fig. 1 along with the reference solution. The presence of nodes in the solutions is a clear indication that the numerical model has both

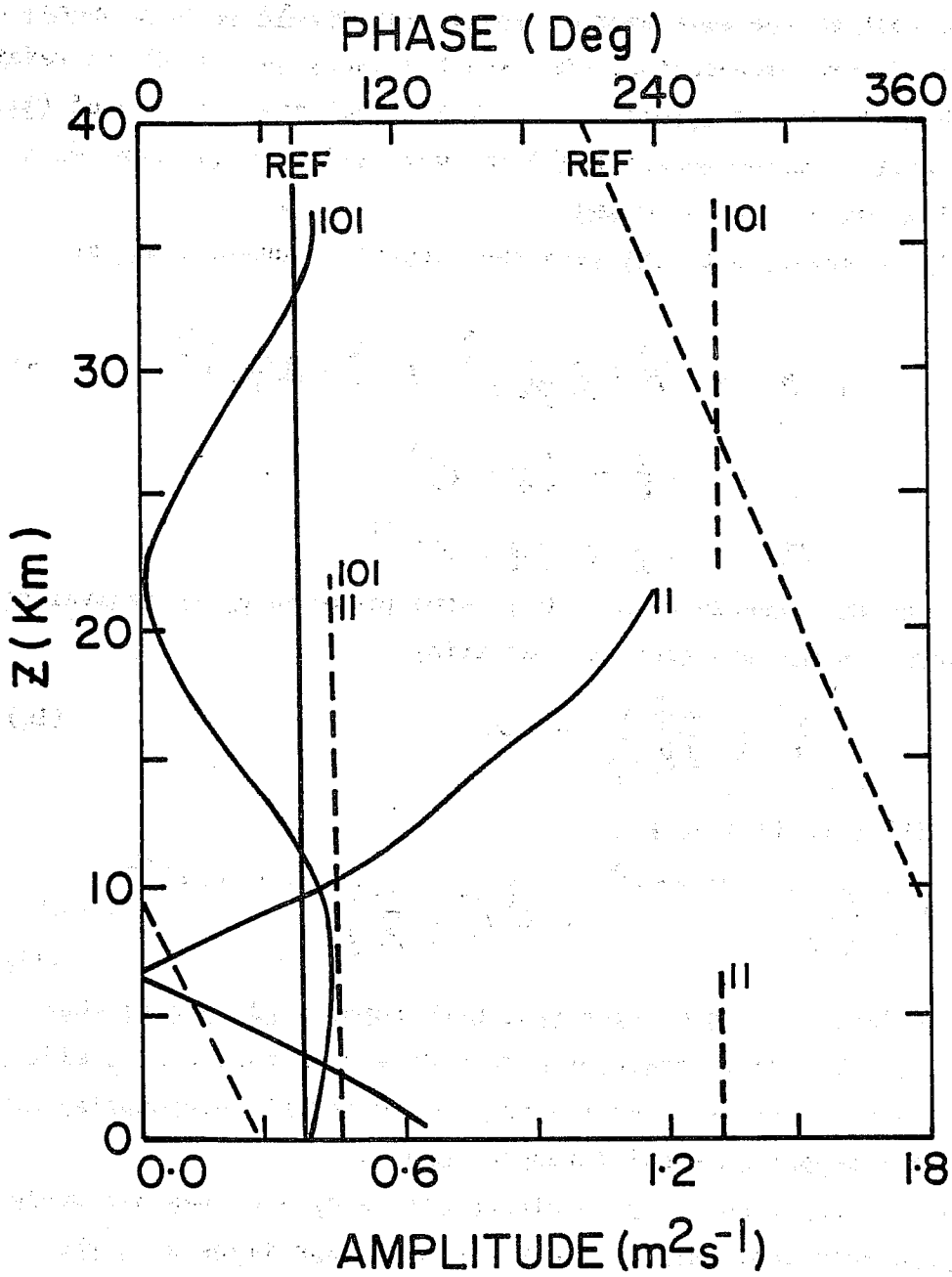

Fig. 1. Vertical distribution of the amplitude and phase of the function $\tilde{\Psi} = \Psi \exp(-Z/2H)$ computed using the reference model (200 levels) and the P model formulation with 101 and 11 levels in the vertical. $\bar{u} = 20$ m s^{-1} and $\alpha_R = 0.0$ (After Kirkwood and Derome, 1977, hereafter abbreviated as KD in figure legends).

an upward and a downward energy propagating part in its solution. In other words the upper boundary condition $\omega(p = 0) = 0$ reflects the upward propagating energy and leads to a standing wave solution. The interference pattern created by the superposition of the components of the solution is seen to be sensitive to the resolution of the model. By the argument of the preceding paragraph the numerical solution cannot be expected to converge as the vertical resolution is increased.

Note that except at the nodal points the phase lines are vertical, implying that there is no wave horizontal heat flux and no vertical energy flux. This is consistent with the fact that when only vertical energy propagation is possible, the latter is equal to $C\bar{u}$ where C is a constant. If the upper boundary condition forces the energy flux to vanish at the top of the model and $\bar{u} \neq 0$ then we find that $C = 0$ and the vertical energy flux vanishes everywhere. This result does not depend on our having taken $\bar{u}$ = constant; it holds for all profiles $\bar{u}(p) > 0$. It is clear then that in simplified models such as the one under study here the upper boundary condition can have drastic effects on the solution. This was pointed out in particular by Lindzen et al. (1968).

If instead of a weak westerly mean zonal wind we now consider a value of $\bar{u}$ = constant sufficiently large to trap the wave, we find quite different results. In that case the boundary condition $\omega'(p = 0) = 0$ does yield information in (11) when we take the limit as $p_T \to 0$. Since now $\gamma < 0$ we must set $\hat{B} = 0$ to have a bounded energy density at infinity. The numerical results (not shown here) do indeed show that the P model with $\omega'(p = 0) = 0$ converges to the correct analytical solution as the vertical resolution increases. The reference model naturally also has a solution in very good agreement with the analytical one.

4. Winter Zonal Wind

We will now examine whether the forced wave solution is sensitive to the upper boundary condition when the mean zonal wind varies with height in a manner fairly typical of winter conditions. We will use the "winter" profile shown in Fig. 2 and we will include the Newtonian cooling mechanism with $\alpha_R(Z)$ as shown in Fig. 3. The profile of α_R between 30 and 70 km is based on computations by Dickinson (1973); below 30 km we have assumed that α_R decreases slowly.

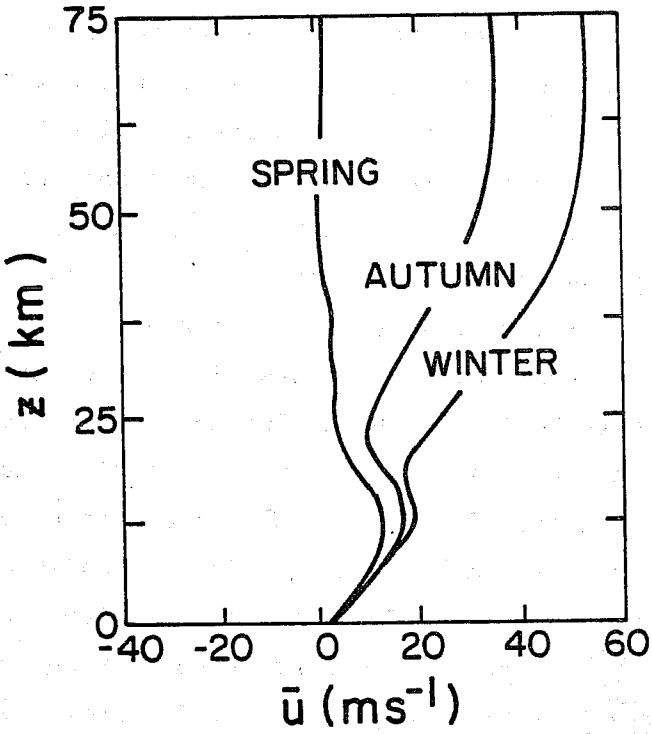

Fig. 2. Vertical profiles of the mean zonal wind for winter, spring and autumn (After KD).

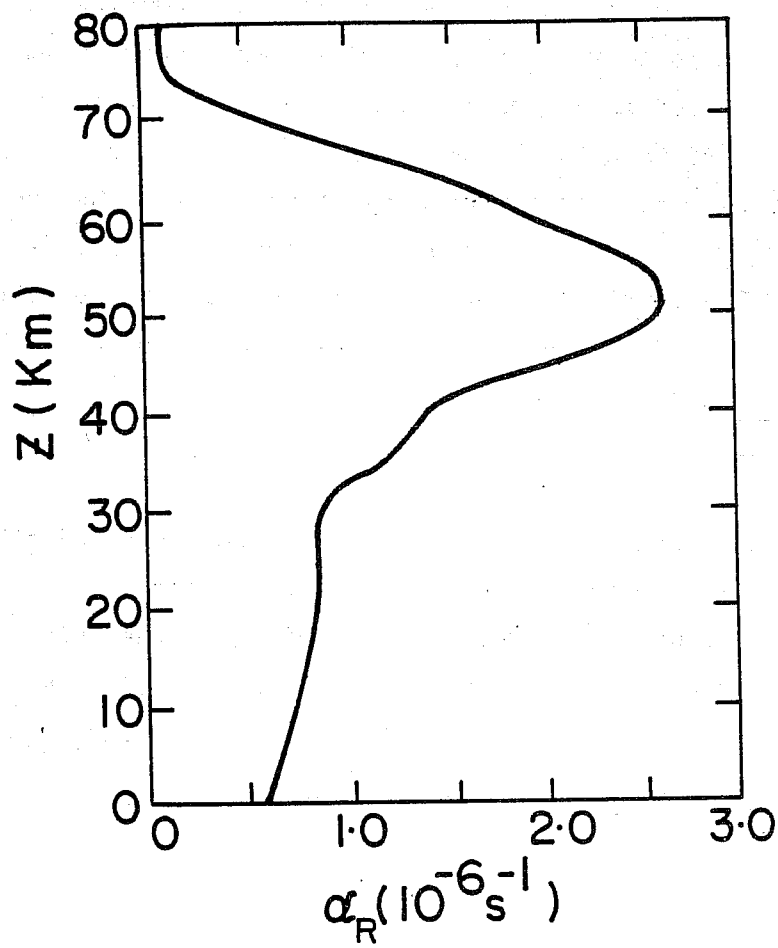

Fig. 3. Vertical profile of the Newtonian cooling coefficient (After KD).

The forced wave structure obtained with the reference model is shown in Fig. 4 together with the structure computed without Newtonian cooling. First we see that with $\alpha_R \equiv 0$ the wave is trapped by the strong stratospheric winds; $|\tilde{\Psi}|$ decays with height in the upper region which acts as a reflector, creating the nodal structure in the lower levels. When the Newtonian cooling is included the forced amplitude is reduced and the nodal structure is replaced by a wave sloping to the west with height.

The observations of zonal harmonic standing wavenumber 1 in January from van Loon et al. (1973) have been averaged between 40-70°N. The resultant vertical profiles presented in Fig. 5 may be compared with the reference solution of Fig. 4. In view of the approximations made in the reference model, the rather good agreement between the computed and observed structures is somewhat surprising.

Let us now see how the P model performs with this $\bar{u}(p)$ profile. Since the strong stratospheric winds prevent the wave energy from reaching the very high levels, it is possible that its reflective upper boundary condition will not have a detrimental effect on the solution. That this is the case can be seen if Fig. (6) which compares the reference solution with that of the P model with 101 levels. Similarly we see in Fig. 7 that even with only 21 levels the P model gives a rather good solution. From Fig. 8, on the other hand, we find that when the vertical resolution decreases to 11 or 6 levels the computed solutions are drastically changed.

One possible explanation for the above behaviour of the numerical solution is that the low resolution P models do not "see" the trapping mean zonal winds in the stratosphere because their uppermost computational levels are too low. To test this hypothesis the computations have been repeated with $\bar{u}$ values everywhere double those presented in Fig. 2. The P model solutions appear in Fig. 9 and support the above explanation. Even with the lowest resolution shown the forced wave is subject to an internal reflection by an upper region of strong winds and the spurious reflection at the upper boundary seems to be negligibly small.

5. Spring Zonal Winds

We might expect quite different results with the "spring" zonal wind profile of Fig. 2 since its very low values of $\bar{u}$ in the stratosphere certainly allow the free upward propagation of the forced wave to infinity, and hence to the reflecting boundary of the P model. As pointed out by

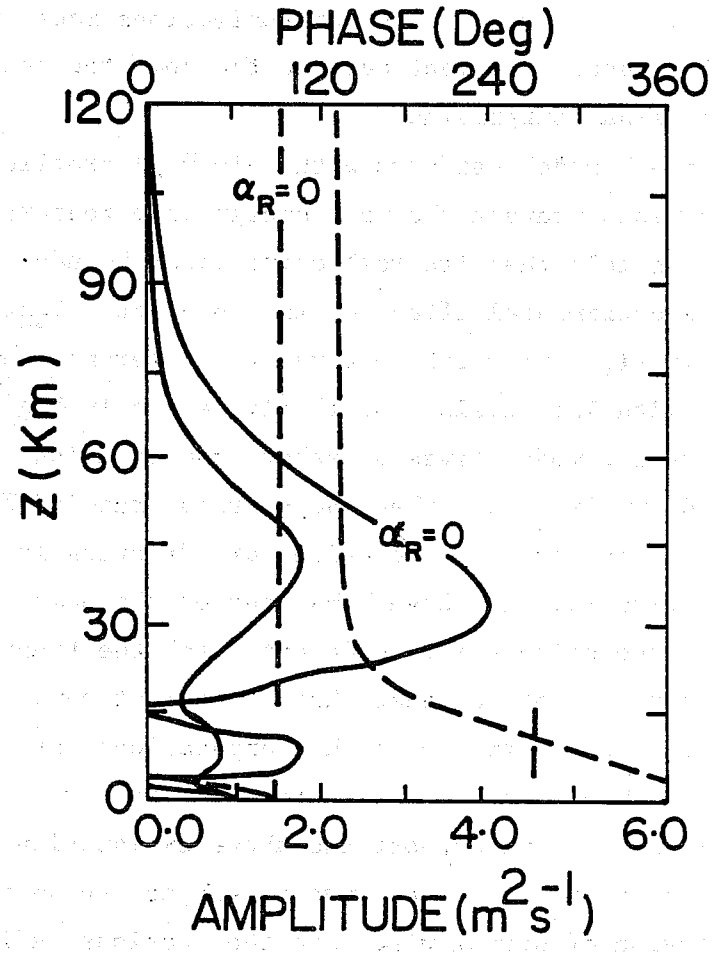

Fig. 4. Vertical distribution of the computed amplitude (solid) and phase (dashed) of $\tilde{\Psi}$. Reference solutions for winter winds without cooling ($\alpha_R = 0$) and with cooling (α_R from Fig. 3) (After KD).

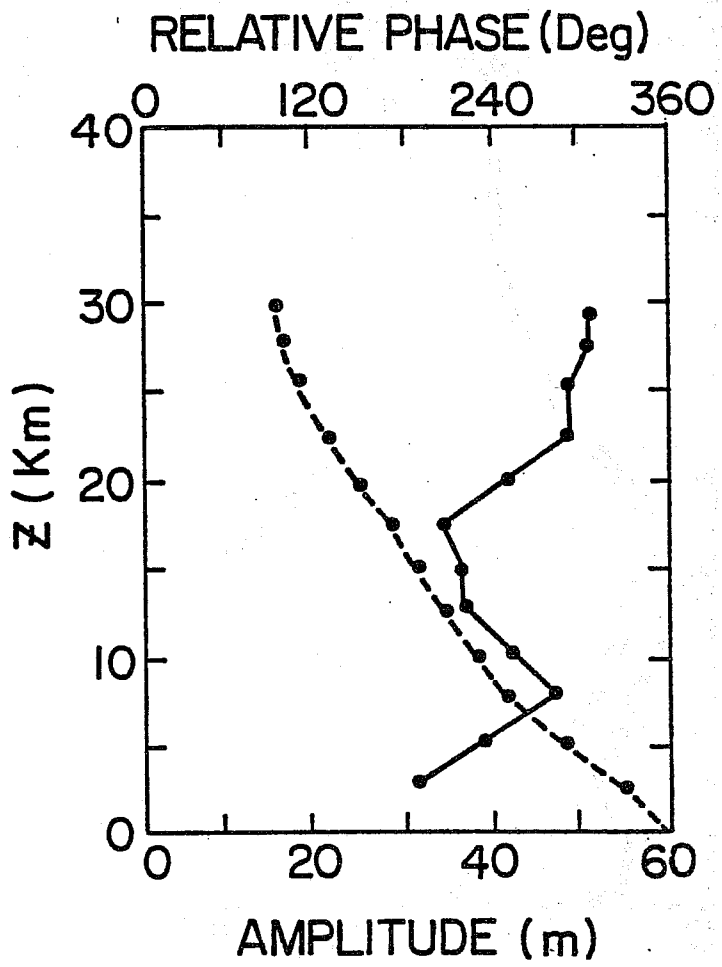

Fig. 5. Amplitude (solid) and phase (dashed) of $\tilde{\Psi}$ of zonal wavenumber 1 obtained from observations in winter.

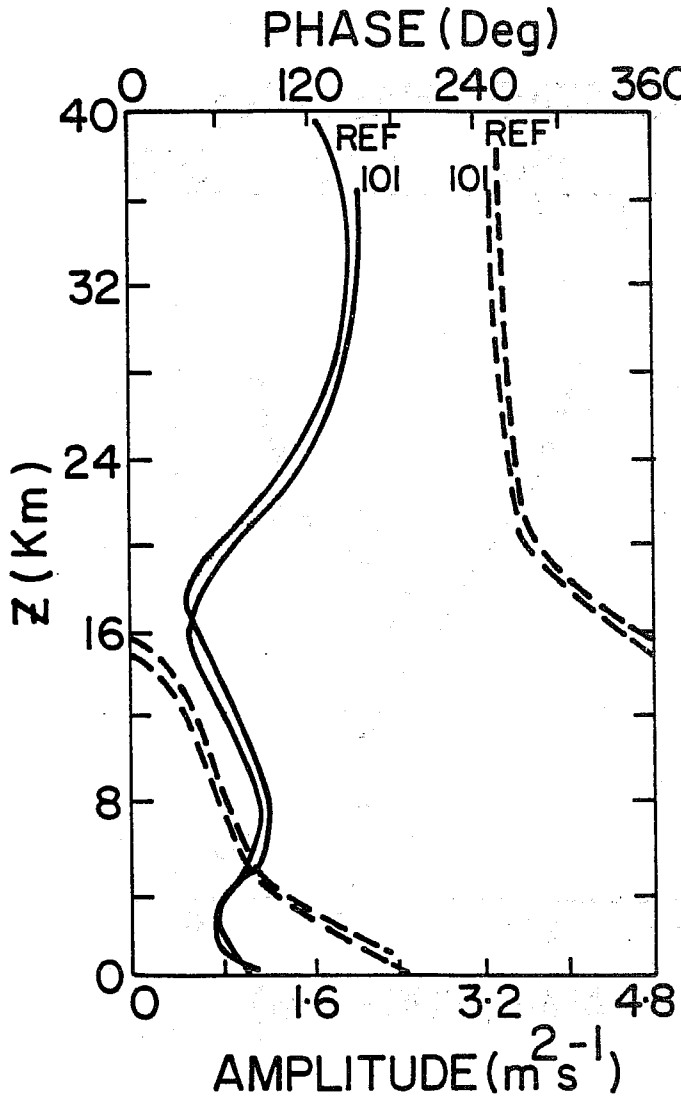

Fig. 6. Vertical distribution of the amplitude (solid) and phase of $\tilde{\Psi}$. Reference and the 101 level P model solutions for winter winds with Newtonian cooling (After KD).

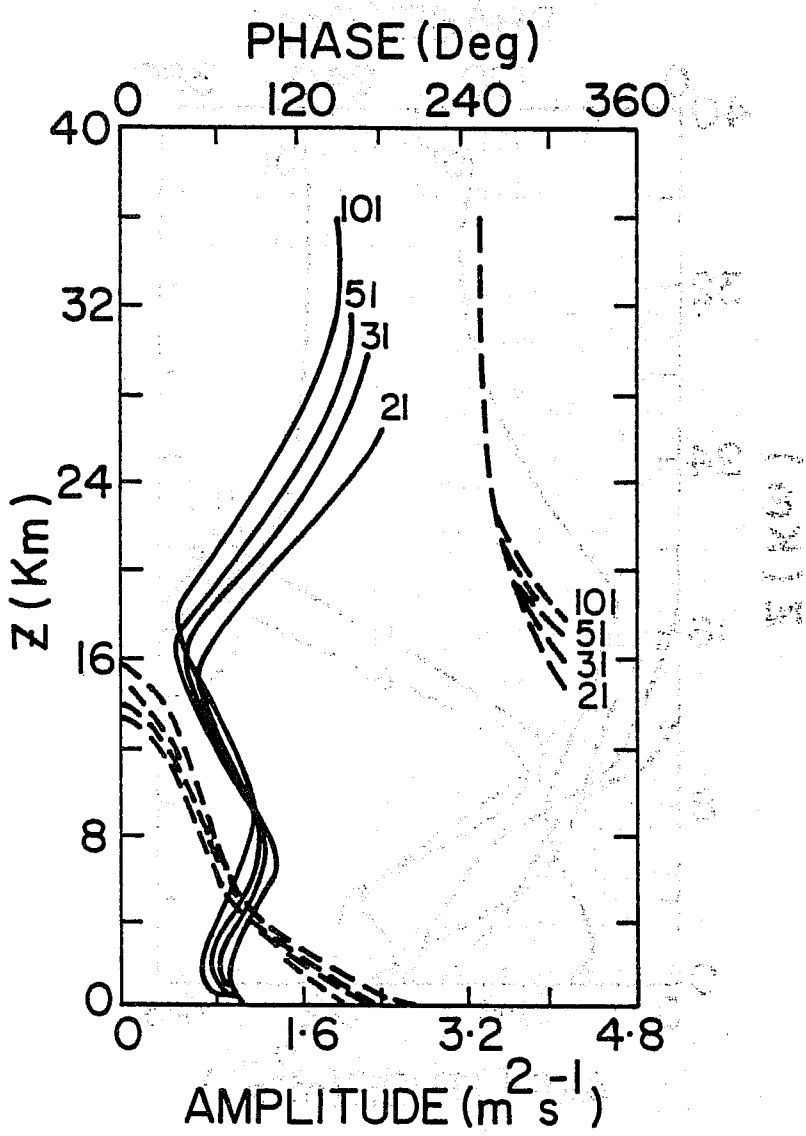

Fig. 7. As in Fig. 6 except that the 101, 51, 31 and 21 level P model solutions are shown.

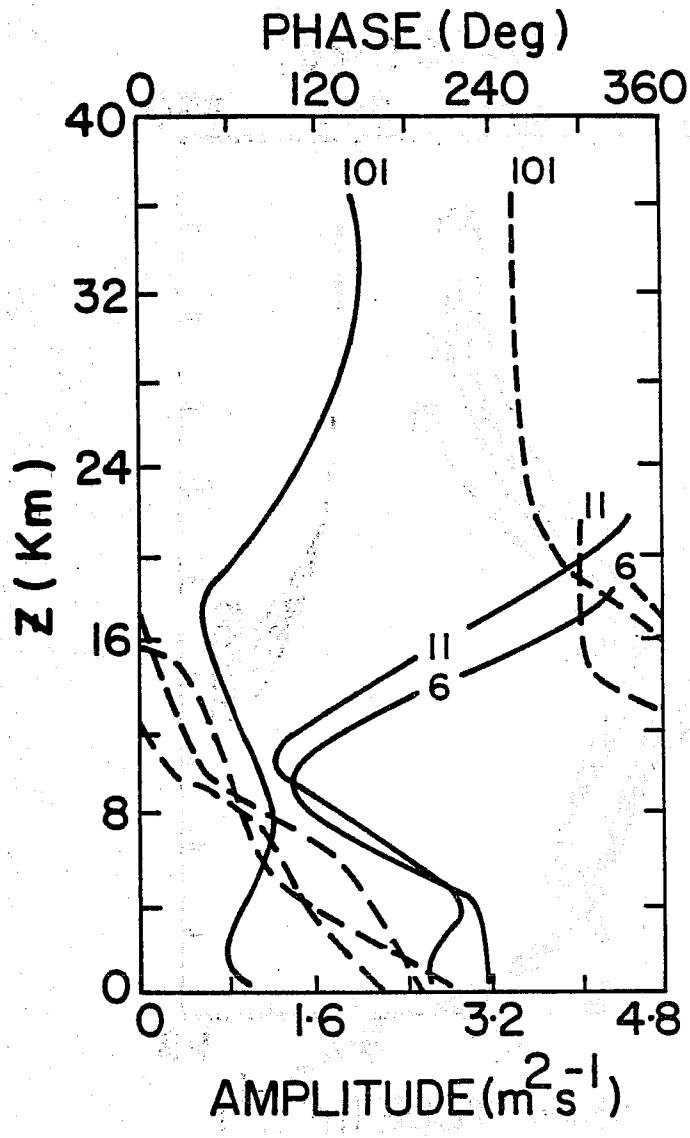

Fig. 8. As in Fig. 6 except that the 101, 11 and 6 level P model solutions are shown (After KD).

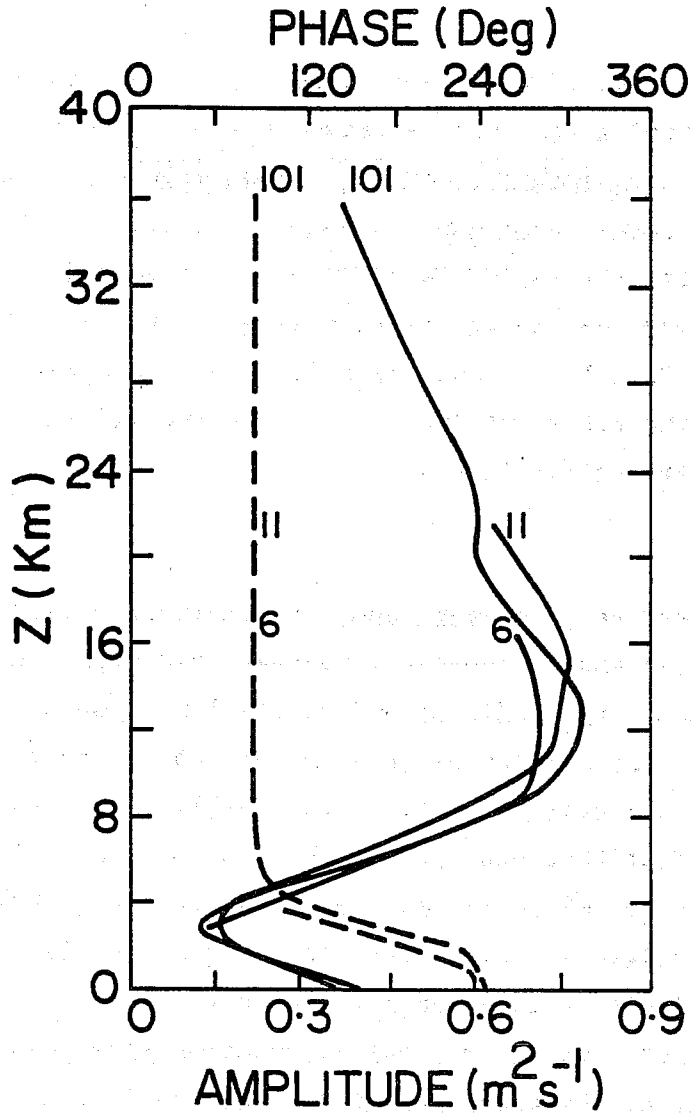

Fig. 9. As in Fig. 8 except that a modified winter zonal wind profile was used (After KD).

Dickinson (1969), on the other hand, the Newtonian cooling mechanism becomes quite effective when $\bar{u}$ is small; thus the dissipation that it provides may prevent the wave energy from reaching the upper boundary.

If we first compare the P model solution with 101 levels to the reference solution (Fig. 10) we find a very good agreement, implying that the Newtonian cooling indeed dissipates the wave energy before it reaches the top.

The wave structures obtained with lower resolutions are shown in Fig. 11. The 31 level model gives quite a reasonable solution but the 6 level model is clearly unacceptable. In Fig. 12 we show the results obtained with the same 6 level model except that at the highest level where α_R enters the problem its value was arbitrarily increased to 2.5×10^{-6} s^{-1}. The improvement in the results is evident. It seems then that in the case of Fig. 11 the main deficiency of the 6 level model (in comparison to the other resolutions) is its inability to "see" the deep dissipating stratospheric layers.

6. Discussion

It is not at all clear that the more complex numerical models used in general circulation studies and in numerical weather prediction are as sensitive to the upper boundary condition and vertical resolution as our linear Beta plane model. The ability of those models to propagate wave energy in the meridional direction as well as vertically, the presence of nonlinear terms and the fact that many of them have more than 10 levels in the vertical, are all factors which may well make the spurious reflections at the upper boundary negligibly small. Very little quantitative information appears to be available on this subject, however.

One study which was done with a general circulation model precisely to investigate the effect of the upper boundary condition is the one by Williams (1976). The stationary waves in two NCAR models with rigid tops were compared. Both models used height as the vertical coordinate with layers 3 km deep; one had 6 layers up to 18 km and the other 12 layers up to 36 km. It was found that in the lowest 18 km both models yielded fairly similar structures for zonal wavenumbers 1 and 3. Wavenumber 2, on the other hand, differed appreciably in the two models, as can be seen in Fig. 13. At (6 km, 60°N), for example, the two wave amplitude maxima differ by a factor of about 2, showing the influence of the reflective

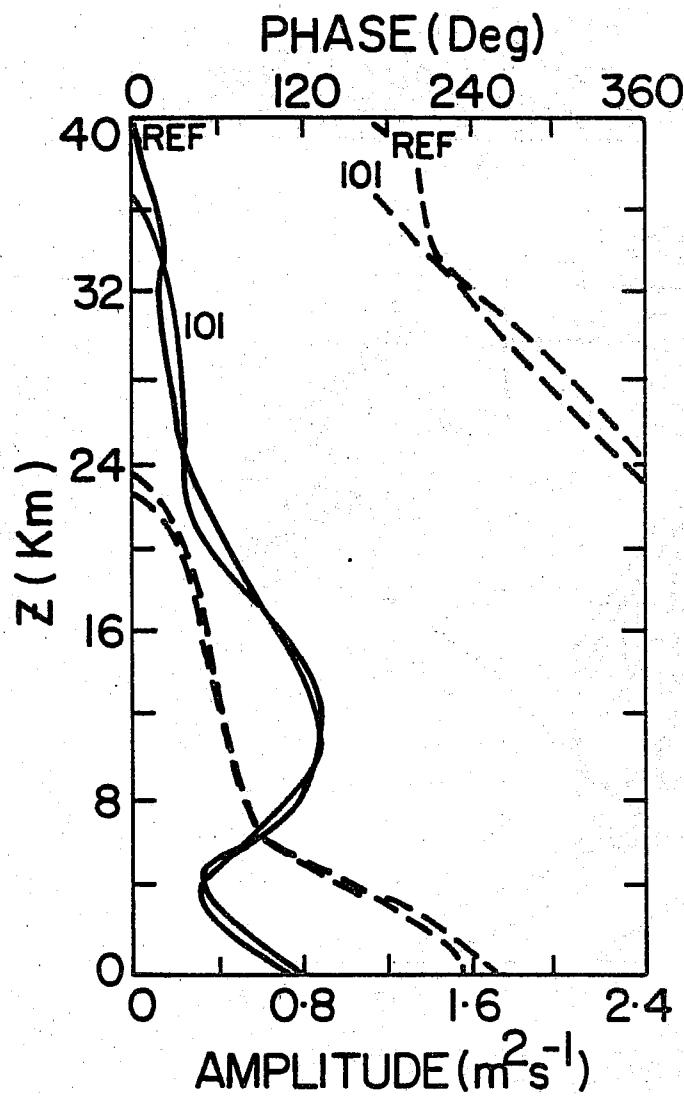

Fig. 10. Vertical distribution of the amplitude (solid) and phase (dashed) of $\tilde{\Psi}$. Reference and 101 level P model solutions obtained with the spring wind profile and α_R from Fig. 3 (After KD).

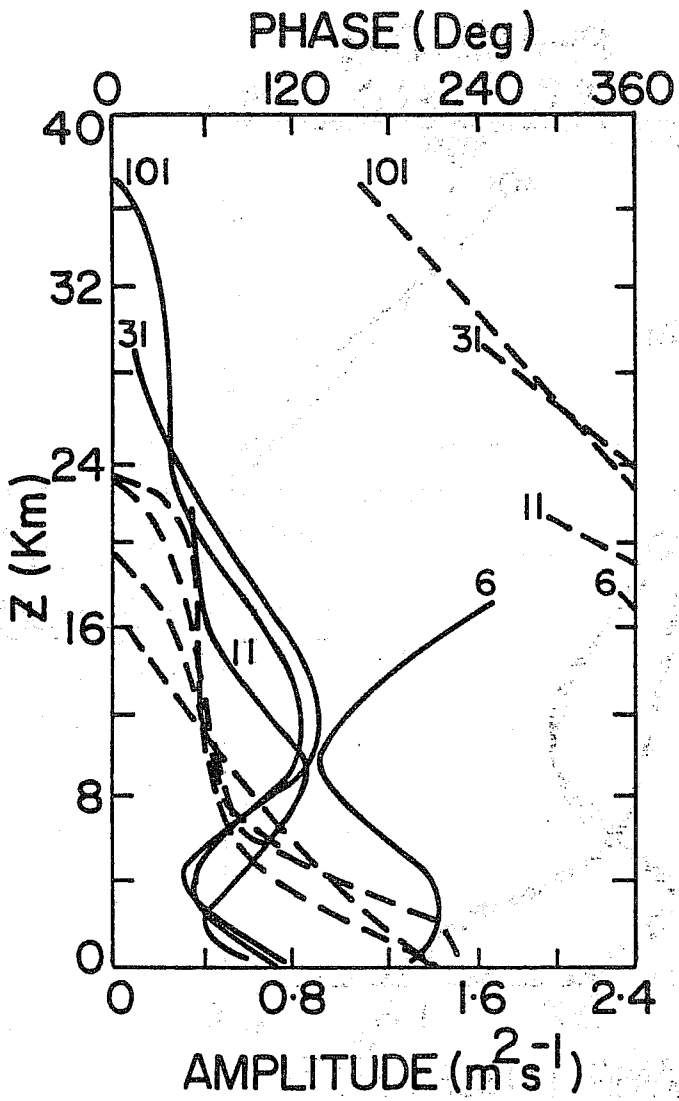

Fig. 11. As in Fig. 10 but for 101, 31 and 6 levels in the P model (After KD).

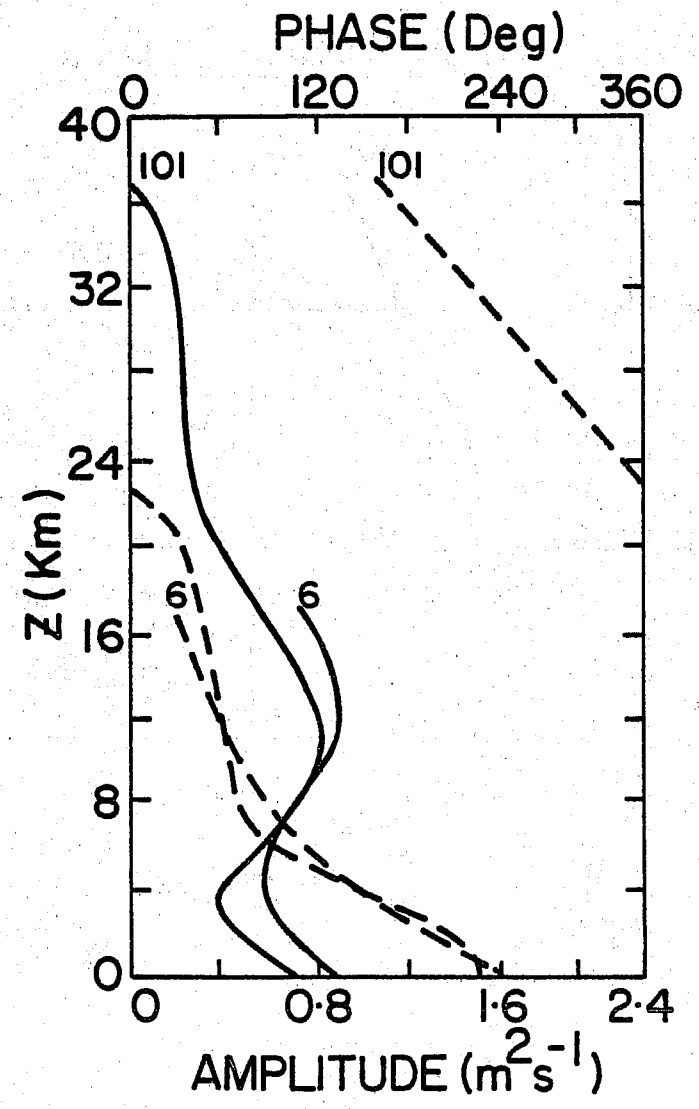

Fig. 12. Vertical distribution of the amplitude (solid) and phase (dashed) obtained using the spring zonal winds, a modified Newtonian cooling coefficient profile and the 6 level P model. The 101 level P model solution is reproduced from Fig. 10 (After KD).

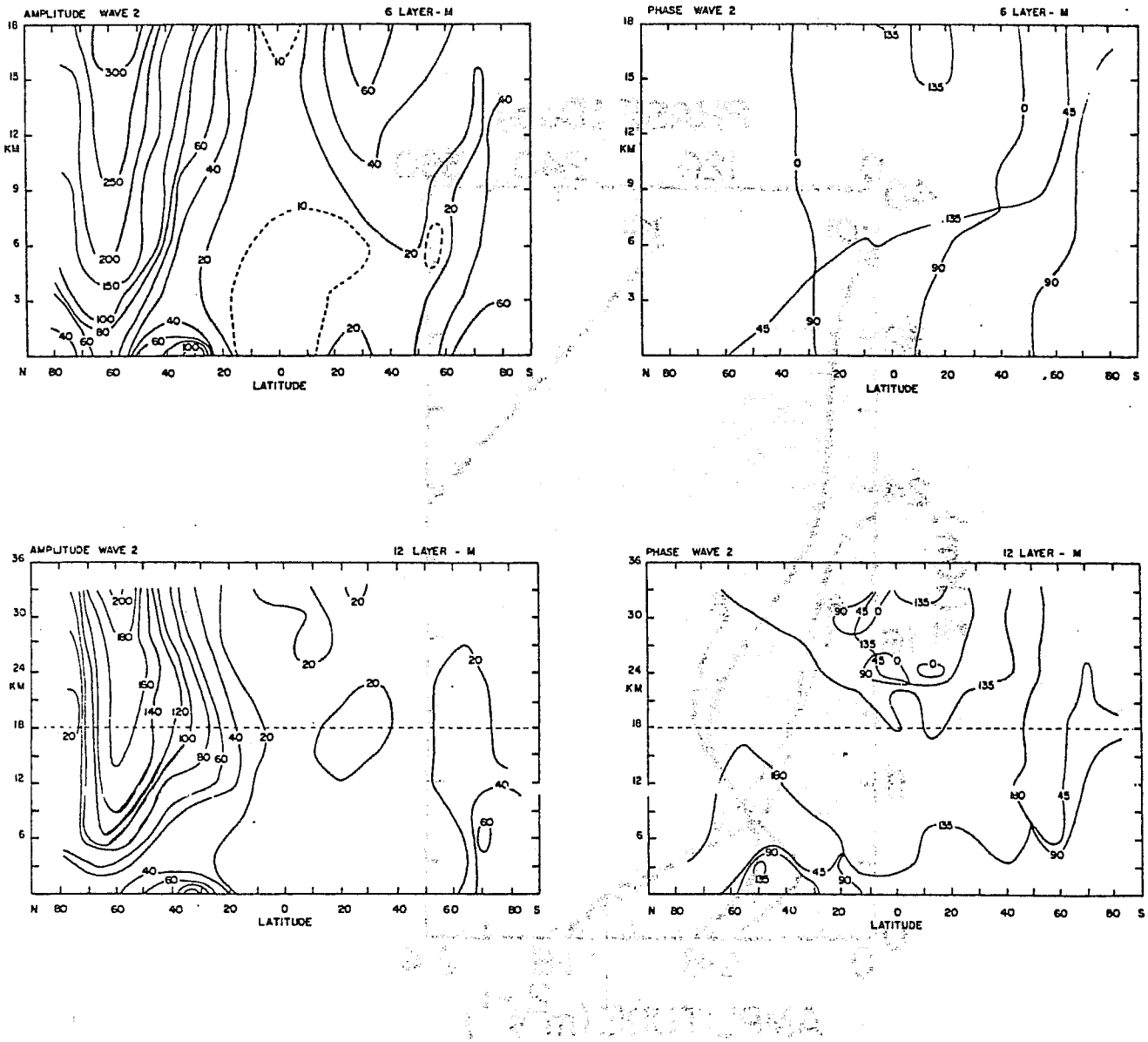

Fig. 13. Latitude-height distribution of the amplitude and phase of zonal wavenumber 2 obtained with two versions of the NCAR model. Upper: 6 layer version; lower: 12 layer version. Amplitudes in metres and phases in degrees east of the Greenwich Meridian (Adapted from Williams, 1976).

boundary condition at 18 km.

7. Implications for Time-Dependent Models

In this section we will examine how the deficiency of a NWP model in representing the stationary forced waves can lead to forecast errors. This arises from the fact that a model which contains a time-independent (or nearly so) wave energy source on the planetary scale, such as topography or land-sea thermal contrasts, can be expected to interpret initial atmospheric data as being the sum of a forced stationary part and a free, travelling part. If the model's stationary component differs from that of the atmosphere, the distribution of initial variance between the free and forced waves will be done incorrectly so that an incorrect amount of energy will appear in the form of travelling waves. The deficiency of the model in representing the forced waves may be related to various factors, such as incorrectly specified heat sources. In the sequel we will assume that the deficiency arises from poor vertical resolution.

We will assume that our forecast model is given by the time-dependent version of (1) and (2), that is,

$$\frac{\partial}{\partial t}\nabla^2\psi' + \bar{u}\frac{\partial}{\partial x}\nabla^2\psi' + \beta\frac{\partial\psi'}{\partial x} = f_0\frac{\partial\omega'}{\partial p} \tag{12a}$$

$$\frac{\partial}{\partial t}\frac{\partial\psi'}{\partial p} + \bar{u}\frac{\partial}{\partial x}\frac{\partial\psi'}{\partial p} - \frac{d\bar{u}}{dp}\frac{\partial\psi'}{\partial x} + \frac{\sigma}{f_0}\omega' = -\alpha_R\frac{\partial\psi'}{\partial p} \tag{12b}$$

with boundary conditions

$$\omega'(x, y, p=0, t) = 0 \tag{13a}$$

$$\omega'(x, y, p=\beta, t) = \bar{u}_s\,\partial h_g/\partial x \tag{13b}$$

where w' is the height-coordinate vertical velocity dz/dt caused by the surface topography $h_g(x,y)$. With the hydrostatic and quasi-geostrophic approximations we can rewrite (13b) as

$$\omega'_s = \rho_s f_0\left(\frac{\partial\psi'}{\partial t}\right)_p + \omega_m$$

where $\omega_m = -\rho_s\, g\, \bar{u}_s\, \partial h_g/\partial x$. The lower boundary forcing ω_m will have the following form

$$\omega_m = D\exp(ikx)\cos ly. \tag{14}$$

The model is then identical to the P model of section 2.1 except for the addition of the $\partial/\partial t$ terms.

The time evolution of the model can be obtained by substituting a solution of the form

$$\psi'(x,y,p,t) = \psi_f(p)\exp(ikx)\cos ly + \sum_{n=1}^{N} a_n \hat{\psi}_n(p)\exp(ikx - ikc_n t)\cos ly \qquad (15)$$

into the model potential vorticity equation. The first term on the right-hand side of (15) is the stationary part of the solution discussed earlier and the second term is a sum of the various solutions to the homogeneous system. In fact the $\hat{\psi}_n$'s and c_n's are the eigenfunctions and eigenvalues of the model. A model with N levels where ψ' is predicted has N possible vertical free modes (eigenfunctions), each one having development and propagation characteristics given by its eigenvalue c_n.

To initialize the model we will assume that the true state of the atmosphere is given by the stationary (forced) solution of the same model with high resolution (101 levels). Thus a correct forecast is one which predicts no evolution in time, and that is naturally the forecast we would obtain if we used the 101-level model to do the prediction. With a low resolution model, however, the flow will evolve and the difference with the conditions at t = 0 will be the "forecast error".

To determine the constants a_n in (15), the initial state (reference solution) is decomposed into a steady-state solution of a low resolution model plus a linear combination of the eigenmodes of that model. Evaluating (15) at t = 0, cos ly = 1 we have

$$\psi'(p) = \psi_f(p) + \sum_{n=1}^{N} a_n \hat{\psi}_n(p) \qquad (16)$$

where ψ' is the control solution, ψ_f is the steady state of the low resolution model and $\hat{\psi}_n$ is the nth eigenvector. The a_n's are easily obtained by matrix inversion.

The forecast error is then

$$E(x,p,t) = \psi'(x,p,t)_{low\ res.} - \psi'(x,p,t)_{reference}$$

$$= \psi'(x,p,t)_{low\ res.} - \psi'(x,p,t=0)_{low\ res.}$$

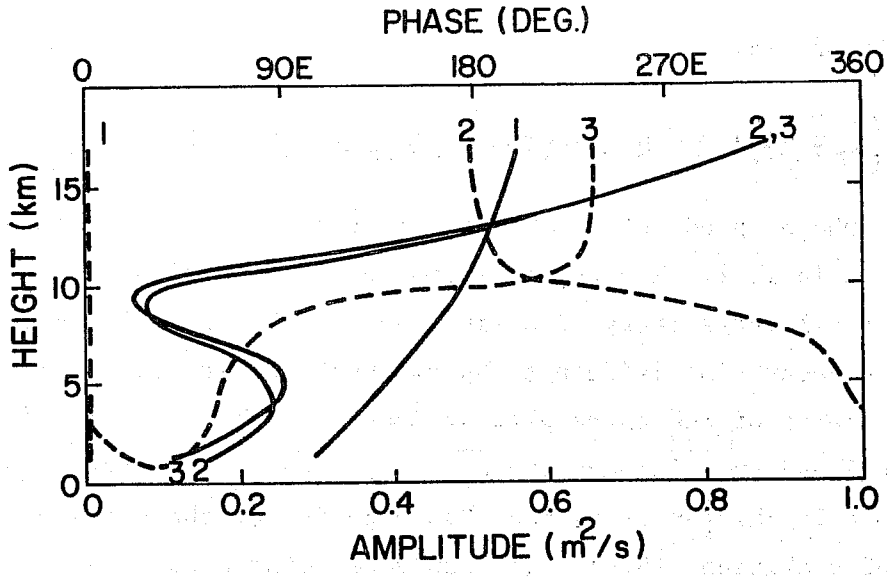

Fig. 14. Amplitude (solid) and phase (dashed) of the first three eigenmodes of the 6 level model with the winter zonal wind profile of Fig. 2. The modes were normalized to have the same RMS (mass weighted) amplitude (After Desmarais and Derome, 1978).

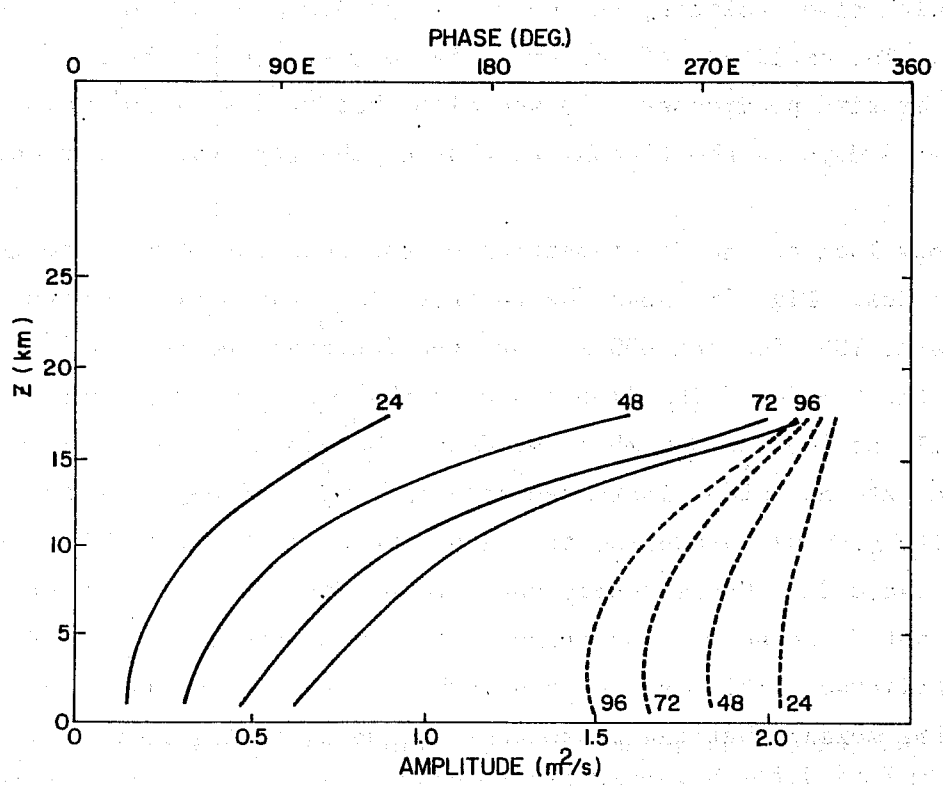

Fig. 15. Amplitude (solid) and phase (dashed) of the forecast error at 24-h intervals, using a 6 level model and the winter zonal wind profile (After Desmarais and Derome, 1978).

or, with the help of (15),

$$E(x,p,t) = \sum_{n=1}^{N} \{ a_n \hat{\psi}_n(p) \exp(ikx - ikc_n t) - a_n \hat{\psi}_n(p) \exp(ikx) \} \qquad (17)$$

The complex phase speeds of the 6 vertical eigenmodes of a 6 level model are given in Table 1. The negative imaginary parts of all phase speeds imply that all modes decay with time, due to the Newtonian cooling mechanism. The e-decay time is seen to be two weeks or longer for all modes. The structures of the three gravest modes are shown in Fig. 14. Mode 1 is vertical and travels westward with a period of 8.1 days. In more realistic models this external mode has a period of about 5 days (e.g. Geisler and Dickinson, 1976). It should be pointed out that Fig. 14 gives the amplitude of the stream function ψ', not $\exp(-Z/2H)\psi'$ as in previous sections. The same applies to subsequent figures.

The forecast errors obtained with the 6 level model appear in Fig. 15 at one-day intervals up to 4 days. We find that the error wave retrogresses with time, pointing to the likely presence of a spurious external mode. The amplitude of the error increases with height and especially so as time progresses. We see also that at 5 km ($\sim$500 mb) the error after 4 days is about equal to that at the top level after only 1 day.

We will now look at the decomposition of the forecast error into the model's eigenmodes. Fig. 16 shows the relative importance of the first 3 vertical modes at 100, 500 and 800 mb, at 24-h intervals up to 96h as well as the sum of the 6 modes. The importance of the westward propagating mode, especially at 500 and 800 mb is evident. We see that the amplitude of mode 1, the external mode, increases with time up to 4 days. After 4 days its amplitude should decrease, to reach a value of 0 after 8.1 days, the period of the mode. Consequently the external mode is predominant in the beginning but decreases in importance later on as the internal modes increase in amplitude. This can be seen mathematically if we rewrite (17), assuming for the moment that the phase speed is real, in the form

$$E(x,p,t) = -2i \sum_{n=1}^{N} a_n \hat{\psi}_n(p) \sin(kc_n t/2) \exp(ikx - ikc_n t/2). \qquad (18)$$

In other words the amplitudes of the various modes in the forecast error are

TABLE 1. The real and imaginary parts of the phase speed c together with the period $2\pi/kc_r$ and the time required for the amplitudes to decay by a factor e, $-1/kc_i$, for the various vertical modes of the 6 level model for winter conditions.

Mode	c_r	c_i	$2\pi/kc_r$	$-1/kc_i$
	m s^{-1}	m s^{-1}	days	days
1	-32.8	-0.28	8.1	151
2	0.7	-0.95	380	45
3	1.2	-2.98	221	14
4	3.3	-2.42	81	18
5	5.9	-2.49	45	17
6	9.2	-2.59	29	16

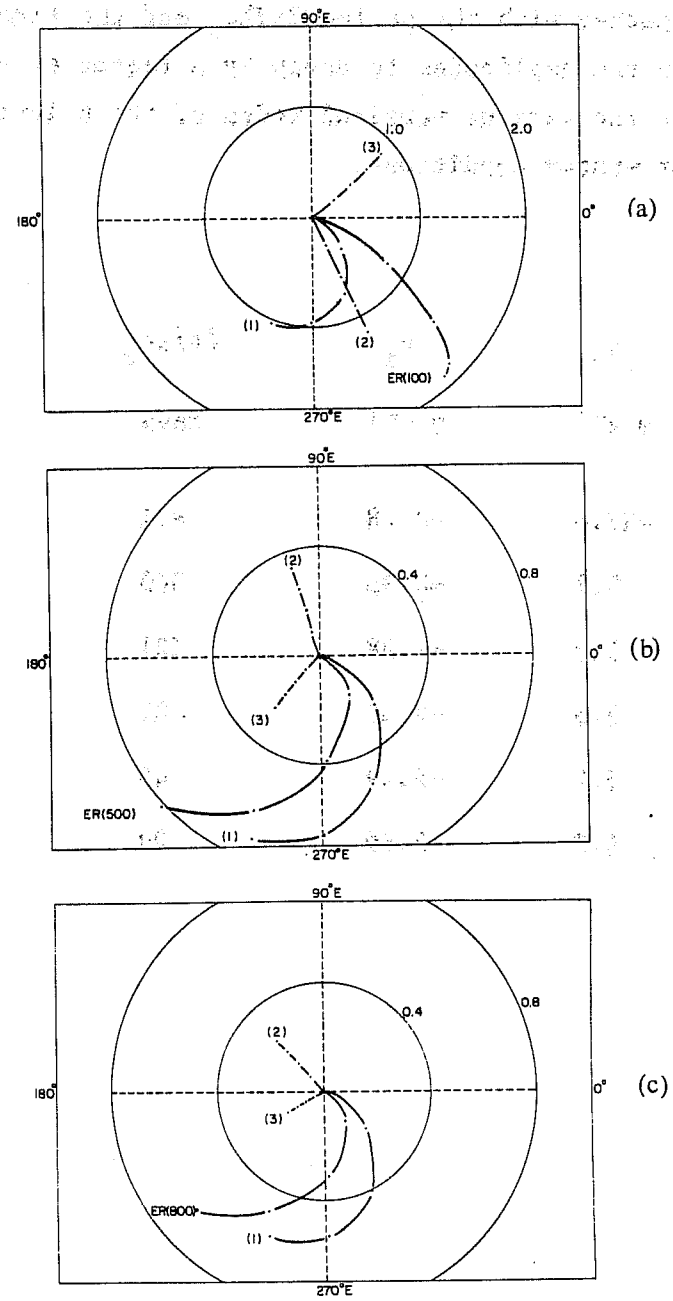

Fig. 16. Decomposition of the total error ER at (a) 100 mb, (b) 500 mb, (c) 800 mb into its components in winter. The amplitude ($m^2 s^{-1}$) scale is written along concentric circles while the phase angle is given by the angle on the polar graph. The mode number is written between parentheses. The origin corresponds to initial time, while the last dot on the curve is at 96h (After Desmarais and Derome, 1978).

modulated by $\sin(kc_n t/2)$ which is zero at $t = 0$ and after one or more complete periods of the mode, i.e., $t = 2\pi m/kc_n$ where m is an integer.

The factor $\sin(kc_n t/2)$ is extremely important in explaining the weight of the external mode in the forecast error. An examination of the factors $A_n\hat{\psi}_n$ for the various modes has shown that it is much smaller for $n = 1$ (the external mode) than for some of the other modes, which means that at $t = 0$ the difference between the reference solution and the low resolution model's forced wave is not projected mainly onto the external mode. The latter, however, has such a high phase speed that it quickly goes to a wrong phase position and leads to an error.

Experiments performed with 11 and 21 levels show that while the forecast errors are smaller than with 6 levels, their main features are qualitatively similar to the one just discussed.

8. Discussion

In closing we stress that while studies such as the above may be helpful first steps in our understanding of forced planetary waves, they must be followed by more complete ones before we arrive at quantitative results that are directly applicable to NWP or GCM models. For example it is likely that the minimum vertical resolution required to achieve a given forecast accuracy can only be determined by performing forecast experiments with the complete model.

Finally it should be kept in mind that there may be no unique and final answer to the problem of the upper boundary condition. Even the Somerfeld radiation boundary condition which we have used in our reference solutions must be considered an approximation. It requires that the wave solution be known above the level Z_T where the condition is actually applied numerically. In our case this meant that the mean zonal wind had to be assumed independent of height above Z_T. In addition it is not clear that the boundary condition can be applied if the flow near the upper boundary becomes highly nonlinear. It is possible that the practical answer to the upper boundary condition problem will be to use a sufficient vertical resolution and to place the upper computational levels sufficiently high so that (a) most of the wave energy will be absorbed or reflected back before reaching the upper boundary and/or (b) the energy that is reflected by the boundary will not reach the lower regions of interest before other forecast errors have degraded the prediction.

REFERENCES

Bates, J.R., 1977: Dynamics of stationary ultra-long waves in the middle latitudes. Quart. J. Roy. Meteor. Soc., 103, 397-430.

Desmarais, J.-G. and J. Derome, 1978: Some effects of vertical resolution on modelling forced planetary waves with a time-dependent model. Atmosphere-Ocean, 16, 212-225.

Dickinson, R.E., 1969: Vertical propagation of planetary Rossby waves through an atmosphere with Newtonian cooling. J. Geophys. Res., 74, 929-938.

_____, 1973: Method of parameterization for infrared cooling between altitudes of 30 and 70 kilometers. J. Geophys. Res., 78, 4451-4457.

Geisler, J.E. and R.E. Dickinson, 1976: The five-day wave on a sphere with realistic zonal winds. J. Atmos. Sci., 33, 632-641.

Kirkwood, E. and J. Derome, 1977: Some effects of the upper boundary condition and vertical resolution on modeling forced stationary planetary waves. Mon. Wea. Rev., 105, 1239-1251.

Lindzen, R.S., E.S. Batten and J.W. Kim, 1968: Oscillations in atmospheres with tops. Mon. Wea. Rev., 96, 133-140.

Nakamura, H., 1976: Some problems in reproducing planetary waves by numerical models of the atmosphere. J. Meteor. Soc. Japan, 54, 129-146.

van Loon, H., R.L. Jenne and K. Labitzke, 1973: Zonal harmonic standing waves. J. Geophys. Res., 78, 4463-4471.

Williams, J., 1976: Zonal harmonic standing waves in the NCAR global circulation model. Mon. Wea. Rev., 104, 249-259.